R-02-03

Strategy for a Rock Mechanics Site Descriptive Model

Development and testing of an approach to modelling the state of stress

Eva Hakami, Hossein Hakami
Itasca Geomekanik AB

John Cosgrove
Imperial College of Scicence and Technology, London

May 2002

Svensk Kärnbränslehantering AB
Swedish Nuclear Fuel
and Waste Management Co
Box 5864
SE-102 40 Stockholm Sweden
Tel 08-459 84 00
+46 8 459 84 00
Fax 08-661 57 19
+46 8 661 57 19

ISSN 1402-3091
SKB Rapport R-02-03

Strategy for a Rock Mechanics Site Descriptive Model

Development and testing of an approach to modelling the state of stress

Eva Hakami, Hossein Hakami
Itasca Geomekanik AB

John Cosgrove
Imperial College of Scicence and Technology, London

May 2002

Keywords: In situ stresses, regional stress field, controlling factors, stress prediction, stress measurements, numerical modelling, Test Case, modelling, fracture zone influence, stategy, Site Descriptive Model

Summary

The overall objective of this project has been to develop, test and establish a method for creating a Rock Mechanics Site Descriptive Model for a site considered in the site investigation programme. The work was divided into three parts, the empirical and theoretical "property models" and the "stress model". The work on the stress model is presented in this report. The work consisted of i) a literature review about geological factors controlling *in situ* stress and a review about the use of numerical models for this subject, ii) the development of recommendations on the methodology to be applied during a site investigation and iii) the Test Case exercise, where the suggested methods were tested.

The main mechanism controlling the *in situ* stress magnitudes in Sweden is plate tectonics causing the stress field to show similarities in most parts of north-western Europe, having a NW-SE trend of the maximum principal stress. The orientation of the stress field is largely determined by the relative movements by the plates. However, the stress orientation may also be influenced by the presence of large regional weak zones, such as the Tornquist deformation zone that lies between Sweden and Denmark. The strike of the Tornquist deformation zone is parallel to the maximum principal stress as observed in central and southern Sweden. The magnitude of the stress is more difficult to estimate, but the general pattern is an increase in magnitude with depth, at least for the upper kilometres. To determine the stress magnitude at a certain site and depth, with reasonable certainty, stress measurement should be used.

A methodology for building a stress model has been proposed. It involves different steps starting with a preliminary stress estimation, followed by steps for interpreting site-specific information. If the stress pattern and structural geology of the site are complex, including major fracture zones intersecting the area, numerical analyses of the stress field is recommended. Different numerical models (*i.e.* alternative geological concepts) can be analysed to provide possible explanations for observed stress patterns. The orientation of fracture zones with respect to the applied stresses determines the direction of fracture zone deformation. Stress measurement results and observations from the site concerning slip directions must be used in the evaluation of the modelling.

The mean orientation for the maximum principal stress may be predicted with a fairly high degree of certainty because both regional stress pattern and the site-specific measurements can be used. The same general trend is expected for the whole central and southern Sweden, but local deviations caused by topography and faults could exist. This prediction applies to rock mass blocks away from major fracture zones. The local spatial variation around the mean can be predicted based on measurement data.

The confidence in the prediction of the stress magnitudes will be dependent on the measurement results and the complexity of the site. Inside, and also in the vicinity of major fracture zones, both the stress magnitudes and stress orientation are expected to vary strongly from point to point. The prediction of the mean stress inside a fracture zone is therefore more uncertain and the predicted local variation will be larger. The stress prediction should include a quantitative estimation of the uncertainty and the variability. Two parameters, u for uncertainty and v for local variability, are proposed.

The aim of a stress model process is to minimize the u-parameter, in rock units where the stress level is of importance for the design and safety assessment.

In the future stress measurement programmes, consideration should be given to the geological model of the site, such that measurement located inside or close to fracture zone units can be distinguished from measurements taken in more intact rock mass units. The measurements should preferably be performed using overcoring techniques or overcoring supported by hydraulic fracturing and HTPF measurements. Overcoring measurement techniques can be used to determine magnitude and orientation of all three principal stresses.

Hydraulic fracturing measurements can be used to determine the magnitude and orientation of the minimum horizontal stress, often coinciding with the minimum principal stress. The maximum principal stresses can be estimated by multiplying the ration between the maximum and minimum principal stress, from overcoring, with the minimum principal stress determined by hydraulic fracturing. Hydraulic fracturing can be performed in existing boreholes. Boreholes for stress measurements are recommended to be located in all rock units, within which a reliable prediction is desired.

Sammanfattning

Det övergripande målet med detta projekt har varit att utveckla, testa, och fastställa en metod för upprättandet av en bergmekanisk beskrivande modell för de platser som skall utvärderas med avseende på lokalisering av djupförvar. Arbetet har delats upp i tre delar; dels en empirisk och en teoretisk modell för bergmassans egenskaper, dels en spänningsmodell. I denna rapport beskrivs arbetet som behandlar spänningsmodellen. Det består av i) en litteraturstudie om de geologiska faktorer som kontrollerar in situ-spänningar och en genomgång av användningen av numeriska modeller för uppskattning av dessa, ii) framtagandet av rekommendationer för metodologin som ska tillämpas vid platsundersökningar, och iii), ”Test Case”-övningen, där de föreslagna metoderna testades.

I Sverige är plattektoniken den mekanism som har störst inverkan på in situ-spänningsfältet. Det innebär att spänningsfältet i stora delar av nordvästra Europa är ganska likartat, med en största huvudspänning ungefär i NV-SO riktning. Orienteringen av spänningsfältet styrs framför allt av plattornas relativa rörelser, men kan också påverkas av större regionala svaghetszoner, som t ex Tornquistlinjen mellan Sverige och Danmark. Tornquistlinjen strykning är parallell med största huvudspänningens riktning i södra och mellersta Sverige. Spänningarnas storlek är svårare att uppskatta, men generellt sett ökar spänningarnas storlek med djupet, åtminstone i de övre kilometrarna av jordskorpan. För att få en bra uppfattning om storleken på spänningarna på en viss plats vid ett visst djup bör spänningarna mätas.

En metodologi för upprättandet av en spänningsmodell har föreslagits. Den utgår från en preliminär uppskattning av spänningarna, följt av olika steg för tolkning av platsspecifik information. Om mätningar visar att platsen har ett varierande spänningsfält och en komplex strukturgeologi (t ex genomkorsad av större sprickzoner), rekommenderas en numerisk analys av spänningsfältet. För att få fram olika förklaringsmodeller till det observerade spänningsfältet kan olika numeriska modeller (alternativa geologiska konceptuella modeller) analyseras. Orienteringen av sprickzoner i förhållande till det regionala spänningsfältet bestämmer riktningen hos uppkomna deformationer. Resultat från spänningsmätningar på platsen och observationer av rörelseriktningar bör användas för att utvärdera modelleringsresultaten.

Den största huvudspänningens genomsnittliga orientering kan uppskattas med relativt god säkerhet, eftersom både kunskap om det regionala spänningsfältet och mätningar från platsen kan användas. Samma generella trend kan förväntas i hela södra och centrala Sverige, men lokala avvikelser orsakade av topografi och förkastningar förekommer. Detta gäller spänningen i bergmassan mellan större sprickzoner. Lokala variationer omkring det genomsnittliga värdet kan uppskattas med hjälp av mätdata.

Konfidensnivån för modellen (prediktionen) för huvudspänningarnas storlek beror av mätresultaten (metod och omfattning) och platsens komplexitet. I och i närheten av större sprickzoner kan spänningarna förväntas variera mycket från punkt till punkt, både till storlek och riktning. Prediktionen av genomsnittliga spänningarna är därför mer osäker i en sprickzon, och den uppskattade variationen är större. En spänningsmodell bör innefatta en kvantitativ uppskattning av såväl osäkerheten som den verkliga

spatiella variationen. För detta föreslås att man använder parametern u, för osäkerhet, och parametern v, för lokal variation. Målet vid upprättandet av en spänningsmodell är att minimera u-parametern i områden där spänningens storlek är av betydelse för ett förvars utformning och säkerhet.

I framtida mätprogram för spänningsfält bör den geologiska modellen beaktas, så att resultat från mätpunkter placerade i eller nära sprickzoner kan särskiljas från resultat från ”intakt” bergmassa. Vad gäller mätmetoder rekommenderas överborrning, eller överborrning i kombination med hydraulisk spräckning eller HTPF-mätningar. Överborrningstekniken kan användas för att bestämma alla tre huvudspänningarnas magnitud och riktning.

Hydraulisk spräckning kan göras i befintliga borrhål och kan användas för att bestämma magnitud och orientering på minsta horisontalspänningen, vilken ofta är densamma som minsta huvudspänningen. Magnituden på största huvudspänningen kan bestämmas med hjälp av kvoten mellan största och minsta huvudspänningen, från överborrning, multiplicerat med minsta huvudspänningens magnitud bestämd med hydraulisk spräckning. Det rekommenderas att spänningsmätningar görs i alla bergenheter för vilka en pålitlig prediktion önskas.

Contents

1 Introduction

1.1 Background

The intact rock and the fractures at a future waste repository would respond mechanically to the excavation of deposition holes and tunnels, and also to the heating of the rock mass during a long period after closure.

During the excavation of tunnels and deposition holes at depth the stresses locally around the excavations will increase and if the *in situ* stress level is high and the strength of the intact rock too low, rock failures close to the walls may occur, so called "spalling". The probability for having this situation, depending on geometry, stress level and rock properties, must be analysed site specifically /e.g. Martin et al., 2001/.

The loading of the near-field rock will become fairly high as a result of the thermal expansion of the rock after the deposition of heat generating waste. The area around the deposition holes and tunnels that would be expected to reach the rock strength limit at different times after deposition may also be analysed /e.g. Hakami and Olofsson, 2000/. Further, the shear stresses on fractures in the rock will increase due to the thermal expansion and the expected amount of shearing of a large fracture intersecting the repository may be calculated /e.g. Hakami and Olofsson, 2002/.

The general conclusion drawn in the SR 97 post closure safety report for a KBS3 type repository /SKB, 1999/ is that neither the thermal pulse from the deposited waste nor the future ice loads would lead to canister damage, unless fractures extending over hundreds of meters intersect deposition holes. So, from a direct canister damage point of view, there does not seem to be any safety assessment requirements as regards the rock mechanics conditions. However, there may be a need to pay more attention to the possible effect of coupled mechanical processes on the retention properties of the near-field and far-field rock. Further, the importance of rock mechanics conditions could be considerable with regards to safety aspects during construction and to feasibility and design issues.

The *in situ* rock stresses represent one of the "suitability indicators" /SKB, 2000/ for the siting and site investigation of a potential repository. It is noted that "Extensive spalling or other extensive overbreak may not occur within a large portion of the deposition area."…"If the repository cannot be reasonably configured in such a way that extensive and general spalling problems can be avoided, the site is unsuitable and should be abandoned." It is therefore vital to determine the *in situ* stresses at a potential site as accurately as possible.

1.2 Objective

The overall objective of this project has been to develop, test and establish a method for creating a "Rock Mechanics Site Descriptive Model" for a site considered in the site investigation programme /Andersson et al., 2002/. The rock mechanics models are intended to be a basis and reference, i.e. provide input data, to the different types of rock

mechanics analyses, mentioned above, that will be conducted prior to the site selection and during design and construction.

The work in the project has been divided between groups such that a “property model”, using theoretical and empirical approaches, and a “stress model” has been developed. The approach to modelling the state of stress has been the objective of this part of the project, presented in this report. The work on approaches to modelling of the mechanical properties is reported in Staub et al. /2002/ and Röshoff et al. /2002/. The result of the project as a whole is summarized in Andersson et al. /2002/.

1.3 Scope

This project concerns the methodology to be applied prediction of the *in situ* stress field at a potential repository site. The work consists of the following parts:

– A literature review with the aim to describe the geological factors controlling *in situ* stress (Chapters 2, 3 and 4).

– A literature review with the specific aim to find examples of the use of numerical models for the subject of *in situ* stress (Chapter 5).

– Numerical modelling (using 3DEC) to investigate and illustrate the possible use of the modelling (Chapter 6).

– The Test Case exercise, where the methods for building a stress model were tested on data from the Äspö Hard Rock Laboratory (Chapter 8).

– Recommendations were developed, based on the experiences from the Test Case, on the methodology to be applied during the site investigation phase (Chapter 9).

2 Factors controlling the *in situ* stress

The aim of this chapter is to determine the factors controlling the state of stress in the Earth's crust and where possible to quantify this. The two most important are *gravity* and *tectonics.*

The former is the result of the overburden and generates both vertical and horizontal stresses in the rocks. These depend mainly on the thickness and density of the overlying rocks and the Poison's ratio of the rock under consideration.

The stresses generated in the crust as a result of tectonics are more varied and depend on the tectonic setting of the part of the crust under consideration. These stresses are most marked at plate margins but can extend many 100s of kilometres into the plate interior in its upper elastic portion. They range from pure extensional stresses, which characterize divergent plate margins such as the Mid-Atlantic ridge to purely compressional stresses at convergent plate margins such as the African/European collision zone represented by the Alpine belt of southern Europe.

The Scandinavian Shield is situated well away from present day plate margins. Never the less, as is discussed later in this chapter, it is likely to be affected by both the extensional regime of the Mid-Atlantic ridge and the compressional regime of the Alpine collision zone.

In addition to the overburden and tectonic stresses mentioned above, the Scandinavian shield has recently been subjected to Glacial loading and is at present responding by isostatic uplift to the subsequent glacial retreat and unloading. Any study of the current stress state in this region will therefore need to consider this relatively local process.

It should be noted that the regional stresses caused by the overburden, tectonic movements and isostatic uplift, can be, and frequently are modified by local heterogeneities within the crust. These heterogeneities may be the result of intrinsic properties of the crust such as vertical and/or horizontal lithological variations, or may be induced by the formation of tectonic structures, particularly fractures such as faults and joints. The dramatic effect of surfaces within the rock mass, which have low shear strength, in locally modifying the orientation and magnitude of the stress, is discussed in Section 3.1.

Finally, in regions of the crust where fluid pressures are high, the role of fluids in modifying the stress state and the related concept of effective stress, σ', defined by the total lithostatic stress, σ, minus the fluid pressure P (i.e. $\sigma' = \sigma - P$) must be taken into account.

2.1 Overburden Stress

In this section the state of stress at a particular depth in the crust resulting from the overburden is considered. The overburden load will generate both vertical and horizontal stresses and these will be determined by the thickness and density of the overburden, the lateral boundary conditions and the physical properties.

2.1.1. Vertical stress

The vertical stress (σ_v) generated by the overburden (Figure 2-1a) is given by:

$$\sigma_v = z \rho g \qquad (2\text{-}1)$$

where z is the depth, ρ is the mean density of the overburden and g the acceleration due to gravity. This vertical stress induces a horizontal stress in the rock and the magnitude of this is determined by the boundary conditions that are operating on the crust. The boundary conditions frequently assumed are those of no lateral strain. I.e. it is argued that the confining effects of the surrounding rock prevent any lateral expansion, which the overburden stress would induce if no lateral constraints were applied. The simple analysis that follows shows that the relationship between the vertical and horizontal stresses is given by:

$$\sigma_h = \sigma_v /(m - 1) \qquad (2\text{-}2)$$

where σ_h is the induced horizontal stress and m is Poisson's number, the reciprocal of Poisson's ratio. The concept of gravitational stresses is schematically illustrated in Figure 2-1.

2.1.2 Derivation of horizontal stress induced in the crust by the overburden

Equation (2-2) can be derived by applying the boundary conditions of no lateral strain to the three dimensional stress/strain relationships for linear elastic materials. The derivation of these relationships is fundamental in understanding the stress state in the crust and it is outlined below. It should be noted that in geological analyses it is usual to label the vertical axis as the z-axis and the two horizontal axes x and y.

By definition the relationship between stress and strain for linear elastic materials (Figure 2-1b) is given by Hook's law:

$$\sigma = E \varepsilon \qquad (2\text{-}3)$$

where E is Young's modulus and e is the strain induced by the stress σ.

In an unconfined specimen a compressional stress in the z direction will induce a contractional strain, ε_z, in the z direction and extensional strains, ε_x and ε_y, in the x and y directions respectively. The ratio $\varepsilon_x/\varepsilon_z$ is termed Poisson's ratio (ν) and is a characteristic property of a material.

$$\varepsilon_x/\varepsilon_z = \varepsilon_y/\varepsilon_z = \nu. \qquad (2\text{-}4)$$

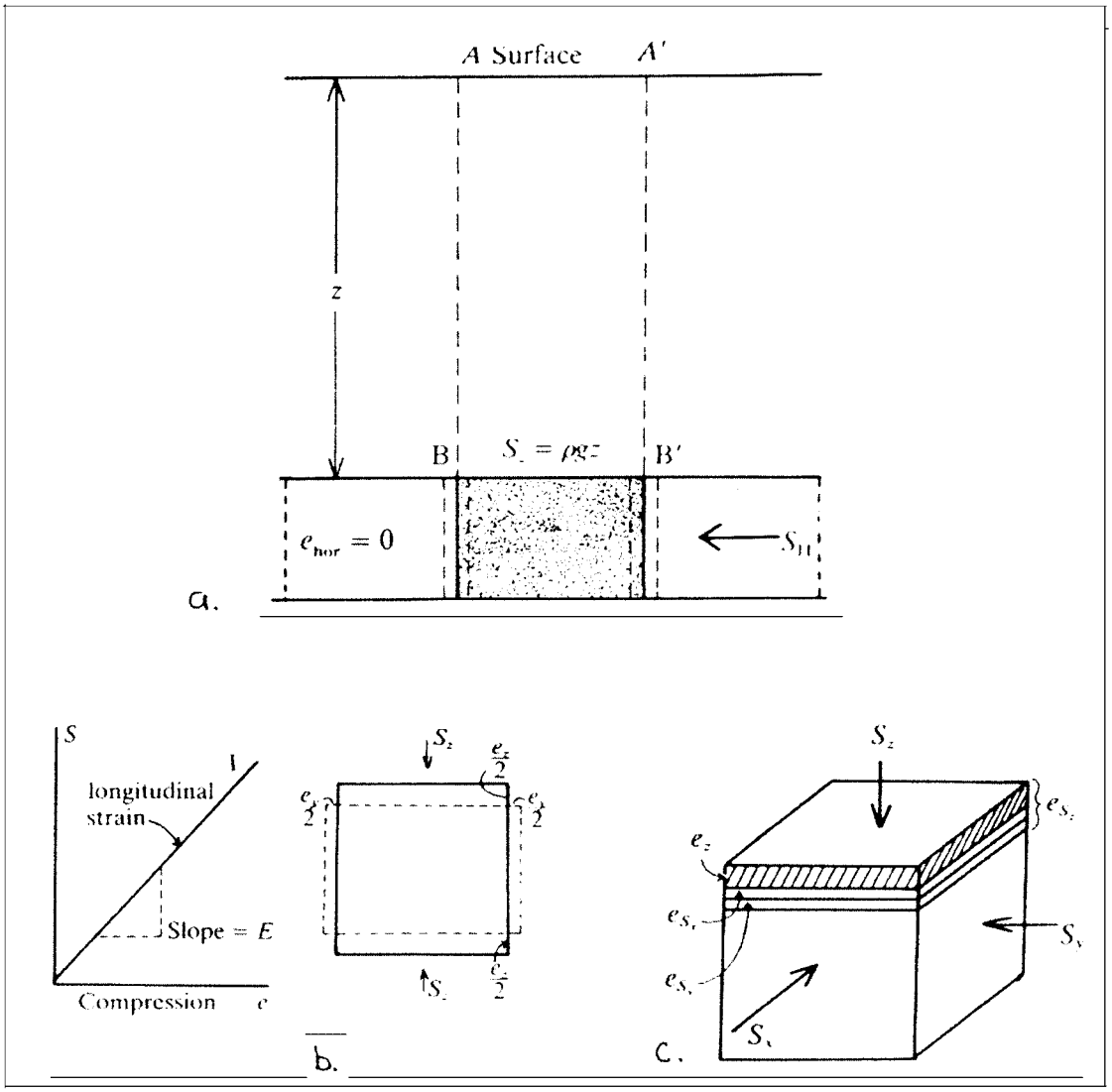

Figure 2-1. *a) A diagrammatic representation of an overburden stress acting on a layer at a depth z. The boundary conditions are such that no lateral extension can occur in response to the overburden. This results in the generation of a horizontal stress. The dashed lines outside the cube show its position if it were not confined by the surrounding rock b) Linear relationship between stress and strain that characterizes a Hookean material and diagram showing the lateral strain induced by a vertical stress when the body is unconstrained. c) Strain components in the z direction induced by the three principal stresses. The vertical stress induces a contraction and the two horizontal stresses extension. /From Price and Cosgrove, 1990./*

The value of Poisson's ratio ranges between 0.5 for an incompressible material, such as a fluid, and 0.0 for an extremely compressible material. Such a material might be approximated by a sponge, or, in a geological context, a highly porous rock. The reciprocal of Poisson's ratio is referred to as Poisson's number and is given the symbol *m*. It ranges in value between 2 for an incompressible material and infinity for an extremely compressible one, ($2 < m < \infty$).

$$\varepsilon_z/\varepsilon_x = 1/\nu = m \qquad (2\text{-}5)$$

By considering the general three-dimensional case of a triaxial stress field with one vertical stress σ_z and two horizontal stresses σ_x and σ_y it is possible to show how the stresses and corresponding elastic strains in three dimensions are related.

It follows from Equations (2-3) to (2-5) that:

$$\varepsilon_x = \varepsilon_y = \varepsilon_z/m = \sigma_z/(m\mathrm{E}) \quad (2\text{-}6)$$

where ε_x and ε_y are the strains induced by the vertical stress, σ_z, in the x and y directions respectively. Consider now the strains in the z direction that will result from the three principal stresses σ_x, σ_y and σ_z represented in Figure 2-1c. Each of the three stresses will contribute to the strain in the vertical (z) direction. Thus the stress in the z direction will give rise to a component of strain ε_z', where:

$$\varepsilon_z' = \sigma_z/\mathrm{E} \quad (2\text{-}7)$$

There will also be a tendency towards an extensile strain in the vertical direction caused by the horizontal principal stresses σ_x and σ_y, which will give rise to two components of strain in the z direction, Figure 2-1c. These may be designated ε_z'' and ε_z''', respectively, where:

$$\varepsilon_z'' = \sigma_x/(m\mathrm{E}) \quad (2\text{-}8)$$

$$\varepsilon_z''' = \sigma_y/(m\mathrm{E}) \quad (2\text{-}9)$$

The dilatational components of strain, ε_z'' and ε_z''', will have the opposite sign to that of ε_z'. The convention in the geological literature is to denote compressive stress and contractional strains as positive and tensile stress and extensional strains as negative. Thus the total strain in the z direction is:

$$\varepsilon_z = \varepsilon_x' - \varepsilon_x'' - \varepsilon_x''' \quad (2\text{-}10)$$

By substituting Equations (2-7), (2-8) and (2-9) into Equation (2-10) the following relationship is obtained:

$$\varepsilon_z = (\sigma_x/\mathrm{E}) - (\sigma_x/m\mathrm{E}) - (\sigma_y/m\mathrm{E}) \quad (2\text{-}11)$$

which can be rearranged to give

$$\varepsilon_z = (1/\mathrm{E})[\sigma_z - (1/\mathrm{m})(\sigma_x + \sigma_y)] \quad (2\text{-}12)$$

By a similar argument it follows that the three stress-strain equations in the x, y and z directions are:

$$\varepsilon_x = (1/\mathrm{E})[\sigma_x - (1/\mathrm{m})(\sigma_z + \sigma_y)] \quad (2\text{-}12a)$$

$$\varepsilon_y = (1/\mathrm{E})[\sigma_y - (1/\mathrm{m})(\sigma_z + \sigma_x)] \quad (2\text{-}12b)$$

$$\varepsilon_z = (1/\mathrm{E})[\sigma_z - (1/\mathrm{m})(\sigma_x + \sigma_y)] \quad (2\text{-}12c)$$

Having derived these general equations for linear elastic materials one can now determine the horizontal stresses generated in a rock by the overburden. If the boundary conditions of no lateral strains are assumed then it can be argued that because the lateral strains are inhibited, it follows that there exists a lateral stress ($\sigma_h = \sigma_x = \sigma_y$), which has a magnitude sufficient to counterbalance the tendency of the vertical gravitational load to induce lateral strain.

The relationship between the vertical and horizontal stresses may be established using Equation (2-12a) or (2-12b). Because e_x and e_y are equal to zero and because 1/E is *not* equal to zero (i.e. E is not equal to infinity), it follows that the expressions in the square brackets in Equations (2-12a) and (2-12b) *are* equal to zero, i.e.

$$[\sigma_x - (1/m)(\sigma_z + \sigma_y)] = 0 \qquad (2\text{-}13)$$

but $\sigma_x = \sigma_y = \sigma_h$ (the horizontal stress) and $\sigma_z = \sigma_v$ (the vertical stress) so the above equation may be written:

$$[\sigma_h - (1/m)(\sigma_v + \sigma_h)] = 0 \qquad (2\text{-}14)$$

which can be rewritten:

$\sigma_h = \sigma_v /(m - 1)$, which is Equation (2-2).

Thus the vertical and horizontal stresses predicted for a crust affected only by an overburden load are given by Equations (2-1) and (2-2). Assuming that the values of density and Poisson's number remain unchanged with depth then these two stress values increase linearly with depths as illustrated in Figure 2-2. It can be seen that the differential stress, $(\sigma_v - \sigma_h)$, increases with depth and it follows from the theory of brittle failure that if failure of the crust is to be induced by this stress field, then the upper portion will be characterized by extensional failure (joints – which form under conditions of low differential stress) and the lower portion of the crust by shear failure (faults – which form under conditions of high differential stress).

The Scandinavian shield has been subjected to several major glacial advances and retreats over the last 100,000 years. The effect has been to modify the vertical load and this can easily be incorporated into the above analysis by either increasing or decreasing the vertical load resulting from the rock overburden. However, the addition or removal of a glacial load is achieved by the advancing or retreating of a glacier and this tends to load the crust asymmetrically resulting in non-parallel uplift or depression of the crust. These asymmetric load boundary conditions may cause a flexing of the crust, which modifies the stress field and may result in the formation of fractures /Price, 1974; Price and Cosgrove, 1990/.

It should be noted therefore that glacial loading and unloading and the associated isostatic motion might generate a stress field more complex than that linked to the simple addition or removal of a vertical load.

In general overburden stresses are not sufficient to cause failure in basement rocks unless abnormally high fluid pressures are present and they need to be modified by tectonic stress regimes before large-scale brittle failure is initiated.

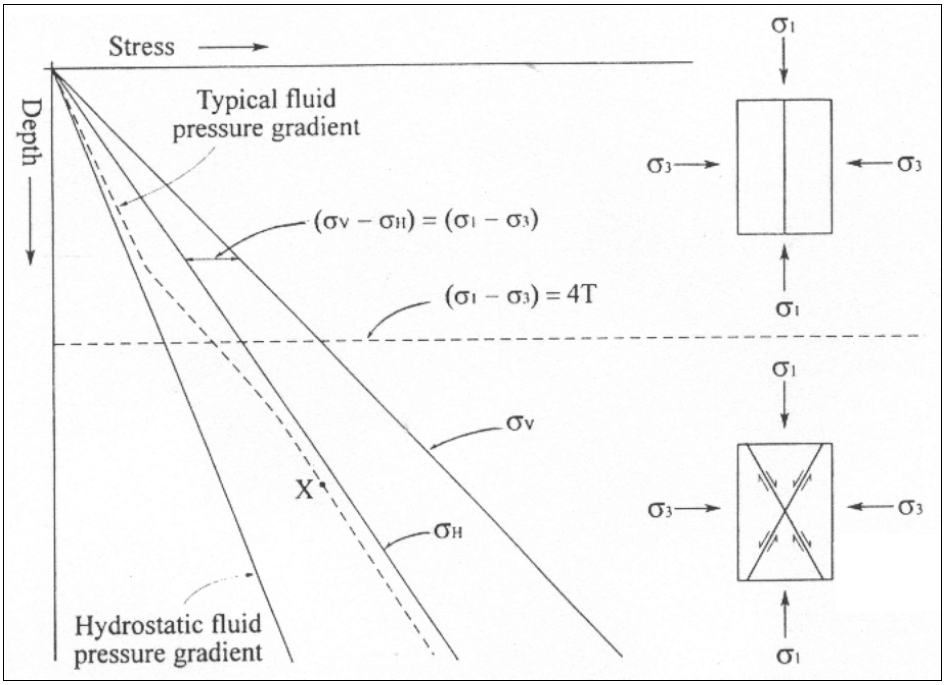

Figure 2-2. *Graphical expression of Equations (2-1) and (2-2), showing the linear increase in both vertical and horizontal stress with depth. The fluid pressure profile is shown as a solid line assuming that the pores (and therefore the pore fluids) remain interconnected. When this does not occur e.g. when compaction isolated the pores, the fluid pressure rises more rapidly as indicated by the dashed line. /From Cosgrove, 1997./*

2.2 Tectonically induced stresses

Large-scale stresses at and near plate margins are generally associated with important deformation processes such as those that characterize the upper crustal fracturing along Mid-Oceanic rifts situated along extensional plate margins and the fold and thrust belt that characterizes collisional belts. Although the plate margin stress regimes die out as one move away from the margins into the plate interiors, they are known to extend for many hundreds and sometimes thousands of kilometres away from the plate edges.

This can be clearly seen in Figure 2-3, which shows a uniform joint pattern generated in the North American plate as a result of the plate collision associated with the Appalachian orogeny. This pattern of deformation also shows that stresses linked to plate tectonics can often be remarkably uniform over many thousands of square kilometres.

Thus if the observable deformation (i.e. the fractures) caused by plate margin tectonics can extend deep into the plate interiors, there can be no doubt that the associated stresses extend even further. Any analysis of stress within the crust, which ignores the possibility of tectonic stresses, is therefore incomplete. As will be illustrated in Section 4.1, the stress state in the Scandinavian Shield, which is at present remote from major plate margins, is never the less significantly effected by tectonics at the plate margins, particularly the Alpine collision to the south.

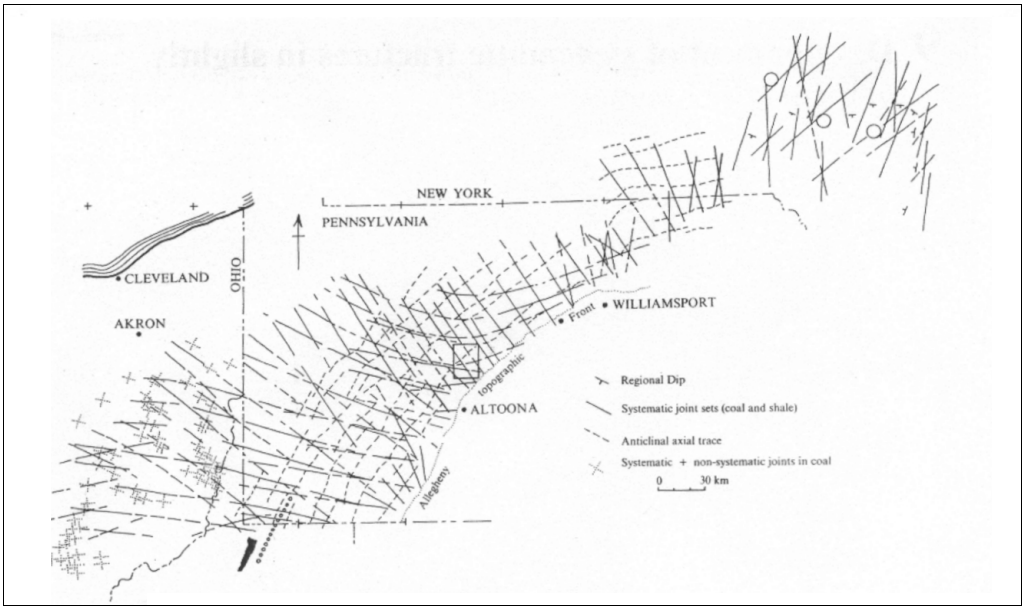

Figure 2-3. *Map of the Appalachian plateau showing the general orientation of the fracture patterns generated by the plate stresses linked to the Appalachian orogeny. /From Engelder and Geiser, 1980./*

3 Factors that might influence regional stresses

This chapter focuses on the way in which different structures such as folds, faults and joints might locally modify the far field stress resulting from the regional tectonics and the overburden.

3.1 The influence of brittle structures on local stress distribution

There is considerable evidence that fractures perturb the far-field stress field in which they are situated. For example Figure 3-1 shows the modification of the principal stress trajectories around a shear fracture. The far-field principal stresses are oriented at 45° to the fracture but inspection of the figure indicates that the stress trajectories rotate into a position either normal to or parallel to the fracture as they approach it. This is because the fracture has no strength across it and as a result the fracture sides are free surfaces i.e. are unable to sustain a shear stress.

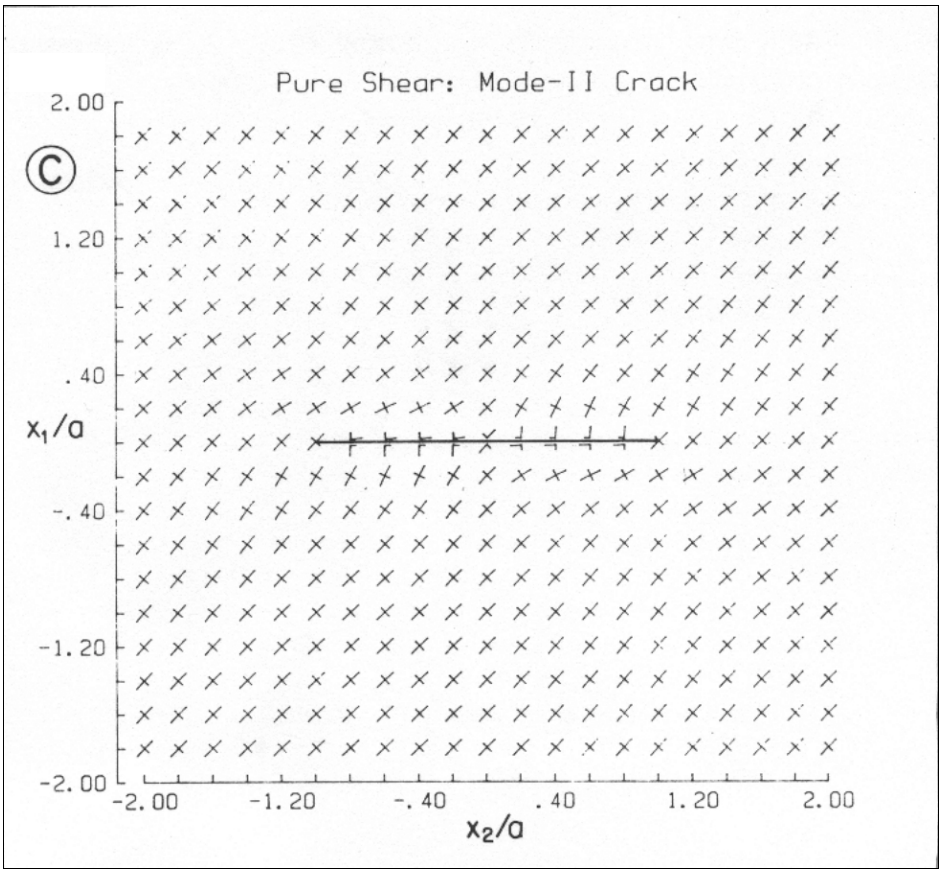

Figure 3-1. *The modification of the principal stress trajectories around a shear fracture. Note that the principal stresses rotate either parallel to or normal to the fracture as they approach it. /From Pollard and Segal, 1987/.*

Figure 3-2. *Two examples of fracture networks from the Liasic carbonates of the North Somerset coast of the Bristol Channel of England. The upper photograph shows the gradual degradation of the younger sets of fractures as they form in response to regional stress fields that have been progressively more degraded by the developing fracture network. The lower photograph shows the effect of early fractures on the later fractures. Later fractures often curve towards and/or abut (terminate) against older fractures.*

If new fractures were to form in response to the far field stress their orientation would reflect that of the trajectories. Extensional fractures form parallel to the maximum principal compression (the long dashes on Figure 3-1). They travel from top right to bottom left of the diagram and when they reach the fracture they rotate. A similar rotation is apparent in the fractures shown in the lower photograph of Figure 3-2. The shorter fractures change their orientation as they approach the longer, earlier fractures so that they intersect at 90°.

This extreme rotation of the stress trajectories reflects the fact that the fracture has no strength across it. If a shear strength exists then the fracture will be able to sustain a shear stress and the rotation of the trajectories will not be as marked. The rotation effect will decrease progressively until the shear strength of the fracture equals that of the country rock. When this occurs no rotation of the trajectories will take place and later fractures will be able to cross the fracture unimpeded and with no change in orientation.

It can be seen from Figure 3-2 that in addition to causing the stress field to rotate, early, low strength fractures also act as barriers to fracture propagation. Evidence of early fractures blocking the advance of later fractures can be found in the numerous abutting relationships shown in Figure 3-2.

3.2 The influence of ductile structures on local stress distribution

Structural geologists have been preoccupied with the relationship between folds (ductile structures) and fractures for some time primarily because fold related fractures often host mineral deposits or hydrocarbons. This study has shown how the folded strata affect the causative and subsequent stress fields. For example Figure 3-3 shows the ‘ideal’ relationship between a fold and the extensional and shear fractures that the causative stress would be expected to generate. The least principal stress is assumed to be parallel to the fold axis and the intermediate principal stress vertical. The stereographic projection (Figure 3-3b) shows the relative orientations of the fold axis, b, the shear fractures R’ and R’’ and the extensional fracture ac. This relationship is termed ‘ideal’ because this is the orientation that would be predicted from the theory of brittle failure assuming that the principal stresses that formed the fold continue to act horizontally and vertically.

In fact the fractures typically ‘observed’ around folds are shown in Figure 3-3c. Although the predicted shear and extensional fractures are formed they do not have the ‘ideal’ orientation but form normal to the layering (bedding) rather than to the Earth’s surface. This is because the bedding planes are planes of low strength. Because they cannot sustain a large shear stress the principal stresses are deflected along them. Thus the principal stresses remain normal or parallel to the bedding. The resulting fractures reflect this and form normal to the bedding. Their orientations are shown in the stereographic projections of Figure 3-3d and e.

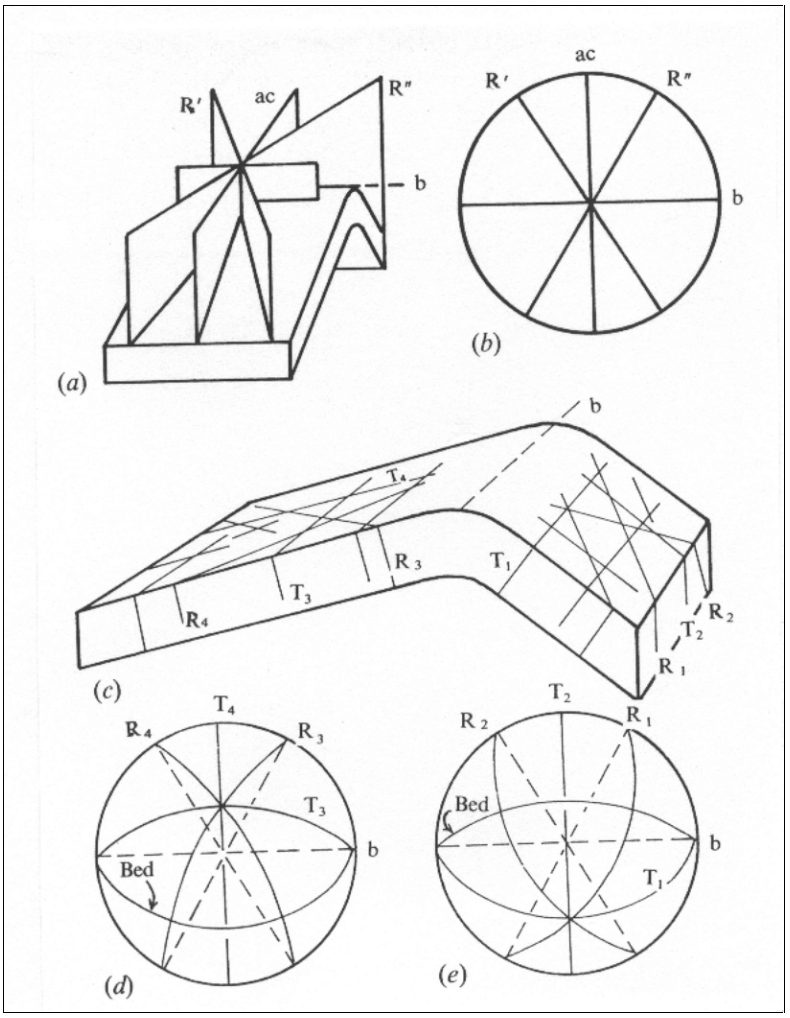

Figure 3-3. *a) Ideal relationship of master joints to a small fold. b) Stereographic plot of fractures shown in a). c) Trends of minor fractures in a folded competent unit. d) and e) Stereographic plots of fractures in the two limbs. R and T are shear and extensional fractures respectively. /From Price, 1966./*

This channelling of the stress by planes of low strength can occur on all scales. In this way the stress field within a fractured basement may bear very little relationship to the far-field plate stresses.

There are other factors in addition to the structures discussed above that might modify regional overburden and tectonic stresses, for example, variations in the mechanical properties of different rocks. These properties may be the intrinsic properties of the rocks or may reflect the fact that the rock has been deformed and the development of fractures has changed the bulk properties of the rock.

3.3 Variations in lithology and its possible effect on the stress field

One of the interesting stress anomalies recorded is the occurrence of a stress "jump" at a certain depth. At this depth there is a sudden increase in the magnitude of the horizontal stress and the discussion in the following section presents some possible explanations for this phenomenon.

As has already been discussed in Section 2.1, if the only stress affecting a rock system is the overburden stress (Equation (2-1)) then the horizontal stress in a layer within the crust at some depth z is a function of Poisson's ratio (Equation (2-2)) and the density of the overlying rocks. If the density of the overburden is constant then the horizontal stress will increase linearly with depth (Figure 2-2), and the slope of the line will be determined by the density. In a layered succession of rocks in which each layer has its own density, Young's modulus and Poisson's ratio, the magnitude of the horizontal stress will be different for each layer and stress jumps will occur at the layer boundaries. The magnitude of these jumps will be determined by the differences in the value of Poisson's ration between the adjacent layers. Thus a model of the crust in which an upper layer of low Poisson's ratio (i.e. a layer which is relatively compressible) is situated above a layer with a high Poisson's ratio, will experience a stress increase in the horizontal stress at the boundary between the two simply as a consequence of the effect of the overburden stress.

The generation of a stress change at a particular depth in the crust outlined above requires only an overburden stress. If it is argued that a tectonic stress (i.e. a horizontal stress linked to plate motion) is also acting (which is the case for Sweden, see Section 4.1.4) then an alternative mechanism for generating a stress jump can be proposed. The way in which the magnitude of the horizontal stress can vary from layer to layer in a multilayer compressed parallel to the layering is illustrated in Figure 3-4. Figure 3-4a shows a multilayer made up of two different types of layer, one relatively weak (b) and the other strong (a). These layers alternate and the bilaminate is shortened (strained) by an amount *e*. The materials are assumed to be linear elastic and their stress-strain curves are shown in Figure 3-4b. It can be seen that if the multilayer is shortened by a constant amount *e*, then the stress in the two types of layer must be different. The magnitude of this difference is determined by the difference in the Young's moduli of the layers.

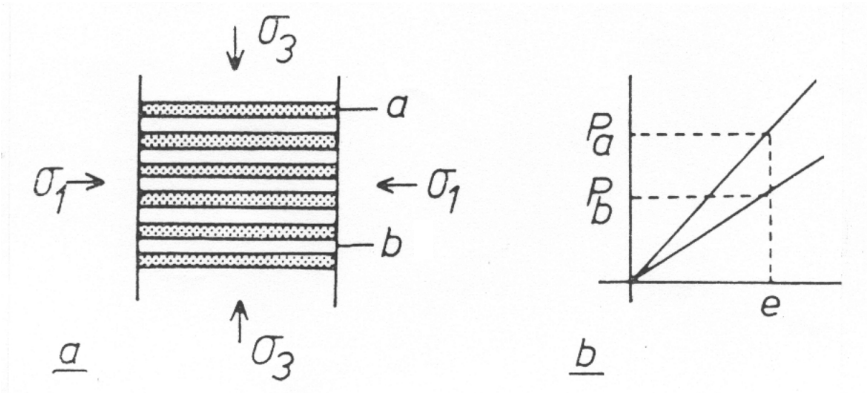

Figure 3-4. *An elastic bilaminate made up of alternating relatively strong and weak layers. The application of a uniform shortening (strain e) parallel to the layering induces different stresses into the two layers (P_a and P_b). The greater the difference in Young's modulus between the two layers, the greater the difference in their layer-parallel compressive stress. /From Cosgrove, 1976./*

A model of the Swedish basement in which an upper relatively weak layer rested on a relatively strong layer could therefore generate a stress increase at the layer boundary. However, it is clear that no such lithological layering occurs. However, it can be argued that the weakness may be the result of a relatively high density of fractures in the upper part of the crust. The properties of the 'fractured rock mass' will be different from the underlying more intact rock. The upper part of the crust is characterised by an abundance of fractures, generated in part by the release of residual stresses which occurs as the rocks become exhumed and is released from its overburden stress and lateral constraints. Thus the weakened layer may be the result of either

1. An intrinsic difference between the two layers e.g. a thick shale on a granite basement or

2. Having the same rock type but where fracturing associated with uplift and the release of residual stresses weakens the upper parts.

In both examples one can treat the idealized model as being made up of two linear elastic materials where the lower, stronger, unit has a greater Young's modulus than the upper. In ii) the fractures affect the bulk properties of the rock (the rock mass properties including the fractures and the crushed zones etc). For example the effective Young's modulus of the fractured rock mass will be less than that for the intact rock and it will behave therefore as a weaker material.

3.4 Listric faults

A third mechanism by which a "jump" in horizontal stress can occur at a particular depth is by the existence of a sub-horizontal fault. Faults tend to fall into one of three categories i.e. normal, wrench and thrust depending upon whether σ_1, σ_2, or σ_3 acts vertically. However, the dip of these faults is 60º, 90º and 30º, i.e. none of them is horizontal.

The Navier-Coulomb theory of shear failure predicts that the fractures will form at approximately 30º each side of the maximum principal compressive stress. In regions of isotropic rocks subjected to a uniform tectonic stress, the faults will be planar features. Many rocks have an intrinsic sub-horizontal planar anisotropy as a result of bedding and the effect of these planes of weakness can be to produce curved faults.

The most important of these are listric (i.e. spoon-shaped) faults and at the surface these faults are often associated with landslides, the slipped mass being bounded by a fault, which is concave towards the mass in both plan, and profile sections. These faults, which are normal faults related to extension, are not restricted to the relatively small-scale surface examples linked to landslides. They occur on all scales and at all depths. As discussed below, listric faults can form in both extensional and compressional tectonic settings. They can form on all scales and in all rock types. The most important feature that seems necessary for their formation is the occurrence in the rock system of a sub-horizontal plane of weakness. One of the most common situations where large-scale listric faults form is that of regional extension such as the present-day North Sea. Here the regional extension associated with the opening of the Atlantic has caused the post-Carboniferous sediments to form large, approximately north-south trending listric normal faults that in their upper portions are steeply dipping. With increasing depth

their dips decrease and the fault eventually becomes parallel to bedding. The faults typically link to a low strength bedding horizon such as a shale or evaporite horizon. On a larger scale, extension and compression of the crust as a result of relative plate motion has resulted in large listric normal and thrust faults which use the brittle/ductile boundary within the crust as the horizon in which they 'bottom out' i.e. become horizontal. Depending on the strain-rate this horizon may either fall within or may coincides with the base of the crust.

3.4.1 Listric faults formed as a result of extension

Many of the large-scale normal faults imaged seismically in the North Sea can be traced from an upper zone where their dip is around 60º to depths where the dip decreases and the fault curves into parallelism with the bedding. These **spoon-shaped** or **listric** fault profiles are extremely common particularly where relatively weak sub-horizontal fractures (such as bedding) or fracture zones occur. These horizons may be clearly defined for example i) a bedding plane, ii) a bedding plane thrust, iii) a thrust plane ramping up the stratigraphy, or may be more diffuse such as i) a mylonite zone, ii) the boundary between the upper, highly fractured part of the crust and the lower less fractured part (discussed in Section 3.3), and iii) the boundary between two meta-morphic zones characterised by mineral phase changes and the associated rheological changes. The formation of crustal-scale listric faults (e.g. Figure 3-5) may be linked to such rheological changes.

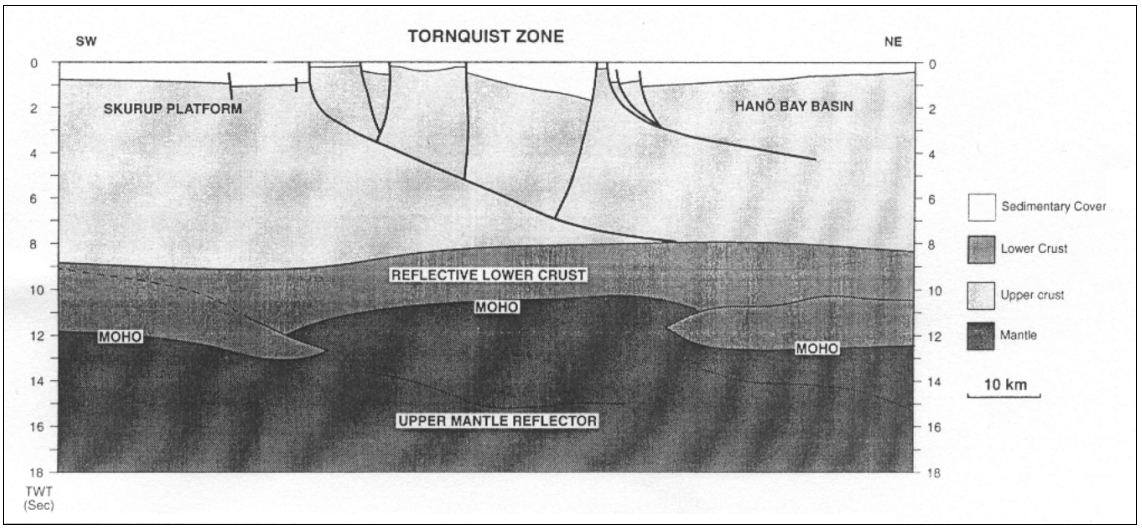

Figure 3-5. *Interpretation of the BABEL seismic section (a detail of which will be shown in Figure 4-7). The steeply dipping, near-surface faults link at depths to a more gently dipping fracture zone, possibly a major thrust. /From Erlstrom et al., 1997./*

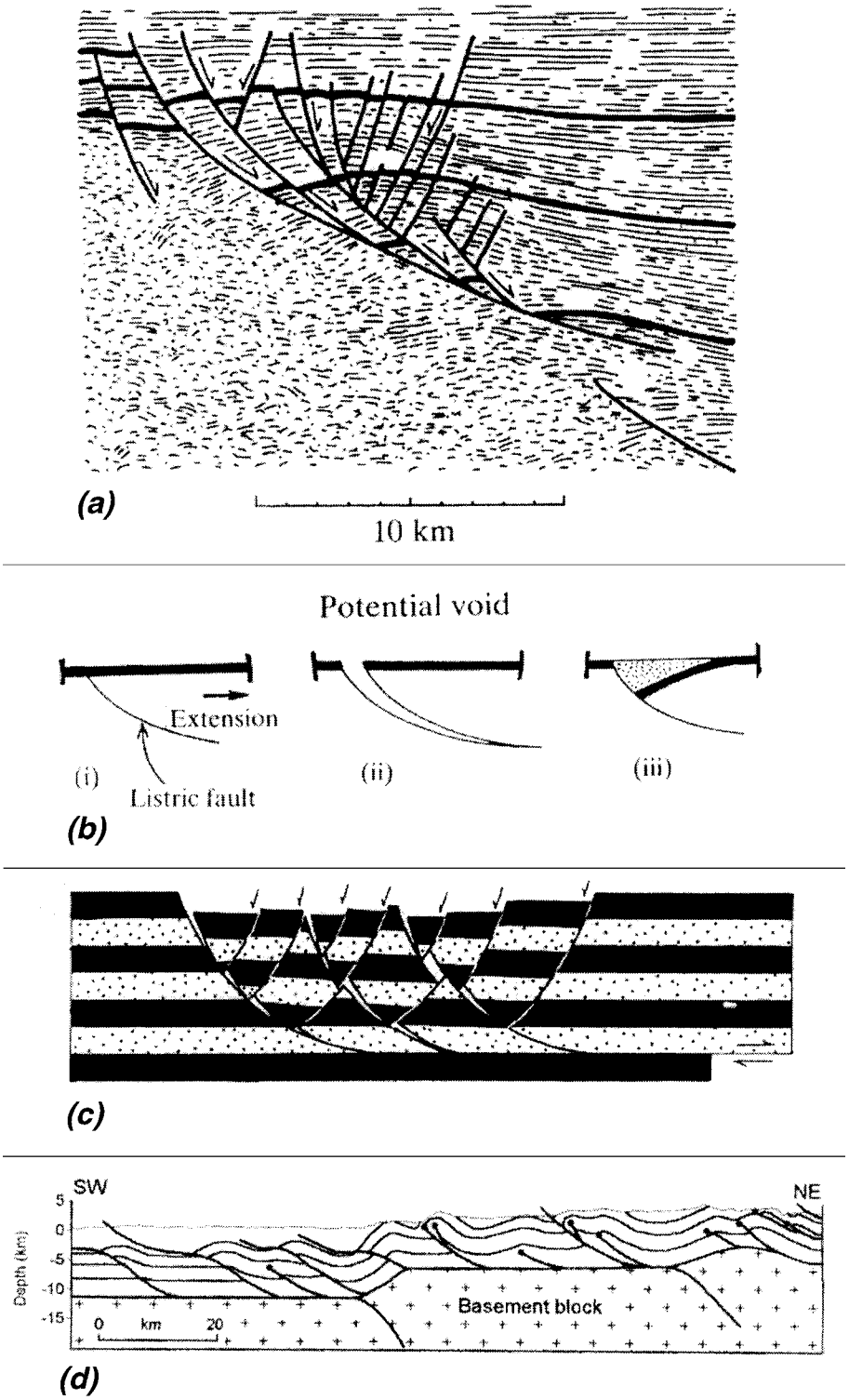

Figure 3-6. *a) Seismic section of a growth fault in the Tertiary sediments of S. Texas part of the Gulf Coast Basin. (b) Dilation associated with movement on a listric fault. The potential gap can be closed in a ductile manner by the formation of a roll-over fold (iii), by brittle failure and the formation of normal faults (c) or by a combination of the two (a). (d) Listric thrusts rising from the basal salt horizon into the cover rocks of the Zagros Mountains.*

3.4.2 Listric faults associated with compressional tectonics

In a region of compressional tectonics the type of fault that forms may be either wrench or thrust depending upon whether σ_2 or σ_3 is vertical. Under boundary conditions appropriate for the formation of thrusts the theoretical orientation of the thrust plane will be one dipping at around 30°. However, when other low-dipping planes of weakness are present the thrust may exploit these in preference to forming a new fracture in the ideal orientation. Thus major thrusts often follow sub-horizontal bedding planes or horizons of weak lithologies. Eventually however, either as a result of the weak horizon dying out or the boundary conditions of the system requiring that the thrust propagate up the stratigraphic succession, the thrust changes its dip and *ramps up* through the overlying rocks (often initially at an angle of 30°) producing a listric thrust. Large-scale examples of this can be seen in Figure 3-6d, which shows thrusting in the 10 km thick cover rocks of the Zagros mountain belt. Here horizontal thrusts initiate in the thick, low strength Hormuz salt at the base of the succession and propagate *upwards* increasing in dip as they do so. This contrasts with listric normal faults which, as noted above, appear to form above the sub-horizontal fracture and curve into parallelism to it as they propagate *downwards***.**

As can be seen from the illustrations in Figure 3-6b (i) and (ii), movement along a listric fault may result in the formation of a gap between the footwall and hanging wall when the fault is reactivated in extension (referred to as a dilatational jog) or to the buttressing of the footwall against the hanging wall when reactivated in compression (referred to as a compressional jog). The generation of these two local zones of high extensional stress and high compressional stress often leads to the local formation of new fractures (Figure 3-6a and c).

Because of the role that listric faults can play in the localization of fractures and the generation of sub-horizontal and low angle faults and because of the effect that such low angle faults might have in controlling the stress distribution in the crust, it is important when making any site investigation, to determine if any steeply dipping faults at the surface continue to be steeply dipping at depth or whether they are likely to curve into any sub-horizontal planes of weakness such as a shale horizon or fracture zone. The particular structural geological conditions in Sweden are discussed in Chapter 4.

3.5 Discussion of the value of the angle of friction ϕ

The angle of friction for a rock can be determined experimentally by plotting the principal stress state at failure for a range of confining stresses. The slope of the resulting failure envelope is the angle of friction (ϕ) and for many rocks this angle is around 30º.

When the rock fails and a shear fracture is formed the shear strength (the shear stress necessary to cause shear failure) drops, i.e. the failure criteria for re-shear on the fracture intersects the shear stress axis below the criteria for the formation of new shears. The two criteria are shown in Figure 3-7a. It can be seen that the failure envelope for re-shear has been drawn with the same slope as the envelope for the formation of new shears implying that the angle of sliding friction is the same for both.

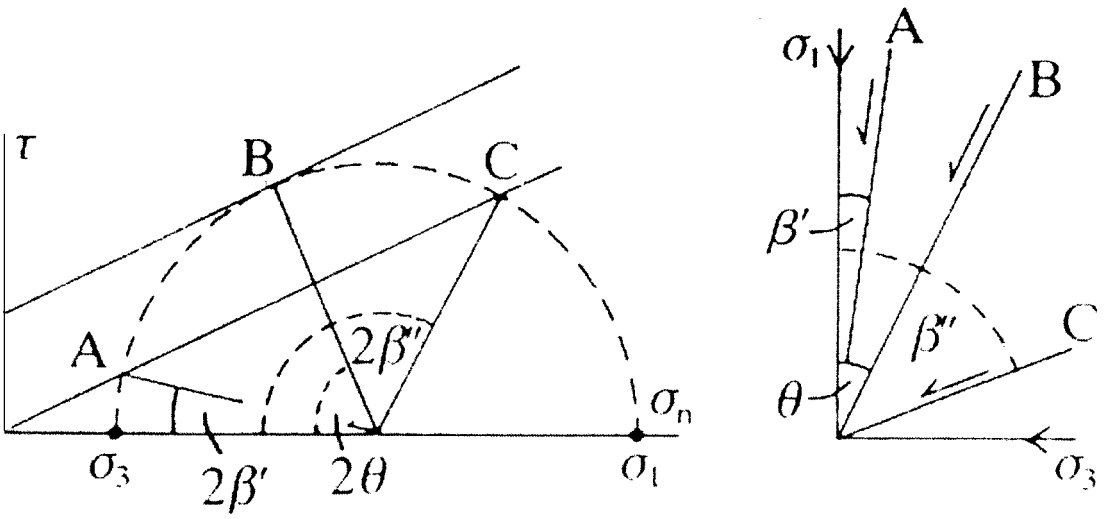

Figure 3-7. *a) Two failure envelopes. The upper slope (containing point B) represents the shear failure criteria for intact rock and the lower envelop (containing points A and C) represents the failure condition for re-shear on a pre-existing fracture. The acting stress is represented by a Mohr circle on the point of coming into contact with the upper failure envelope. b) B is the orientation that a new shear fracture would have with respect to the maximum principal compression* σ_1 *and A and C represent the range of angles in which pre-existing fractures must fall if they are to be re-activated in shear.*

Numerical modelling of possible slip on existing fractures requires that a value of ϕ be selected. It is therefore necessary to consider whether or not the assumption that the value is the same for new shear and re-shear, is valid. The following brief discussion indicates that it is not.

When a shear fracture forms in a rock movement along it generally generates a 'fault product'. This can range from a fault breccia, through a fault gouge, a mylonite and ultimately a pseudotachylite. The properties of these products are very often different from those of the intact rock. Some, such as the breccia and gouge, are generally weaker and others such as the mylonite and pseudotachylite are often stronger. The migration of fluids along faults lined with breccias and gouge can cause alteration and weathering which can further reduce the angle of friction. In addition the presence of water along the plane will also tend to reduce ϕ. Thus the assumption that the angle of friction is the same for intact and fractured rock seems unrealistic and it seems likely that in the upper levels of the crust where faults are characterized by breccias and gouges, the value of ϕ for a fractured rock mass will be considerably lower than for the intact rock.

4 Stress state in Sweden

In this section an outline of the geological history of the Scandinavian plate is given and its implications regarding the present stress state in the crust considered.

4.1 Stress history leading to the current stress regime

An understanding of the geological history of the study area is useful as it can be used to determine the evolution of the stress regime in which the site is situated. This enables the likely pattern of fractures to be determined (a factor that may dramatically affect the local effect of current regional stresses, see Section 3) and may also enable the likely orientation of residual stresses locked in the rock to be established.

The study area for the Test Case (see Chapter 8) in this project is situated on the west coast of the Baltic Sea at Äspö Hard Rock Laboratory in southern Sweden. The site is on the western margin of the Baltic Sea Basin, an inter-cratonic basin sitting on Early Proterozoic crust of the East European Craton. The following discussion is divided into three sections. The first briefly discusses the evolution of the Precambrian shield, the second the evolution of the Baltic Sea Basin and the third the break-up of the shield from the Cambrian to the present day.

4.1.1 Precambrian history of the East European Craton

The relationship of the East European Craton to the rest of the North Atlantic Precambrian shield is shown in Figure 4-1a. The Äspö area lies on Early Proterozoic crust, which experienced its last important deformation around 1.8 Ga ago as a result of the Svecofennian orogeny. The subdivision of the East European Craton is shown in Figure 4-1b, where the region of Svecofennian deformation is termed Fennoscandia, and the main provinces and structures of the Fennoscandian segment are shown in Figure 4-1c.

Inspection of Figure 4-1c and Figure 4-2 shows that the East European Craton is bounded to the northwest and southwest by two important structures namely the late Precambrian Caledonian collision belt characterised by the Iapetus Suture and the Tornquist Line respectively. The age of the Tornquist Line is uncertain. However, it is cut by the Caledonian belt of the Iapetus Suture which it clearly post-dates (Figure 4-2), it is also thought to be of approximately Caledonian age.

As shown in Figure 4-2, three intra-cratonic sedimentary basins occur on the Fennoscandian segment of the East European Craton (Figure 4-1b). These are the Bothnian Bay Basin, the Bothnian Sea Basin and the Baltic Basin. They developed in response to Middle Proterozoic and Late Proterozoic tectonic events, separated in time by about 800 my, /van Balen and Heereman 1998/. Only the Baltic Basin (i.e. the basin adjacent to the Äspö area) was subsequently affected by the Caledonian orogeny and Mesozoic rifting. Crustal extension was minor or did not take place during the Proterozoic evolution phases of this basin.

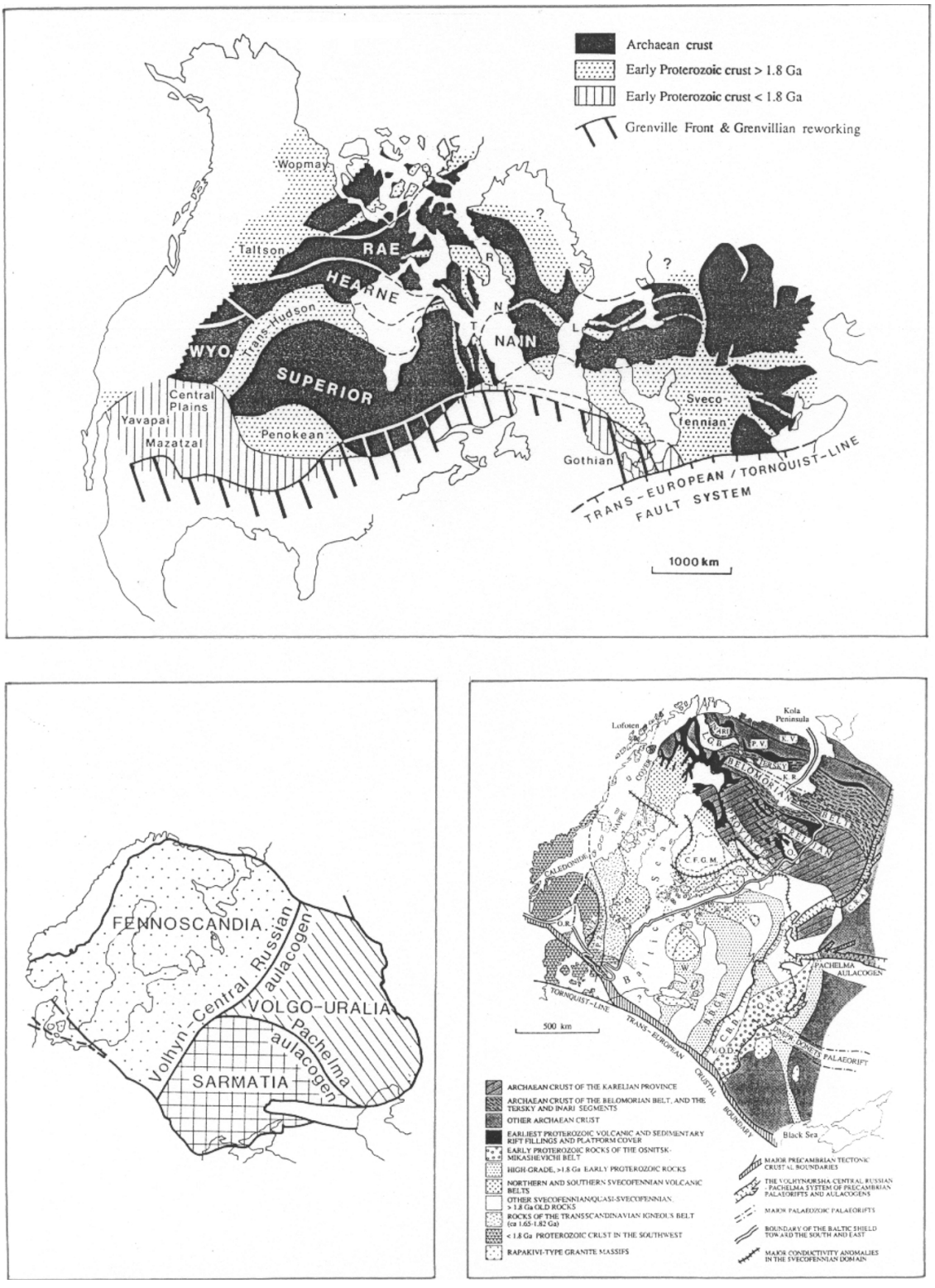

Figure 4-1. *a) The relationship of the East European Craton to the rest of the North Atlantic Precambrian shield. b) Crustal segments of the East European Craton. c) Main provinces and structures of the Fennoscandian crustal segment. /From Gorbatschev and Bogdanova, 1993./*

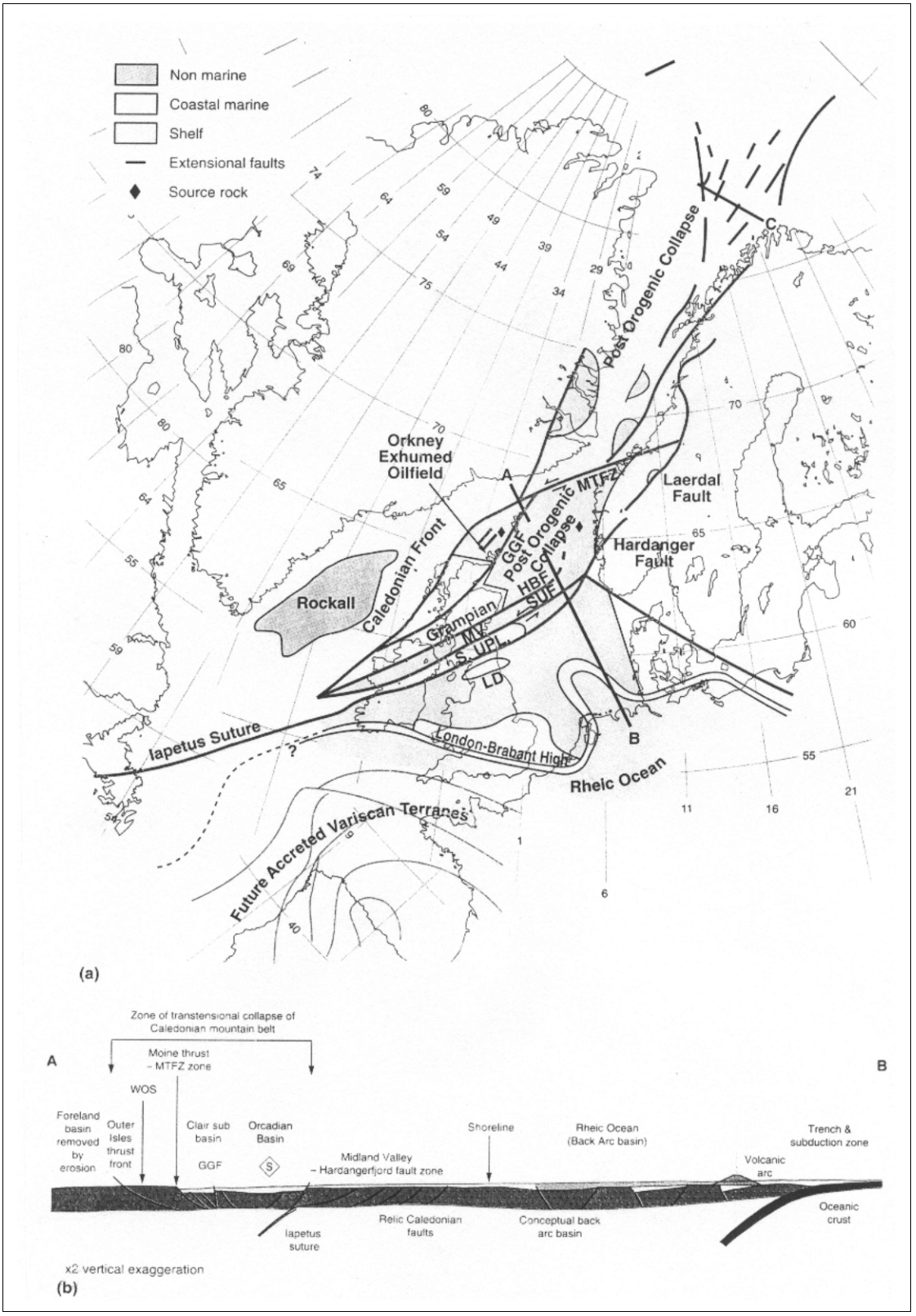

Figure 4-2. *The Scandinavian Peninsula bounded by the northeast-southwest trending Caledonian Suture and the northwest-southeast trending Tornquist Line, see also Figure 3-6c. /From Roberts et al., 1999./*

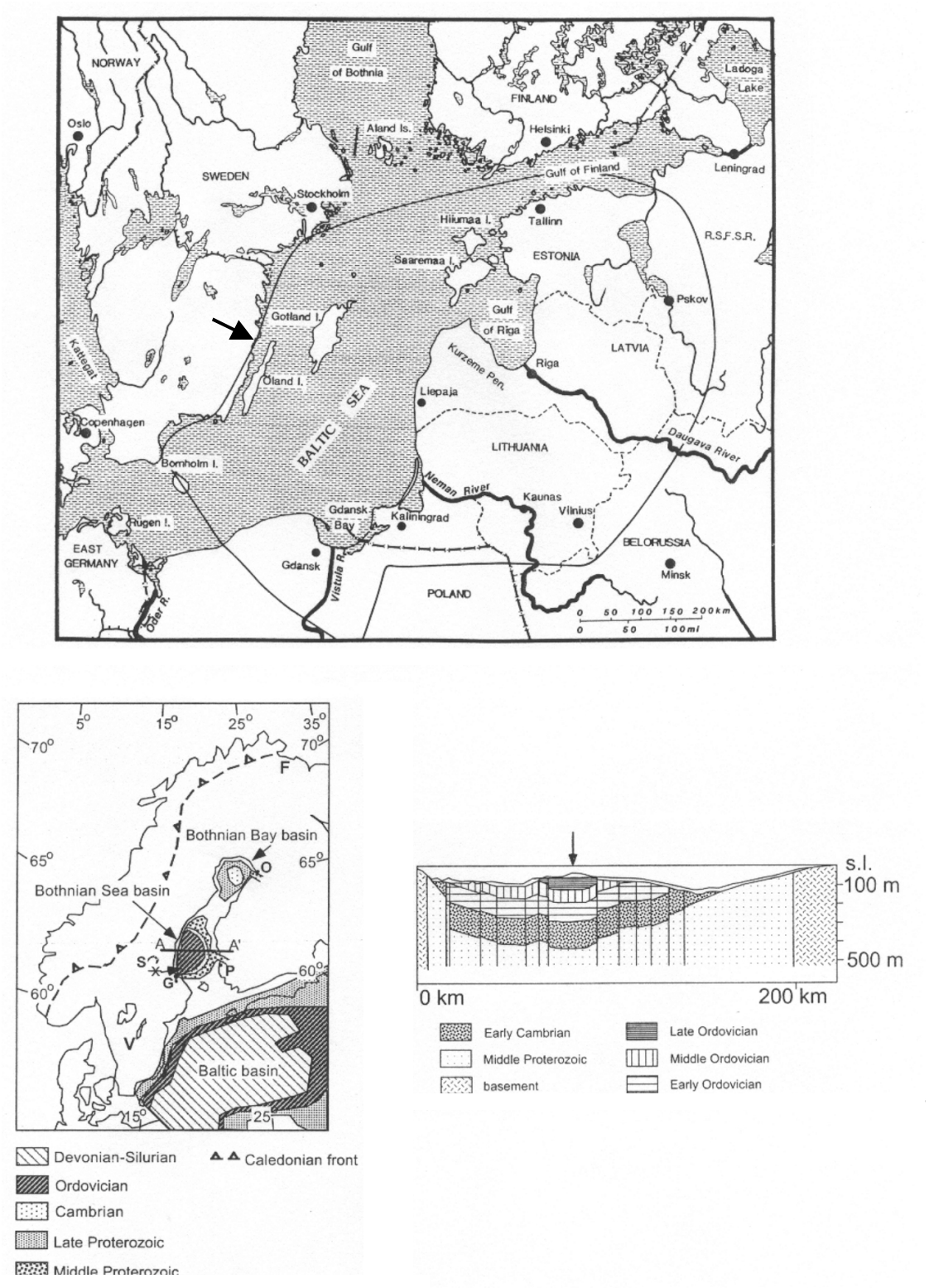

Figure 4-3. *The top diagram shows the geographical extent of the Baltic Basin and the proximity of its western margin to the Äspö region (arrow). /From Ulmishek, 1991./ The bottom left diagram shows the location of the central Baltoscandinavian Intra-cratonic Basins. Line A-A' indicates the location of the cross section on the bottom right. /From van Balen and Heeremans, 1998./*

The outcrop and subcrop geological map of the Caledonian sequence in the Baltic Basin is shown in Figure 4-3a /Ulmishek, 1991/. The southwest and northern boundaries of the basin are clearly fault controlled. The nature of the north-western margin (on which the Äspö Hard Rock Laboratory is situated) is more problematic. It is not marked as a fault on Figure 4-3a but the linear nature of this boundary which coincides with the present-day Baltic coastline of southern Sweden, the orientation of the major normal faults of the Central Baltic Sea rift system (Figure 4-3b) and the fact that the north-northwestern margin of the Bothnian Sea Basin *is* fault bounded (Figure 4-2a) indicate the likelihood of this margin being controlled in some way by a major fault. Nevertheless the two sections illustrated in Figure 4-5 show that fundamental differences exist between the margin of the basin with the Tornquist Line (section BB'), which is clearly fault controlled, and the margin of the basin on its north-western margin, which is characterized by a marginal monocline (section CC'). On shore, a major rift (the Vättern rift, Figure 4-6) occurs. It is parallel to the coastline and to the major normal faults of the Central Baltic rift. Together they indicate the existence of an important and long-lived NNE-SSW fracture set and provide further support for the suggestion that the Swedish coast in the Äspö region is fault controlled.

4.1.2 Post-Cambrian tectonics associated with the Tornquist Line

Äspö is situated on the north-western margin of the Baltic Basin only 200 km northeast of the Tornquist Line. Movement on this major crustal fracture zone from the Cambrian onwards has produced a series of basins which straddle the zone and the analyses of their sedimentary history has revealed that the region has been subjected to a succession of tectonic events, all of which are likely to have affected the rocks at Äspö. The fault complex associated with the Tornquist Line and its proximity to the Äspö area is shown in Figure 4-6 and Figure 4-7a.

A southwest-northeast seismic section through this fault complex is illustrated in Figure 4-7b. It shows that initially the individual faults were normal faults. This can be demonstrated by examining the displacement of the "Top basement" horizon across the most southwesterly of the three main faults, which still displays a significant net normal movement. However, the displacement of higher stratigraphic horizons such as the "Base of the Upper Cretaceous" shows clearly that the fault was subsequently reactivated in a reverse sense and that this reversal (or inversion) occurred in post Triassic times.

Deeper seismic sections (Figure 3-5) indicate that the steep faults of this line, which characterise the upper portion of the crust, merge into gently dipping faults as they approach the lower crust. It appears as a large listric (curved) normal fault, downthrown to the northeast, which has subsequently experienced inversion (i.e. reactivation with a reverse sense of movement). The fault may be an earlier, Precambrian thrust which was used in the Post Cambrian as an extensional fault. Clearly from the point of view of understanding the sets of fractures that might be generated in the Äspö area as a result of the evolution of the Tornquist Line it would be necessary to consider the possibility of a northeast-southwest compression followed by an extension in the same direction during the post Cambrian normal faulting and finally a return to compression during the inversion of the sedimentary basins marginal to the Baltic Basin in post Triassic times.

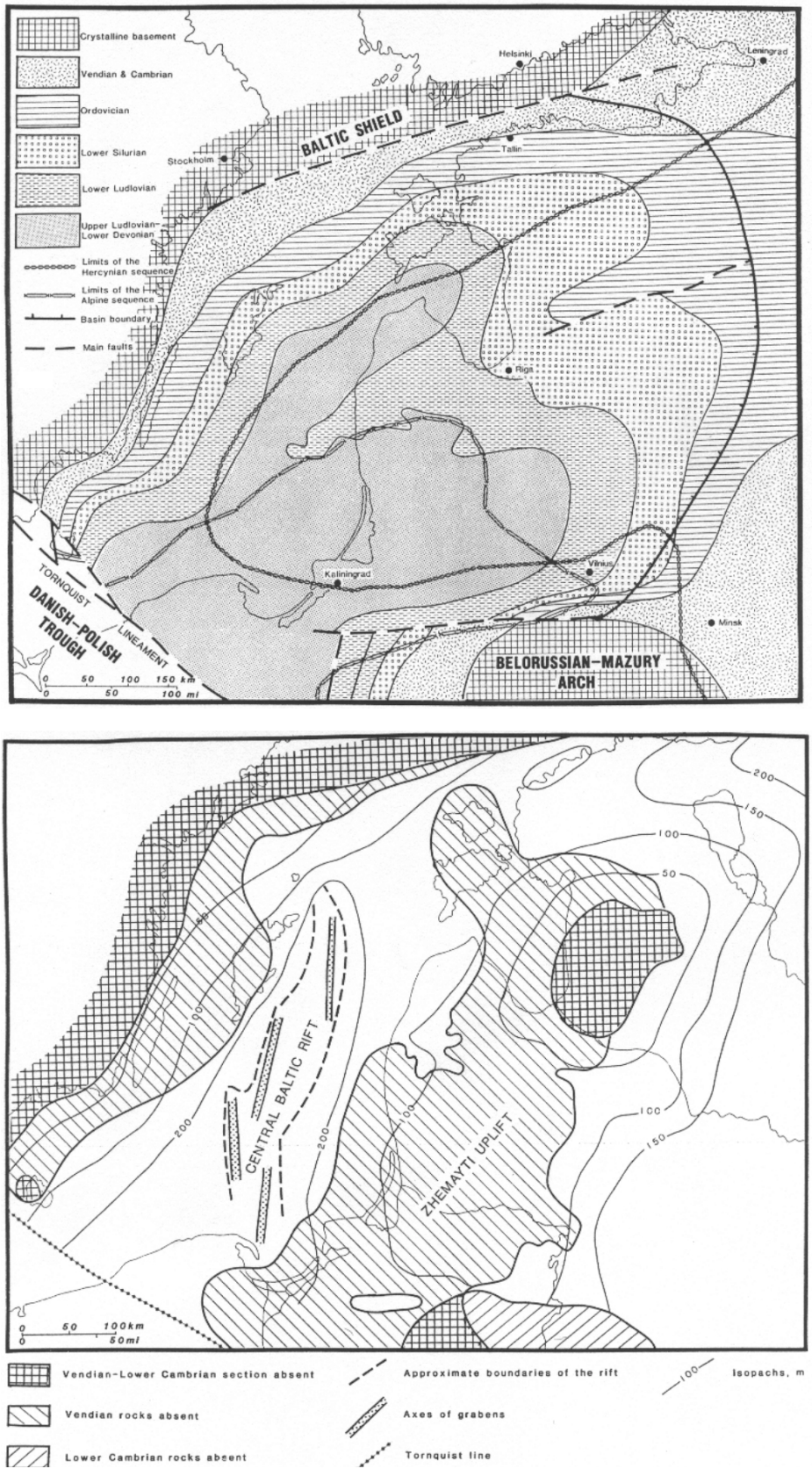

Figure 4-4. *The upper diagram shows the outcrop and subcrop geological map of the Caledonian sequence in the Baltic Basin. The lower diagram shows the orientation of the major normal faults in the Central Baltic Sea rift. /From Ulmishek, 1991./*

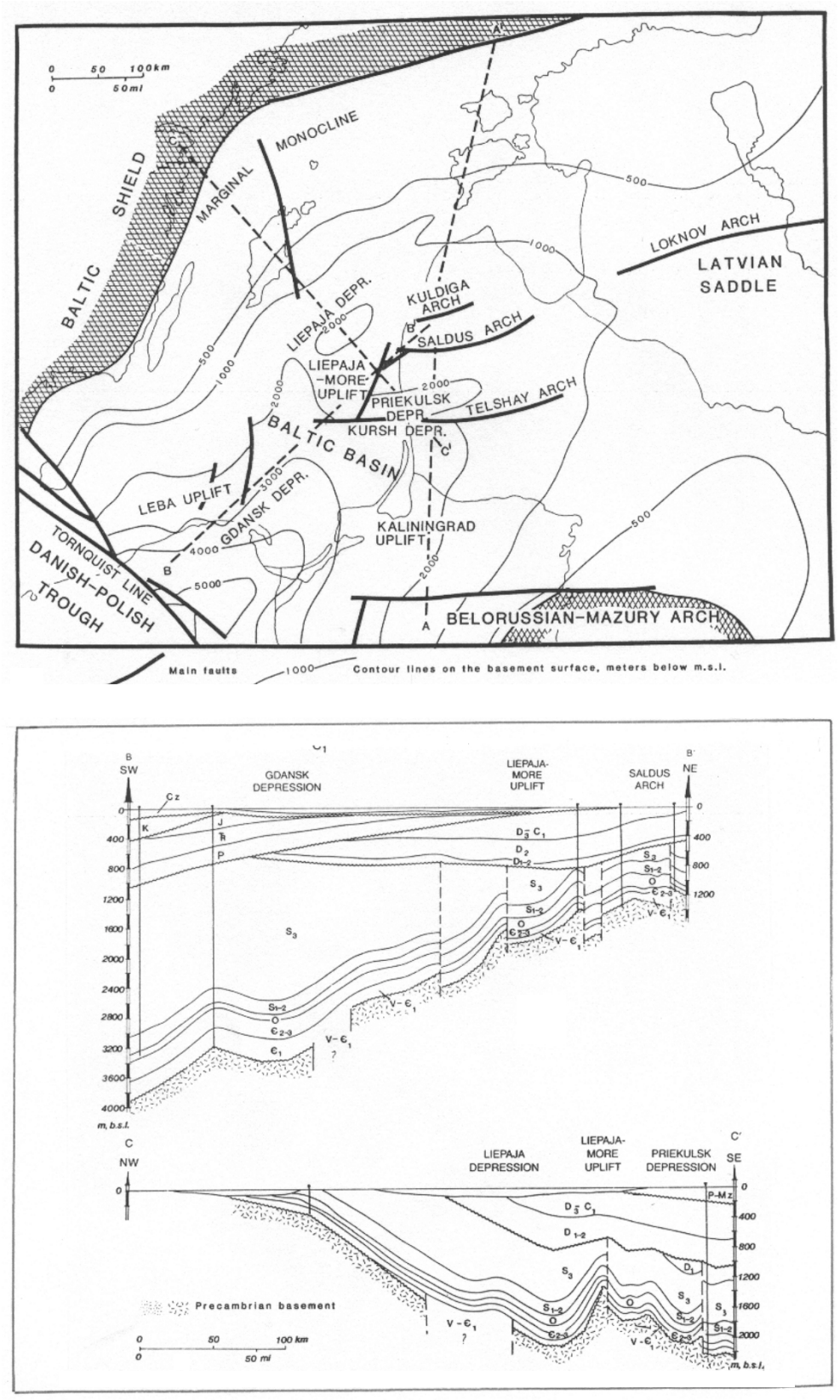

Figure 4-5. *a) Main tectonic features of the Caledonian sequence in the Baltic Basin. b) Cross sections through the Baltic Basin. BB' across the south-western margin defined by the Tornquist Line and CC' across the northeast-southwest margin defined by the present coast of southern Sweden. /From Ulmishek, 1991./*

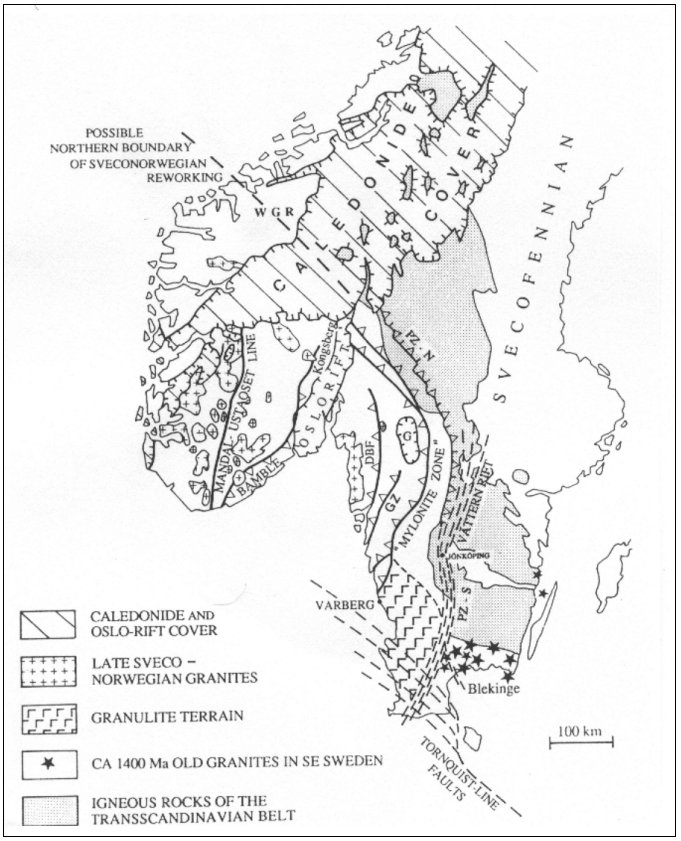

Figure 4-6. *Structure of the southwest Scandinavian domain. Of particular note is the occurrence of a major north-northeast south-southwest trending rift, the Vättern Rift, which parallels the Swedish coast in the vicinity of the ÄHRL site. /From Gorbatschev and Bogdanova, 1993./*

Figure 4-8 shows a schematic reconstruction of the Devonian to resent tectonic evolution across the Tornquist Line. Following an Early Devonian uplift, southwest-northeast extension occurred associated with the break-up of the northwest European plate during the onset of Atlantic rifting. This extension continued through to the late Cretaceous when the Alpine collision between the African and European plates imparted an approximately north-south compression, which caused the inversion of the basins.

It is interesting to note that some of the important normal faults in the North Sea associated with the rifting of the Atlantic (e.g. some of the faults bounding the Central North Sea Graben), trend approximately north-south, i.e. are appropriately oriented to have been generated by this east-west extension. However, in regions of the crust were important pre-rift fractures in different orientations exist, as for example along the northwest-southeast trending Tornquist fracture zone, the normal faulting exploits these early structures rather than generating new fractures with the ideal north-south orientation. The use of this fracture zone, which is oblique rather than normal to the regional extension direction of the time, results in a component of strike-slip motion occurring along the faults and the formation of *oblique-slip normal* faults rather than pure normal faults. Such deformation along the Tornquist zone would be termed *transtensional*. Similarly, during the north-south compression which resulted from the Cretaceous collision between the African and European plates, reactivation of these oblique-slip normal faults would have accommodated the required north-south shortening by *oblique-slip reverse* faulting and the fracture zone would have been characterized by *transpressional* deformation.

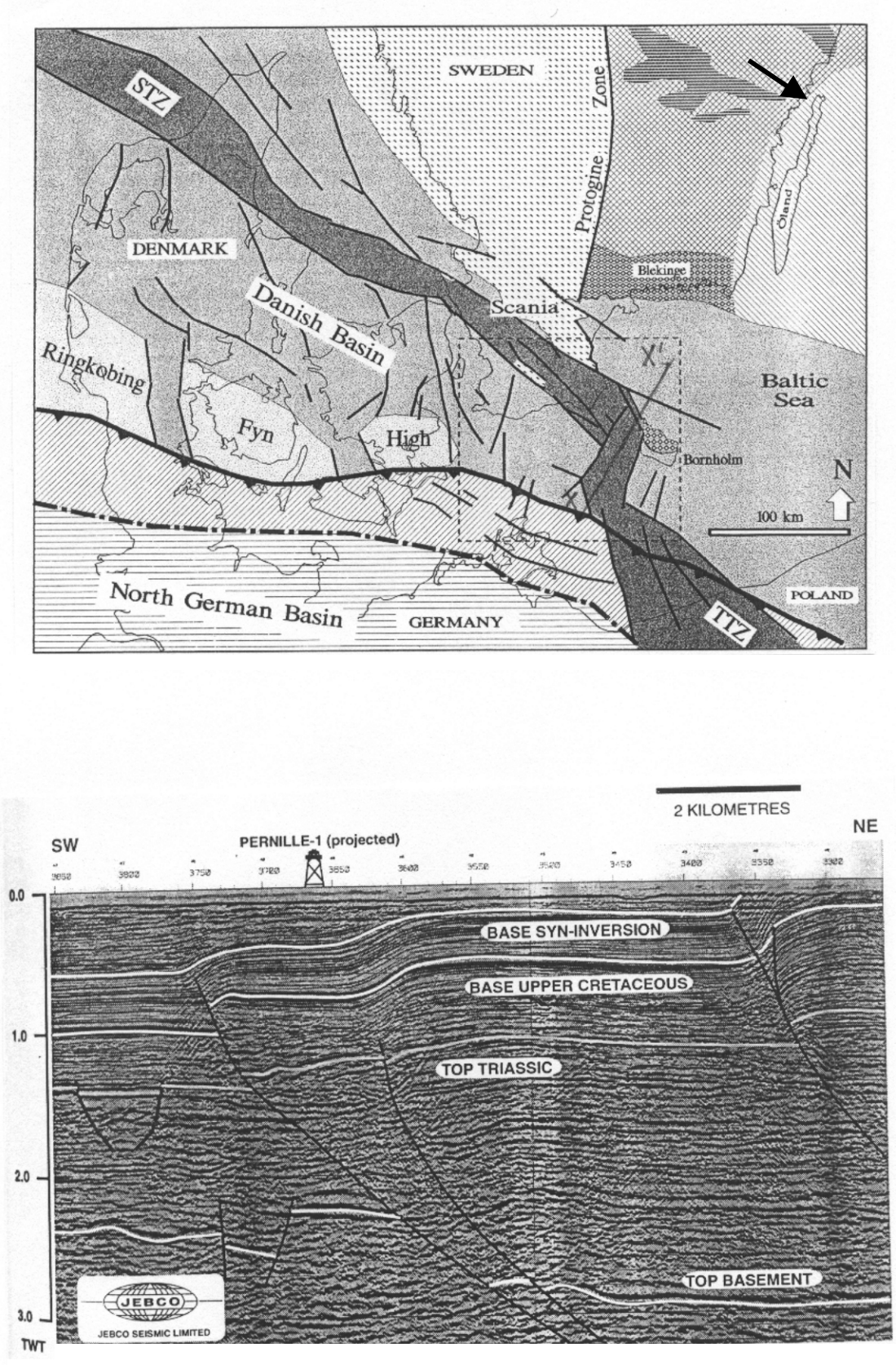

Figure 4-7. *(a) Map showing the proximity of the Tornquist Zone (STZ TTZ) to the Äspö area (arrow). (b) The seismic section XX' shows reverse movement on some of the northwest-southeast trending normal faults that characterize the Tornquist zone. /From Erlstrom et al., 1997./*

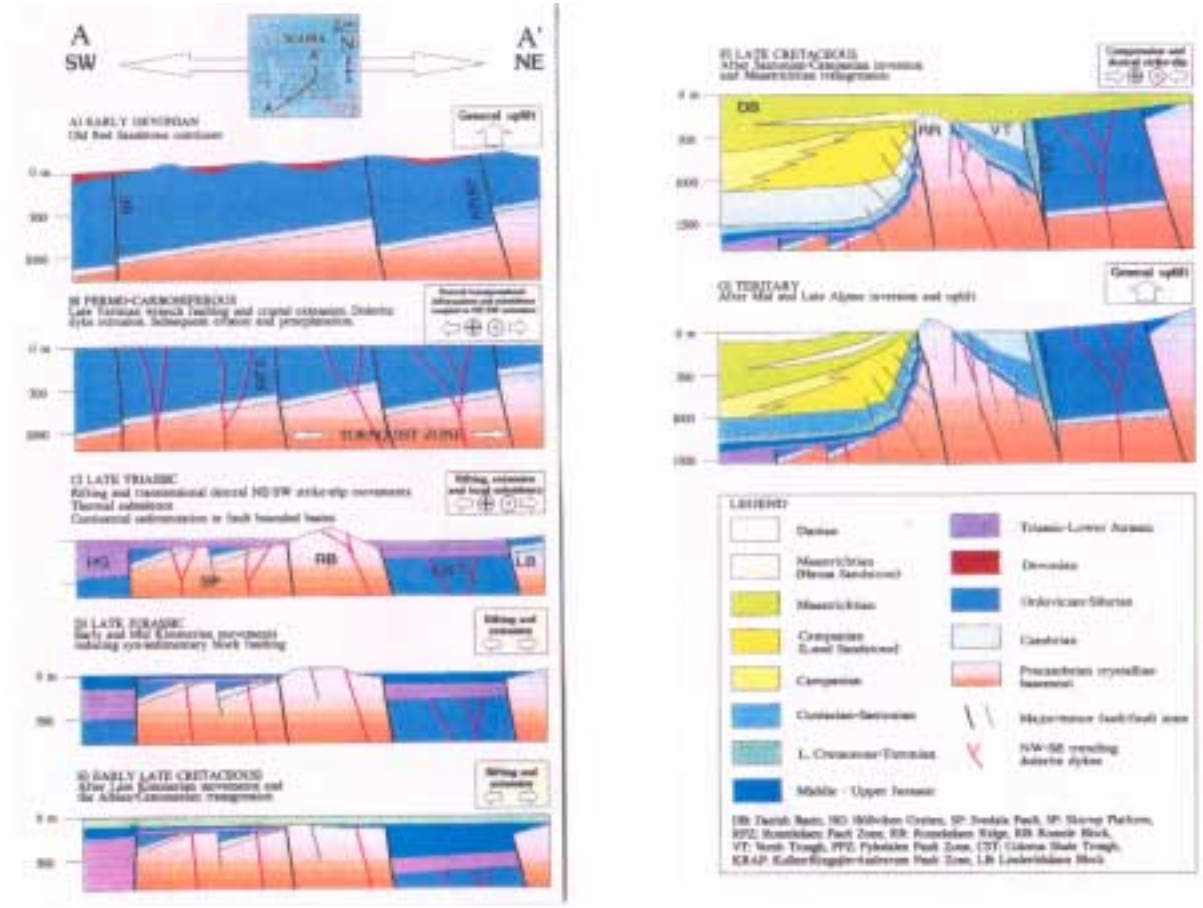

Figure 4-8. *A schematic reconstruction of the tectonic evolution across the Tornquist Zone showing the interplay of extension, compression and uplift. /From Erlstrom et al., 1997./*

The reactivation of old fracture sets during later deformation events even when they are not ideally oriented is discussed in the following section.

The discussion of the tectonic evolution of the Äspö region outlined in this section shows that through its long history the Scandinavian plate has been subjected to a series of major deformation events most of which have left important fractures (faults, joints or both) as evidence of their occurrence.

The existence of fracture sets and fracture networks in a rock mass can dramatically influence:

- Whether or not new fractures form in response to later stress fields
- The orientation of new fractures (see Section 4.1.3) and
- The orientation of the current stress field within the vicinity of the fractures (see Section 4.2.3).

4.1.3 The influence on ancient fracture sets on subsequent fracturing

When a fractured rock mass is subjected to stress in the brittle regime it may respond by either the reactivation of old fractures or the generation of new ones. Which of these two possibilities occurs depends upon the relative orientation of the applied stress and the pre-existing fractures and the relative magnitudes of the shear strength of the fracture and the intact rock.

This can be illustrated using the Mohr circle representation of the stress state and the failure criteria for shear failure of intact rock (upper line containing point B, Figure 3-7a) and for reshear on a fracture (lower line containing points A and C, Figure 3-7a). The stress state has been selected to be such that the next increment of stress will be sufficient to cause shearing of the intact rock. Until this increment is added no new shear fractures will form. However, it can be seen that the existing stress state is of sufficient magnitude to cause re-shear on fractures in a range of angles to the maximum principal compression σ_1, from β' to β'', Figure 3-7b.

An interesting example of the use of old fractures rather than the generation of new, occurred during the opening of the rift valley system in East Africa. Here an east-west extension exploited ancient fractures in the basement. These had a variety of orientations including northwest-southeast, northeast-southwest and north-south, Figure 4-9. As noted in the previous section a similar situation probably arose in the Scandinavian shield during the approximately east-west extension linked to the opening of the Atlantic, which began in the Permian. Two important fracture sets which developed in the shield in the vicinity of Äspö and which pre-date the opening of the Atlantic are the approximately north northeast-south southwest fractures (e.g. the fractures associated

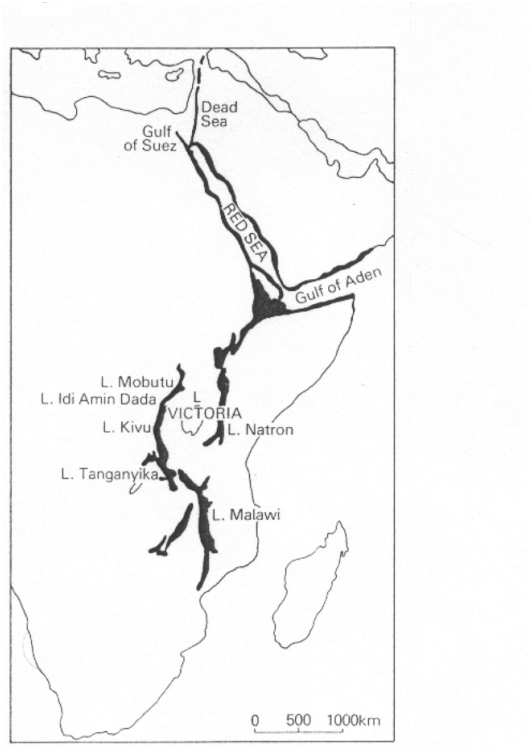

Figure 4-9. *The rift system of East Africa. Note that the rift is made up of segments with different orientation reflecting the influence of pre-existing fractures in the basement.*

with the Central Baltic rift (Figure 4-4), the Vättern rift (Figure 3-3), the Baltic coast of southern Sweden that parallels them both and the approximately north-south trending Central North Sea Graben) and the northwest-southeast trending fractures linked to the Tornquist Line (Figures 12 and 15). Both sets were reactivated during the extensional deformation linked to the Atlantic rifting.

4.1.4 The role of current plate motion on the present day state of stress in the NW European plate

The present day stress state in the NW European plate is shown in Figure 4-10 and Figure 4-11. The far-field stresses within the plates are the result of the relative plate motion and a considerable database now exists relating to this topic (see e.g. Minster and Jordon, 1978; Grunthal and Stromeyer, 1992).

The stress map shown in Figure 4-11 is made up from data from a variety of sources including *in situ* over coring measurements, well bore breakouts, fault plane solutions and repeated precise geodetic triangulations. Zoback /1992/ points out that in general the broad-scale regional mid-plate stress patterns are though to be mainly the result of compressional forces applied at plate margins and that these are primarily ‘ridge push’ and ‘continent collision’.

In the context of the NW European plate these forces would be an E-W directed compression from the Atlantic ridge and an approximately north-south compression from the Alpine margin. It can be seen from Figure 4-10 and Figure 4-11 that NW Europe is characterized by a northwest-southeast directed maximum compressive horizontal stress in western Europe and a west northwest-east southeast directed stress in Scandinavia. Müller et al. /1992/ note that this stress orientation is sub-parallel to the direction of relative plate motion between Africa and Europe and is rotated 17° clockwise from the direction of absolute plate motion.

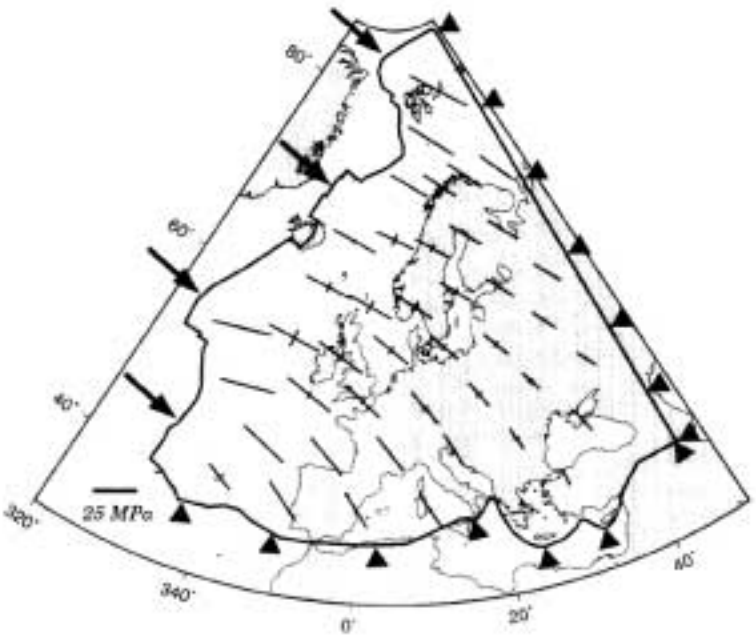

Figure 4-10. *Predicted European tectonic stresses based on mid-Atlantic ridge push. /From Gölke and Coblentz, 1996./*

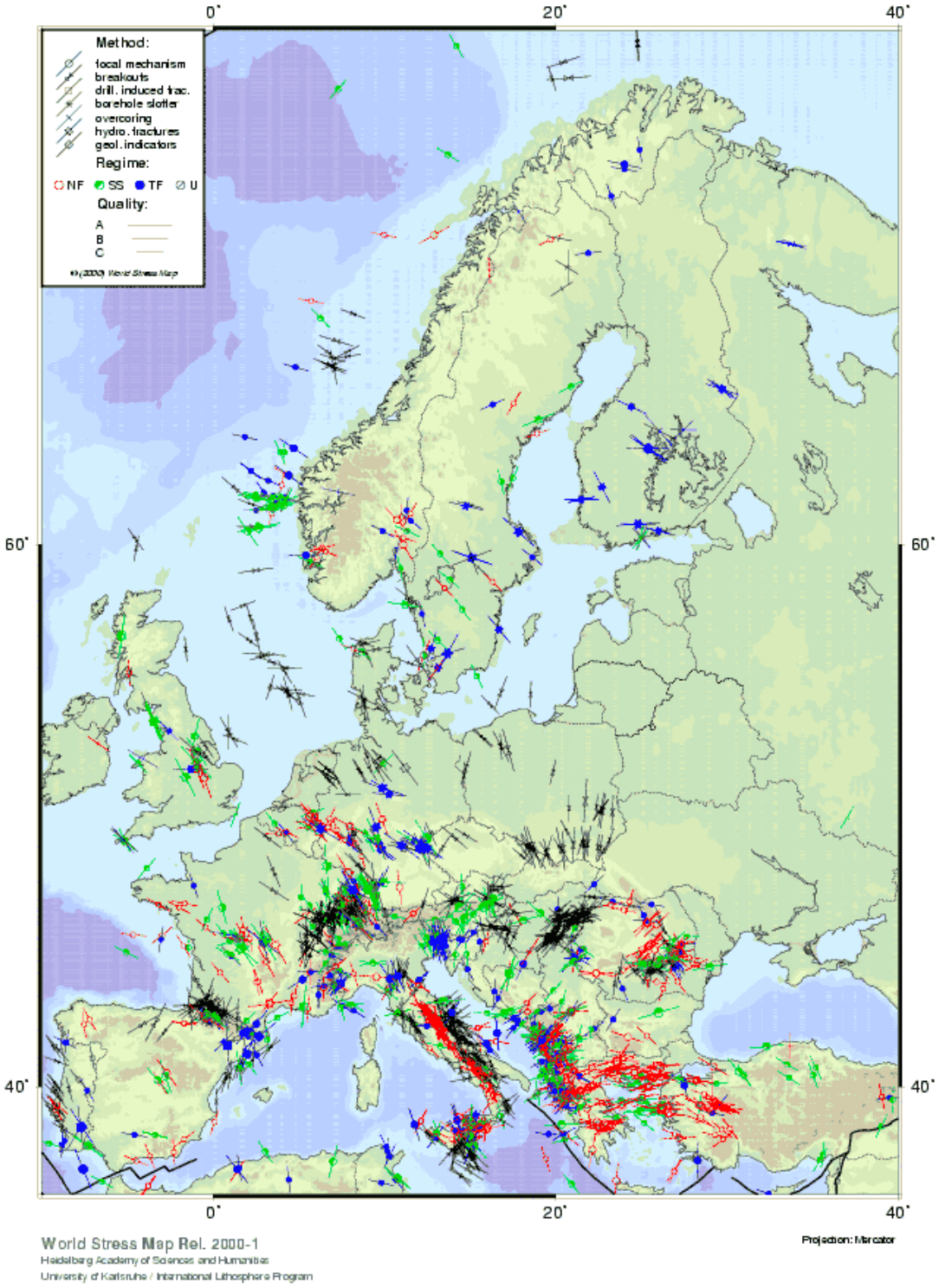

Figure 4-11. *European component of the World Stress Map. /From Müller et al., 2000./*

It appears therefore that the stress field within the European plate is at present dominated by the Alpine collision to the south and the role of 'Ridge push' from the Mid-Atlantic Ridge is negligible. Superimposed on these first-order stress fields linked to plate motion are second-order stress fields that are associated with specific geological or tectonic features, Zoback /1992/. Three specific types of features need to be considered in Scandinavia. These are:

- Variations in lithospheric thickness,
- deglaciation flexuring and
- the existence of important fracture sets within the shield.

These are discussed briefly below but the relatively uniform stress field that currently pervades the European plate Figure 4-11 indicates that they do not modify the stress regime significantly.

The model of the lithosphere usually assumed is one of an elastic layer resting on a viscous substrate. In such a model plate motion would generate a viscous drag. However, Minster and Jordon /1978/ point out that the European plate is hardly moving in an absolute reference frame and that consequently viscous drag would be negligible. In addition by using stylolites as palaeo-stress indicators it can be demonstrated that the current northwest-southeast directed compression has been operating throughout most of the Tertiary and was probably initiated by the onset of the Alpine collision in the Late Cretaceous. It is argued therefore that the effect of this collision has consistently overwhelmed the effect of any 'ridge push' from the west.

4.2 Factors other than plate motion that influence the stress in the NW European plate

In the previous section three features were identified that might modify the plate stresses in Scandinavia. These are variations in lithospheric thickness, deglaciation flexuring and the existence of important fracture sets in the shield.

4.2.1 The effect of variations in lithospheric thickness on the stress field

Müller et al. /1992/ note that "the uniformly oriented stress field in western Europe coincides with thin to medium lithospheric thickness (50–90 km) and high heat flow (>80 mW/m^2) and that the more irregular horizontal stress orientations in Scandinavia coincide with thick continental lithosphere (110–170 km) and low heat flow (<50 mW/m^2)." They argue that the cold, thick lithosphere in this region may result in lower mean stresses associated with the far-field tectonic forces and that these allow the stress field to be more easily perturbed by local, second-order stress fields.

4.2.2 The effect of removal of glacial load

A brief review of the studies of lithospheric loading (e.g. as a result of sedimentation or glaciation) is presented by Zoback /1992/. Figure 4-12 shows the orientation of the maximum horizontal stress from Scandinavia plotted on a map of surface uplift rates for glacial rebound. The regional northwest-southeast trend of the stress field is still

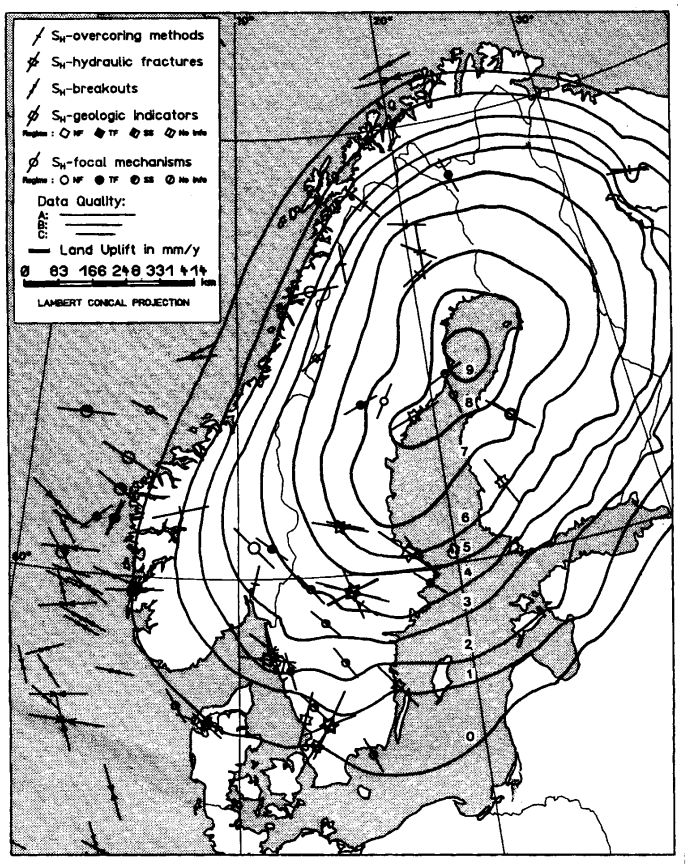

Figure 4-12. *Maximum horizontal stress orientation for Scandinavia plotted on a map of surface uplift rates (mm/yr) for glacial rebound. /From Müller et al., 1992./*

apparent and is not dramatically disturbed by the deglaciation flexuring. In addition, Gregersen /1992/ considers some of the local stress anomalies in the shield and reports that "no correlations with geological provinces or province boundaries were found" and that …"there does not appear to be any clear correlation between anomalous stress orientations and post-glacial uplift in the present earthquake activity". He notes that "This lack of correlation is in sharp contrast to geological evidence in the form of large faults indicative of large post-glacial earthquakes occurring right after the end of the latest ice age 9000yrs ago". Taken together this evidence suggests a tremendous change of stress field in Holocene times, from one dominated by post-glacial unloading immediately after the ice age to one dominated by the present plate motion today.

4.2.3 The effect of pre-existing fracture sets

It was noted earlier in Chapter 3 on factors that might modify the magnitude and orientation of regional stresses, that fractures, particularly those with a low shear strength compared to the host rock, cause a deflection of the stress trajectories into orientations either normal or parallel to the fracture.

The NW European plate is characterized by an important NW-SE trending fracture set (i.e. the Tornquist Line fractures). The correlation between the maximum horizontal compressive stress and these fractures is unlikely to be a coincidence and it is probable that the stresses were deflected by these major fractures into an orientation parallel to themselves.

5 Methods for numerical analysis of in situ stress conditions – a review

5.1 General

The *in situ* stress distribution in a rock mass has been studied for various purposes. A major industry sector where *in situ* stress predictions are necessary is the mining industry. A good knowledge of *in situ* stress distribution plays an important role in safety and contributes to the improvements in overall mine economy. Another area where a sound knowledge of the *in situ* stresses is very important is tunnelling and other underground facilities, in particular in mountainous areas with weak rock types. For this type of projects the rock stability is crucial and should not deteriorate over many decades.

The approach taken in the numerical simulation of stresses would, however, be quite similar, regardless of the type of construction being considered. It is the geological setting in the area of concern that is the main factor influencing the stress distribution would determine how the problem is to be analysed. In the following sections a number of examples will be given of studies where a numerical analysis has been used in an attempt to predict or explain the *in situ* stress field. The examples are arranged to illustrate the effect of various stress influencing factors including topography (over-burden), rock stiffness differences, tectonic load, faults and fracture zones and glacial loading.

5.2 Influence of topography

At the Wellenberg repository site in Switzerland various methods have been used to determine the *in situ* stress field /Konietzky et al., 1995/. Basic data were collected from borehole measurements such as hydraulic fracturing stress measurements, analysis of borehole breakouts and drilling-induced fracturing. Additional data were collected by resorting to the geological-tectonic stress indicators.

A numerical stress field model of the area was built with the following aims:

- to estimate the *in situ* stresses over large areas,
- to separate gravitational and tectonic components,
- to check assumptions made during interpretation of stress measurements,
- to investigate the influence of different parameters on the stress field.

Since this area has high mountains, a marked topographic relief was expected, and consequently three-dimensional modelling was considered. However, to help in determining the adequate model dimension for the 3D model, simple 2D models were first performed for three cross-sections, see Figure 5-1. The vertical boundaries were moved from outside inwards and the resulting effects on the stress distribution in the interior of the model were investigated.

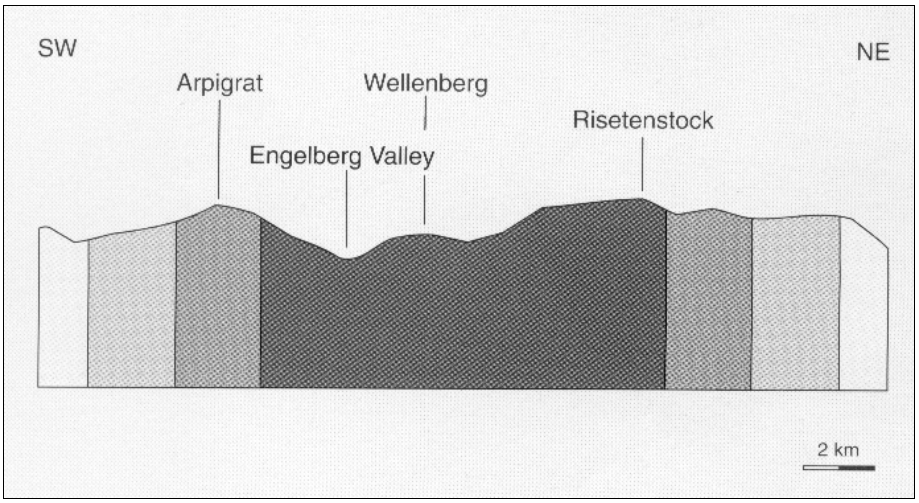

Figure 5-1. *2D-model of investigation area in order to determine the size of 3D-model. /From Konietzky et al., 1995./*

Based on the results, a model covering approximately 600 km^2 was selected for the 3D model (Figure 5-2). The horizontal base was set at 3000 m below sea level. Eight different formations, based on the geological section, were incorporated into the model. The numerical mesh was finer closer to the planned repository. The model consisted of a total of 65,000 elements and an elastic material law was used.

The calculation sequence was divided into several stages and the first stage was the consolidation of the model under purely gravitative stress. Secondly the reaction forces from the larger 2D model were applied as stress boundaries for the 3D model. A comparison of the modelling results for the simple gravitational condition with the measured stresses showed clear discrepancies. It could therefore be concluded that the stress effects from the topography could not alone explain the observed stresses and tectonic forces also had to be taken into account.

Figure 5-3 shows an example of results from the 3D model. Also in this model, apart from the effects from the topography a tectonic stress component was included, simulated with fixed stress boundary conditions. The boundaries were changed until a satisfactory agreement was reached with stress measurements in the boreholes. Another further detailed study of the area was performed in /te Kamp et al., 1999/, using a similar approach, (Figure 5-4). It can be seen that the effect of topography, i.e. the effect of different overburden can be simulated by letting the model area reach the ground surface. In this model also the effects of the difference in material properties (different rock types) was simulated. It was shown that on the potential repository level the variations in the stress field coincided with material boundaries and regions where plastification has taken place.

In general it may be concluded that the effect of topography on the stress variation will be significant only fairly close to the ground surface and in mountainous areas.

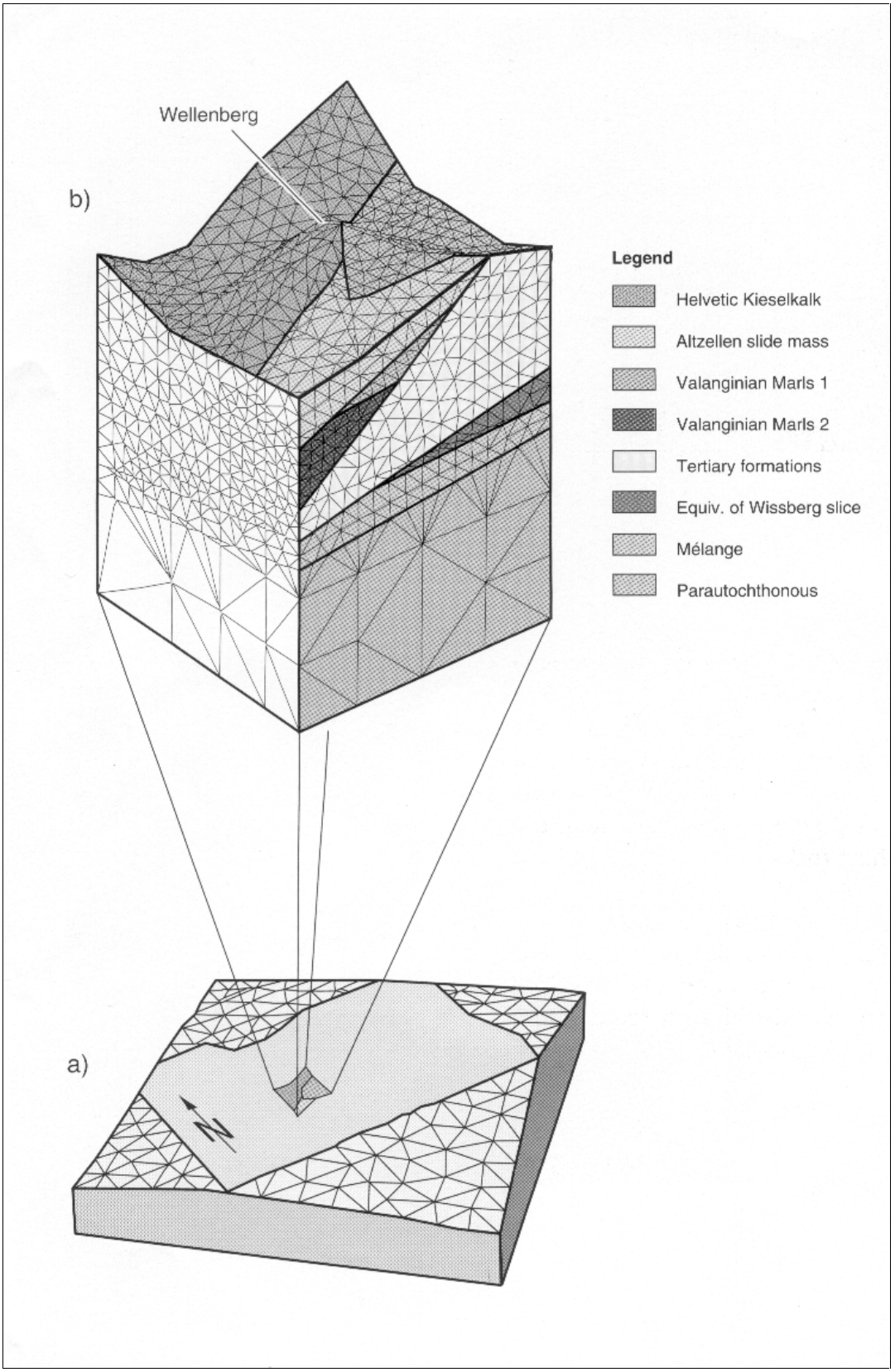

Figure 5-2. *The 3D-model for rock mass modelling at Wellenberg. In order to increase resolution the elements in the area of interest are smaller than those at the edges of the model. /From Konietzky et al., 1995./*

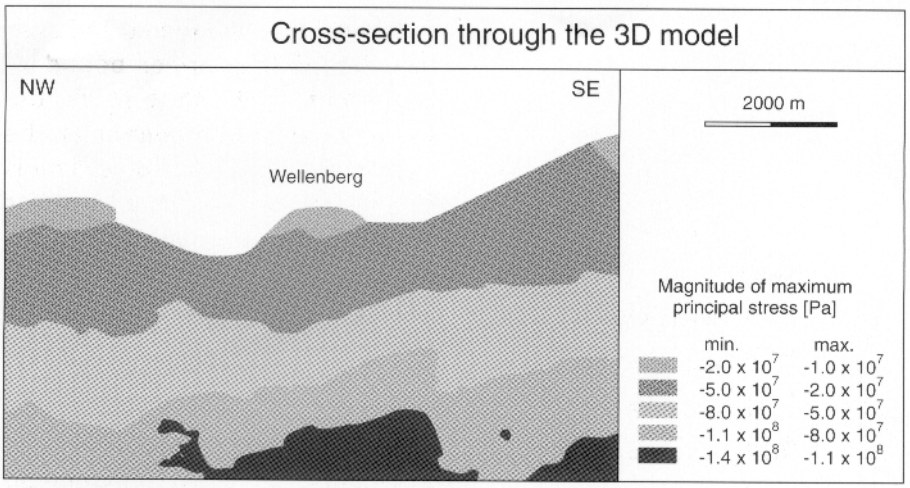

Figure 5-3. *The 3D-model for rock mass modelling at Wellenberg. In order to increase resolution the elements in the area of interest are smaller than those at the edges of the model. /From Konietzky et al., 1995/.*

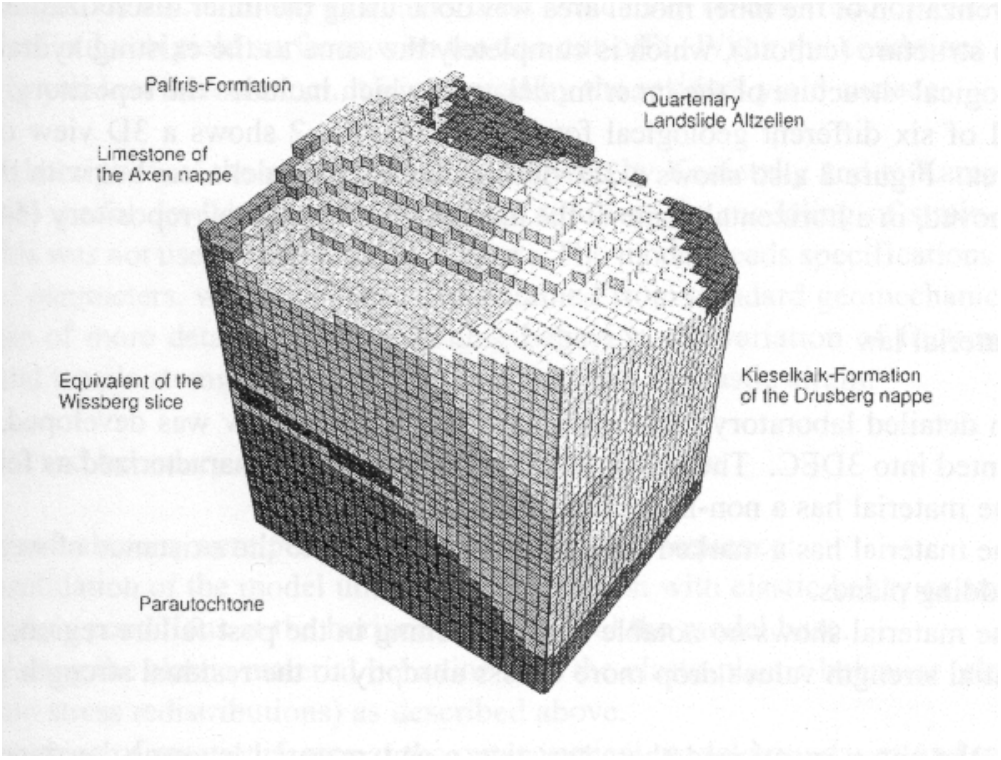

Figure 5-4. *3D view of the inner area in the 3DEC model from Figure 5-2. Different shades correspond to different rock materials. /From te Kamp et al., 1999./*

5.3 Influence of stiffness differences

The work by Whyatt /2000/ on the Coeur d'Alene mining district in North America is an example of a study where the mineralogical properties of the rocks play an important role in controlling the stress distribution. In this comprehensive study, which drew on extensive laboratory testing, it was concluded that the strongest rock type (silicified vitreous quartzite) had a uniaxial compressive strength (240 MPa) 3–6 times higher than the weakest rock type (siltite-argillite) and an elastic modulus about 3 times larger, on the rock mass scale.

In this example these differences in rock deformation properties could be correlated to the observed differences in the stress field. Figure 5-5 illustrates the interestingly large differences in vertical stress from different mines in the district. Variations in topography could only account for stress variations that fell within the shaded area of the figure and it was concluded that the stress values outside this range were the result of variations in the stiffness of the different rock units.

The simple cases of the stress variations around a circular or elliptical softer or stiffer inclusion may be solved analytically. The largest stress concentration, expressed as the ratio between stress inside the inclusion ands stress applied on the boundary, reaches 3 times when the stiffness ratio is 3 (see Figure 5-6).

Whyatt /2000/ further investigates the more complicated geometrical case of a stiffer fold and ring using numerical modelling (FLAC3D). It is concluded from these simple models that the level of stress concentration apparent in the Coeur d'Alene district (2:1) can be accounted for by stiffness variations given the range of modulus contrast encountered (up to 3:1). The approach to the continued analysis was to consider the five major periods of tectonic deformation that had affected the area, assuming that the whole district has undergone a uniform loading history. It follows that similar inclusions containing similar rock would create similar local perturbations of stress regardless of

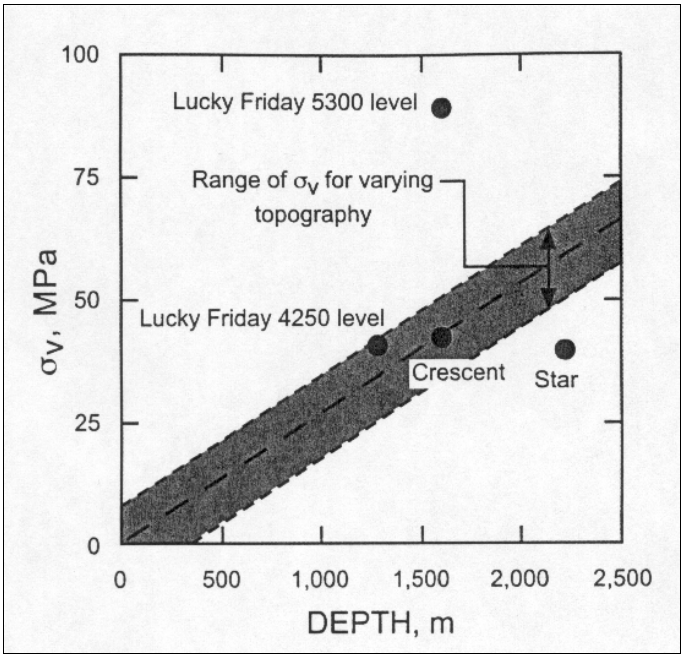

Figure 5-5. *Vertical stress measured at the Lucky Friday mine. /From Whyatt, 2000./*

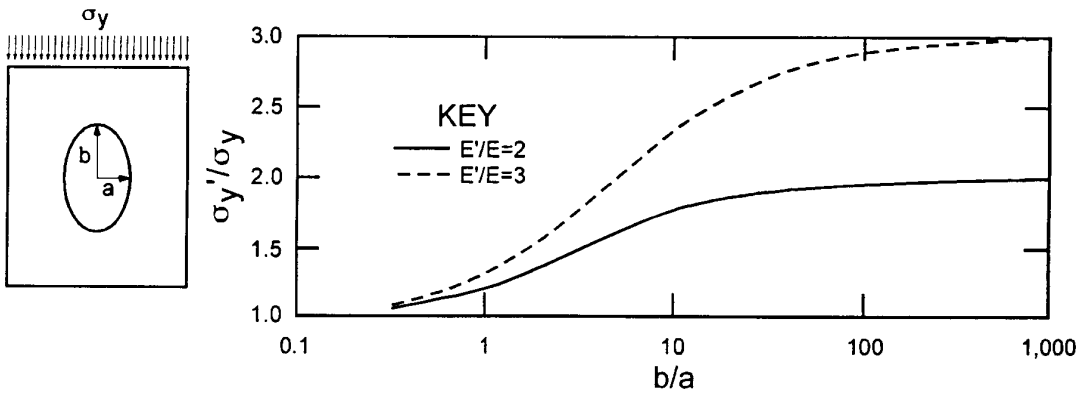

Figure 5-6. *Stress ratio vs E-modulus ratio for elliptical inclusion of different elongation. /From Donell, 1941./*

location in the district. A large series of analyses using FLAC2D and FLAC3D was thereafter performed. To compare the different models (with different load components) the sum of square error for each model was calculated and a best-fit model was found that gave a better fit to the measured stresses in the whole region compared to the simple model assuming a linear stress distribution with depth.

5.4 Influence of tectonic stress

As already mentioned, the stresses in many places cannot be explained only with gravitational forces and therefore the tectonic stresses must be included in realistic models. In Figure 5-3 and Figure 5-4 examples are given on models by Konietzky et al. /1995/ and te Kamp et al. /1999/, where the boundary conditions were calibrated to get a good fit to measurements. The actual sources of the stress forces were not simulated. The stresses at the boundaries were assumed and varied and measurements were required to select the model in which there was most confidence, in a “data-fit” process.

Another example of numerical modelling of in situ stress is given by Homand et al. /1997/. They performed an extensive study to explore and explain the stress distribution in a cole mine region, the Arc syncline in Provence. The geology in the area was represented in a UDEC model (two-dimensional distinct element code). They applied tow types of loading after consolidation calculation of the model, 1) loading corresponding to current tectonic situation (CT) and 2) Lading involving the steps of tectonic history (TH), see Figure 5-7. Three different model geometries, including different number of faults were also compared in the study.

As an example of the results presented by Homand et al. /1997/ the calculated $\sigma 1$ magnitude along an E-W profile through the centre of the model is shown in Figure 5-8. The different curves in the figure correspond to the different tectonic stages simulated (cf. Figure 5-7). The modelling results clearly illustrate the dependence of geological structures on the in situ stress. Stress distribution are approximately similar for both loading cases (CT and TH), but the simulating including the tectonic history tends to slightly reduce $\sigma 1$ and increase $\sigma 1$ and deflect the major stress towards the northeast.

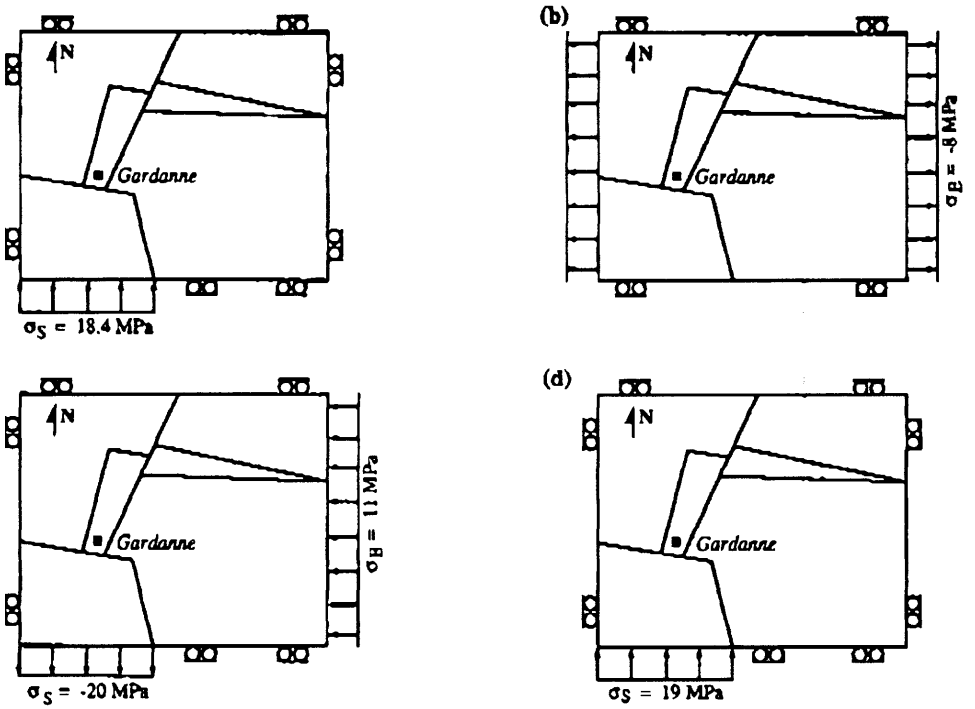

Figure 5-7. *Loading involving tectonic history of the region (i.e. loading TH) a) N-S compression during the Eocene period, b) E-W extension dated from the Oligocene period, c) ENE-WSW compression during the inferior Miocene period, and d) N-S compression starting from the superior Miocene period. /From Homand et al., 1997./*

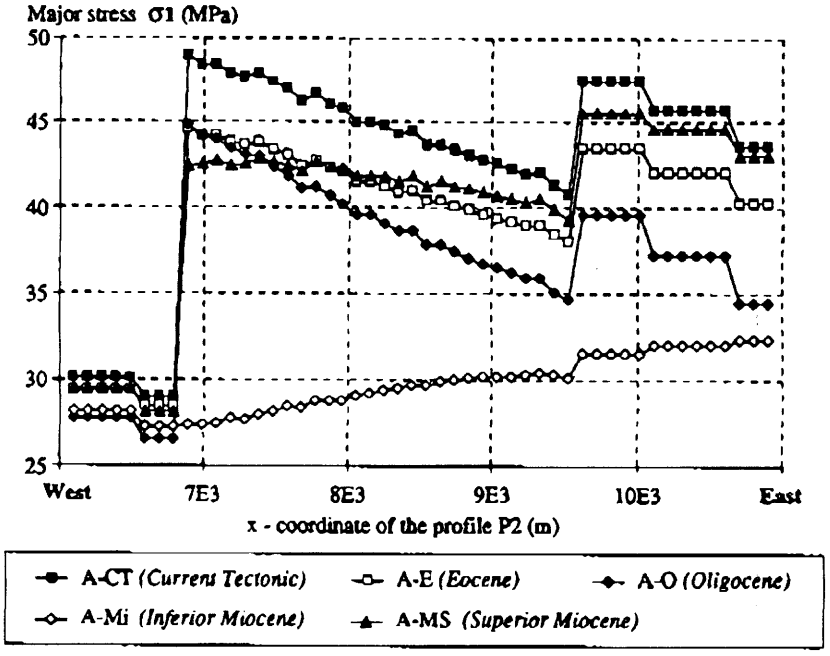

Figure 5-8. *Major principal stress magnitude along an E-W profile at the centre of the model. The curves correspond to the different loading steps. See in Figure 5-8. /From Homand et al., 1997./*

The best results were obtained when minor faults in the south were also taken into account. Despite the fact that the modelling was two-dimensional Homand et al. (op cit.) considered the modelling work helpful in explaining the stress distribution and loading increments in the studied area.

5.5 Influence of faults and fracture zones

The assessment of stress determination methods was one of the elements of the research program carried out at the Underground Research Laboratory (URL) in Canada. Chandler and Martin /1994/ describe how they used numerical tools to understand the *in situ* stress field at URL. Within the rock surrounding the URL, there exist two major fracture zones. These are thrusts, i.e. low-dipping faults along which reverse-dip displacement has occurred. The stresses measured can be grouped into three domains separated by the fracture zones. Thus this area clearly illustrates a case where subhorizontal structures influence both stress magnitude and orientation (Figure 5-9).

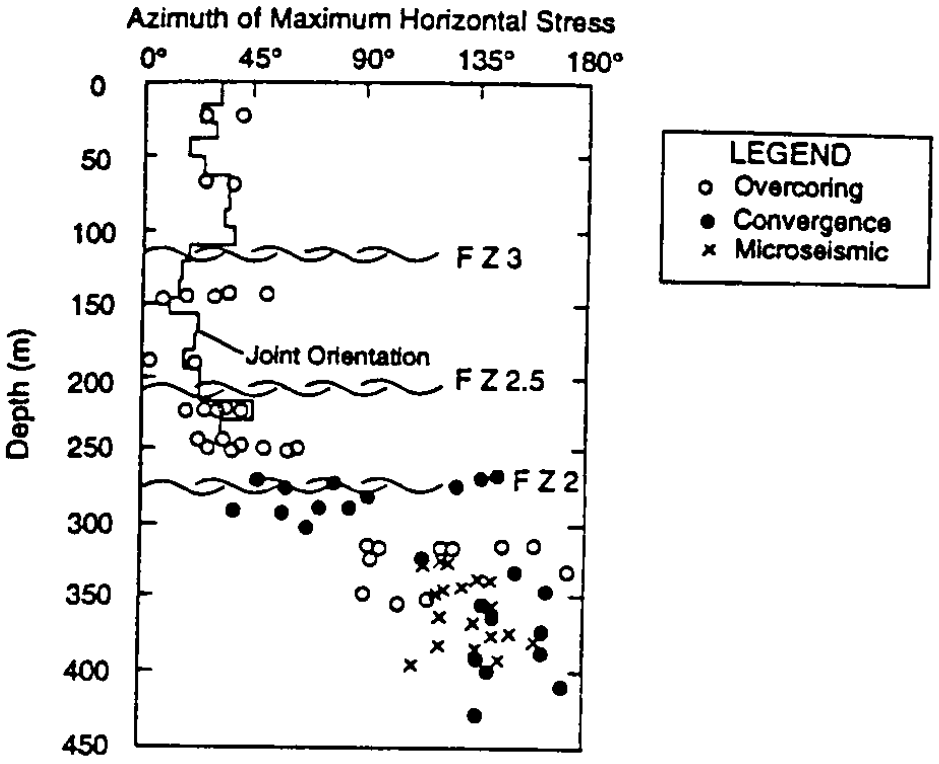

Figure 5-9. *The measured orientation of the maximum horizontal stress at the URL. Note the 90° rotation across Fracture zone 2. /From Chandler and Martin, 1994./*

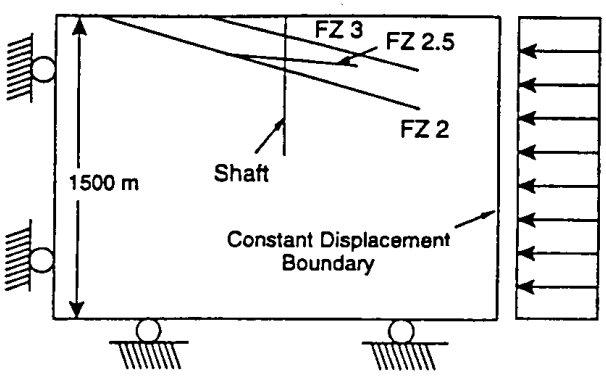

Figure 5-10. *The boundary conditions imposed in the UDEC and FLAC numerical models of URL. /From Chandler and Martin, 1994./*

Figure 5-10 shows the set-up of the two-dimensional numerical model using UDEC and FLAC that was analysed. The model represents a vertical section through the area in the dip direction of the zones. The horizontal distance between the boundaries was decreased until stresses at the 420 m depth were representative of measured values. The dip-direction stresses are the stresses calculated by the model and the strike-direction stresses are the out-of-plane stresses necessary to satisfy the plane-strain condition.

Figure 5-11 and Figure 5-12 shows the calculated horizontal stress magnitudes together with the measured stresses. It can be seen that the numerical model produces a stress increase in the zones, due to the slip, and a constant stress at depth, similar to the measured values. In addition the model captures the change in direction of t maximum stress that was observed in the field (Figure 5-9).

In the URL example the fracture zones extends all the way up to the ground surface and a large shear displacement and stress relief can occur. However, even in the situation where fractures are located inside the rock the stress will still be affected as a result of slip. Both numerical and analytical analyses of such discontinuity-loading configuration can be found in the literature. One example is here given in Figure 5-13 /from Hakami and Olofsson, 2002/. The figure shows a plot of stress trajectories from a part of a UDEC model including an enclosed fracture. The tip of the fracture lies in the centre of the plot (the dotted line is the continuation of the fracture which has been given very high strength properties). The overall pattern of a maximum stress in the horizontal direction is deflected at the fracture such that the principal stresses become roughly parallel and perpendicular to the plane of the fracture that has reached slip failure. In this case the stress magnitude in the direction parallel to the fracture will change distinctly when moving from a point on the upper to the lower side of the slipping fracture.

The slip occurs along the entire surface with the largest slip occurring at the centre of the fracture and decreasing to zero at the fracture tips. The upper fracture surface has moved towards right and this has caused a stress concentration at the upper side of the tip (the longest trajectory line is located there). Just below the fracture tip on the right side the rock gets tensile stresses (the circular signs). The actual stress concentration will be overestimated to some degree in a model with elastic material properties. In a real rock mass the tensile stress concentrations that can be built up will be limited by the tensile strength of the rock and the creation of fractures (fracture propagation) at the tip.

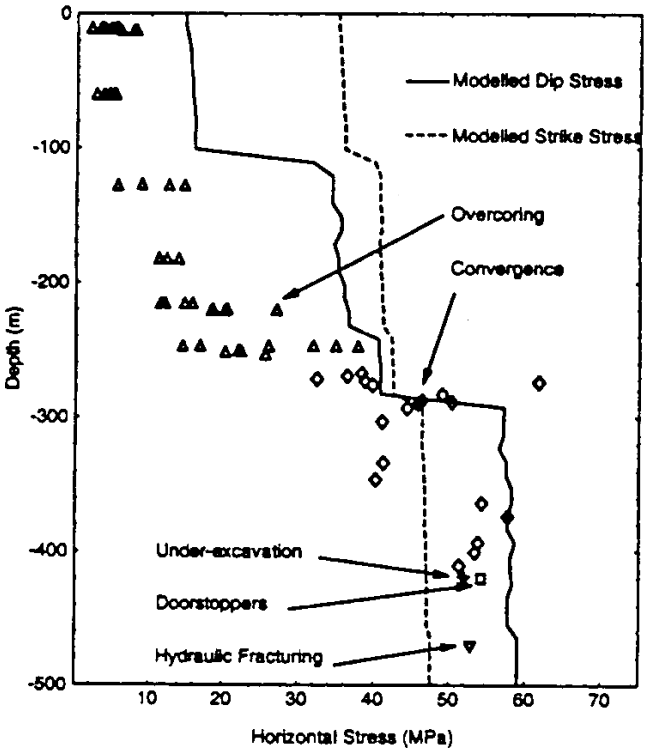

Figure 5-11. *Horizontal stresses calculated using UDEC and the measured stresses measured in the dip direction of Fracture zone 2 /from Chandler and Martin, 1994/.*

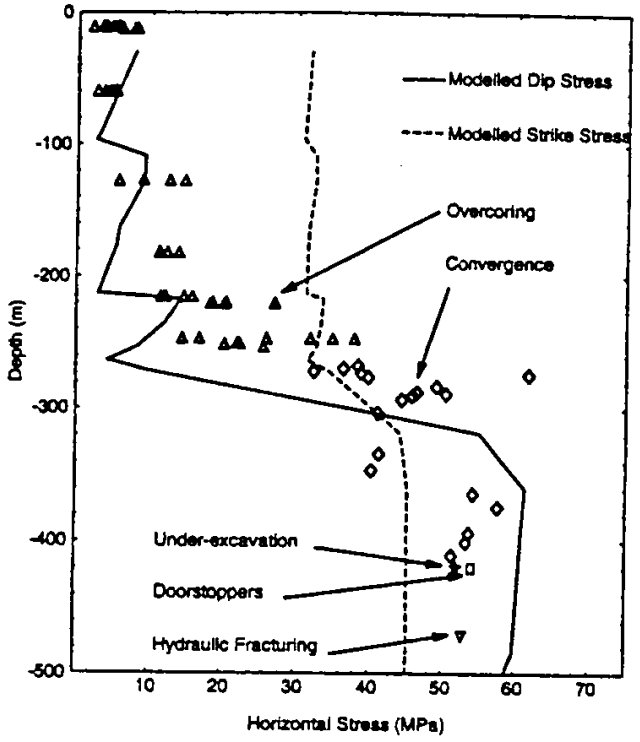

Figure 5-12. *Horizontal stresses calculated using FLAC and the measured stresses measured in the dip direction of Fracture zone 2. /From Chandler and Martin, 1994./*

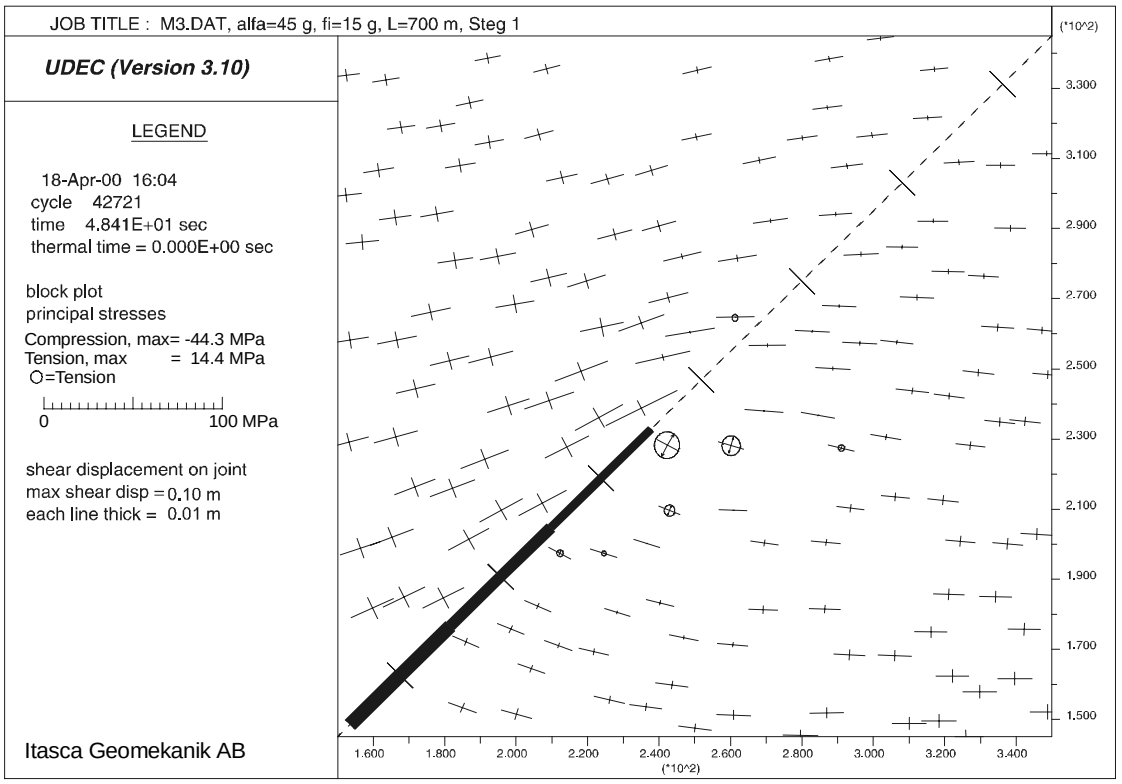

a)

Figure 5-13. *Principal stresses around upper end of the fracture in a UDEC model (two-dimensional model). The length of the lines in the cross corresponds to the stress magnitudes and the directions of the lines are the directions of the two principal stresses. The thickness of the lines at the fracture corresponds to the magnitude of the shear displacement. /From Hakami and Olofsson, 2002./*

Depending on the geometry (size and dip) of the fracture, the orientation and magnitude of the stresses and the material properties of the surrounding rock and the fracture (or fracture zone), the magnitudes of the effect on the stress regime will be different. In modelling the influence of fractures also the type of numerical model used, boundary conditions selected and the discretization of the model, may influence the results.

5.6 Influence of glacial loading

The function of a nuclear waste repository is to maintain its integrity as long as the waste is highly radioactive. It is therefore necessary to assess the stress modification at a repository site that would result from any glacial advance that might be associated with the next ice age. Rosengren and Stephansson /1990/ carried out UDEC-calculations in an attempt to simulate the rock mass response to a coming glaciation and deglaciation.

However, for the purpose of the present project whose aim is to predict the stress regime at a site before repository construction, it is the effect of *previous* glaciation periods, which is the main focus of interest, particularly if it impacts on the present state of stress. The influence of glacial loading and unloading was mentioned in Section 4.2.2.

It was noted that Gregersen /1992/ presents geological evidence for a major modification of the stress field linked to the glaciation, but that he found no evidence that any stress effects remains today. He suggests that the current stress state relates directly to the present plate motions.

6 3DEC modelling of the influence of large scale structures on the in situ stress field

6.1 Objectives

The objectives of performing numerical modelling in this project was to develop a methodology that could be used to build a descriptive *in situ* stress model in future site investigation. The numerical modelling shall help in *explaining* the stress variation found from measurement in boreholes and should also be used to support a prediction of the stresses in points *between* measurements.

6.2 Modelling approach

In the following the suggested general modelling approach is presented and some discussion on influencing factors is made. In Chapter 8 the modelling approach will be further illustrated by the modelling performed in the Test Case exercise. The computer program suggested to be used is 3DEC (Three-dimensional Distinct Element Code), Itasca /1998/.

6.2.1 Assumed geological mechanisms

A single numerical model cannot answer all possible rock mechanics questions related to hazardous waste at the same time, but all models must be built with the attempt to answer a very specific question. For this project the issue concerns the *in situ* stress (i.e. the stress before excavations), further the geological setting of interest for SKB is that of Southeast Sweden where the investigation sites are located. As has been discussed in Section 4.1.1, the rock types will be hard crystalline rocks and the region of interest is tectonically fault controlled.

During the geological history the stress state has varied, both concerning stress magnitudes and stress orientations, and faults existing today have been re-activated several times. To simulate the whole geological development would be impossible, because of the lack of detailed information and deep understanding that this would require. Therefore, a large simplification of the mechanical situation is needed.

It is in this approach assumed that the major fracture zones, that have experienced substantial slip during the geological history, are currently in limit equilibrium state with the surrounding stress field. This is not necessarily true but has been suggested by different researchers. For the performed modelling it is further assumed that a regional stress field of similar magnitudes and orientation as the *current* stress field could have caused *the latest* movements on the fractures, i.e. that the regional stress field has not changed dramatically since the latest fault movements occurred. This means that, *if* the important geometrical and property features are captured in the model, the stress distribution at equilibrium will reflect the current stress pattern.

The geological mechanism, included in the proposed modelling approach, is thus the *shear reactivation* of pre-existing major fracture faults, due to current regional stress field. The stress field redistribution that would be the result from regional compression, due to *stiffness variations* in fracture zones and rock mass, is another mechanism that may be analysed with this approach.

6.2.2 Modelling sequence

The different steps of the applied modelling sequence are illustrated in the in flowchart in Figure 6.1. The steps undertaken and the assumptions made are summarized in the following:

1. Grid geometry includes the geometry of the block for prediction The Major fracture zones incorporated are based on the idealized structure geological model provided by the geological descriptive model of the site.

1a. Fracture zones are normally modelled as planar discontinuities with finite length. A fracture zone as modelled has its ends within the computation grid and the ends are sufficiently far from the grid boundaries. The size (extension) of the fracture zones can be chosen with some support from the structure geological surface maps. The uncertainty description of geological model should be taken into account *(*i.e. the mechanical model will never become certain if the existence or characters of major fracture zones are uncertain).

1b. The blocks between the major fracture zones represent the "rock units" of the comparatively less fractured rock mass. Note that the scale chosen when selecting the major fracture zones would determine what type of minor zones that must be considered to exist inside the rock units.

2. The *in situ* stresses prior to the onset of the last shearing episode are assumed to vary linearly with depth. The equations that yield the *in situ* stresses are selected based on SICADA database and other sources.

3. The computation grid should be clearly larger than the area of investigation in question; in order to eliminate any boundary impact on the stress redistribution that takes place because of slip along fracture zones. Boundary conditions may be chosen such that no displacement is allowed all over the bottom and the vertical boundaries.

   As an alternative to 2 and 3 one could also consider a modelling sequence where the boundaries are forced to move. Also in this case the stresses will be calculated for equilibrium, but the stress level will develop due to an assumed compression (or tensional movement). In this case the *general movements* of the region are hypothesized (i.e. overall compression direction on a larger scale) instead of the general stresses.

4. Rock mass outside fracture zones is considered to be a continuum with rock mass equivalent properties based on values derived by "theoretical and empirical mechanical property models" (the different parts of the approach for developing a rock mechanics descriptive model are described in Andersson et al., /2002/. Rock mass may be assumed to consist of only one or several lithological unit. Spatial distributions of rock mass properties may be considered in the models (if there is

any reason or support for doing so). Material model for the rock mass can be chosen to be elastic, elasto-plastic (Mohr-Coulomb) or following other constitutive law, but elastic is recommended if the result is not expected to be sensitive to this choice.

5. In comparison to the stiffness of a discrete fracture of a small size obtained in the laboratory, the stiffness of a fracture zone is assumed to be reciprocally proportional to the estimated thickness of that fracture zone. The stiffness may be estimated based on stiffness estimation for the rock mass inside fracture zones, which is part of the mechanical "property model".

   It has been assumed that the shearing which is produced through the numerical simulation reflects the last, or rather the latest episode, of many slip episodes taking place all over a fracture zone over million of years elapsed since the genesis of the fracture zone. The shearing strength, i.e. the resistance against shearing movement that is mobilized when the tectonic forces are reactivated, should be selected represent the residual shear strength. Accordingly the magnitudes of cohesion as well as friction coefficient are those that are expected to emerge in the post-rupture domain. The selection of parameters may be chosen based on "property model" estimates or data from literature.

6. The numerical model is run to solve the problem for equilibrium. If needed, the model structure displaces and deforms until the model is stable. When stable, the resulting stress components (now more or less different from the initiated stress values) from each model element may be presented.

   Parallel Runs are those runs where the, often considerable, uncertainty associated with selection of input parameters – such as the geometry of fracture zones, friction angle for fracture zones etc – are incorporated into a series of computations (see Figure 6-1). Parallel Runs are performed to estimate the span of uncertainty associated with the results obtained from the different computations.

7. The results of analyses are evaluated and the need for additional modelling efforts assessed.

8. *Alternative Simulations* refer to those runs, in which an essential change has been introduced into the computations. Examples of such essential change may be a new conceptual model regarding the rock mass /fracture zone constitutive laws, introduction of sub-horizontal fracture zones into the computations, a significant change in the deformation modulus of the rock mass with depth, change in loading sequence etc.

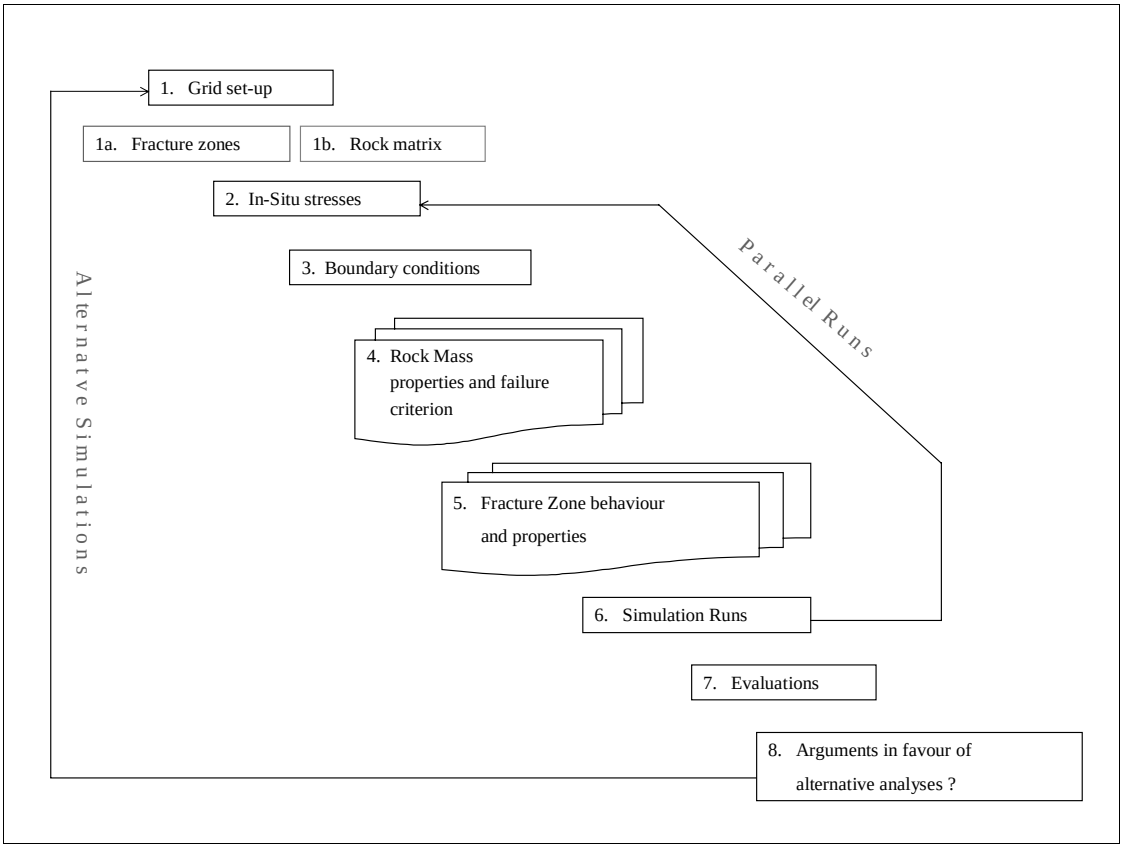

Figure 6-1. *Flowchart illustrating the different steps of a numerical modelling analysis.*

6.3 Factors influencing model results

6.3.1 Orientation between stresses and fractures

The orientation of a fracture zone in relation to the stresses applied is of vital importance to the deformation (compression, opening, shear, slip) of the zone. Therefore the zone orientation is a factor that must be considered when possible stress effects is analysed. Largest effects from a zone will be found if the zone allows for large slip and stress redistribution. This is the case when the angle to maximum stress is moderate, and the confinement against deformation is low. For Swedish stress conditions, with highest stress horizontal, this occurs when a fracture zone has a gentle dip and is entering the ground surface.

To illustrate the large stress influence from such a case, a 3DEC model was built that included a subhorizontal zone starting at mid-height of the model and entering the ground surface (Figure 6-2). Three steeply dipping fractures were also included in this model. The boundaries of the models were fixed and high horizontal stresses, simulating tectonic forces, was initiated in the model and thereafter the deformation required to reach equilibrium was calculated. Figure 6-3 shows the calculated stress magnitudes along two vertical lines, simulating two measurement boreholes, intersecting the subhorizontal fracture zone at two different depths. In the same ways as was shown with the 2D-analysis for the URL case (see Section 5.5), the stress magnitude experiences an

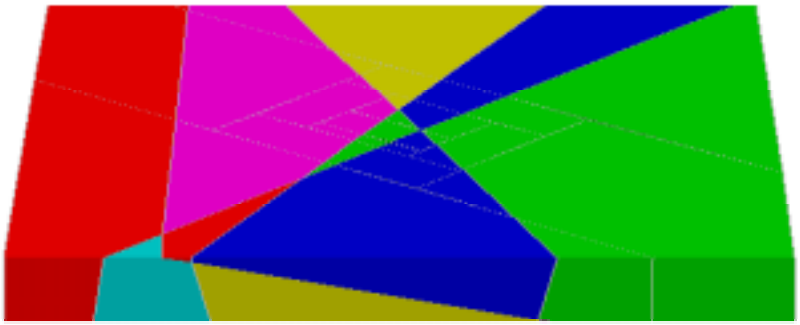

a)

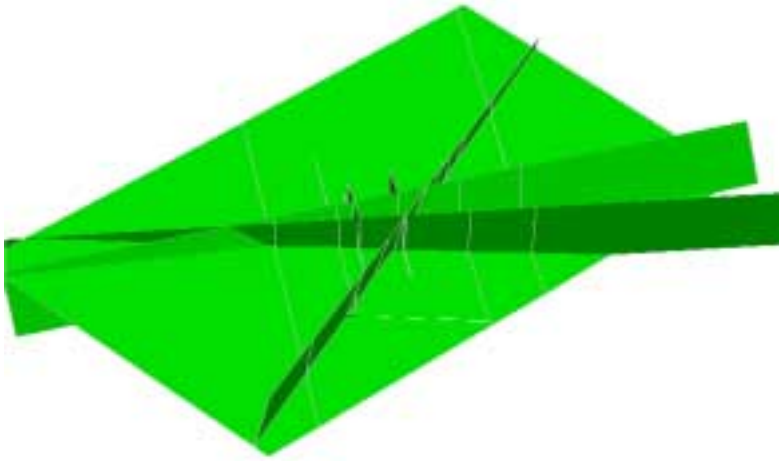

b)

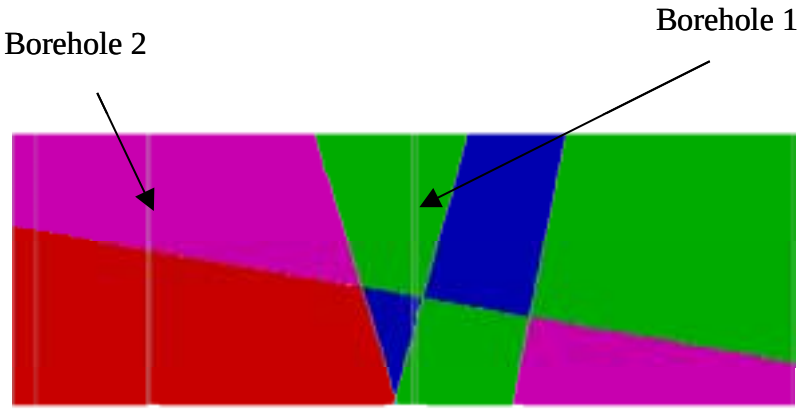

c)

Figure 6-2. *3DEC model including a subhorizontal structure. a) Isometric view. b) Fracture zones planes. c) Vertical section.*

instant increase at the depth of the fracture zone (stress jump). The explanation is that stresses have been released in the rock mass above the fracture zone during the slip. The magnitude of the jump will be dependent on the amount of the shear and this will depend on the relation between applied load (magnitude and orientation) and the properties of the fracture zone (geometry, orientation, strength).

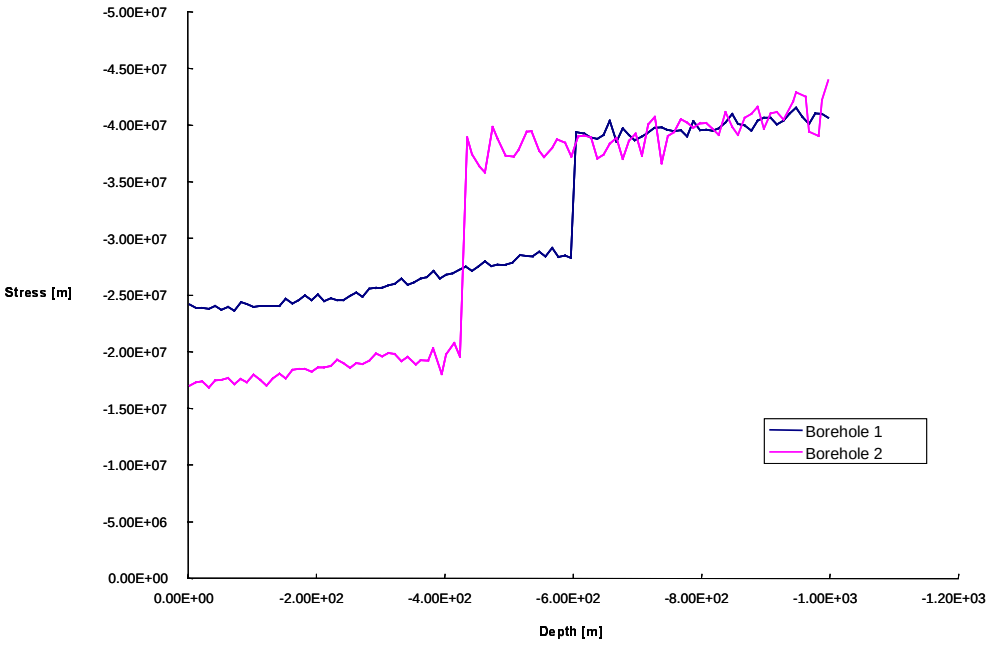

Figure 6-3. *Major principal stress as a function of depth along two "boreholes" for 20° assumed friction of the fracture zone planes. See Figure 6-2.*

Not only the stress magnitude but also the stress orientation will change in case of a slip as in this example. The principal stress trajectories turn to become parallel and perpendicular to the zone.

It should be noted that the shear movement may not only be towards ground surface such as in this example but the shear slip may take place in any direction and also at depth (see Figure 6-4). When both the maximum and the minimum principal stresses are horizontal the largest shear stress component also lies in the horizontal plane. Therefore, when a fracture plane is steep but strikes in the direction of the large shear stress it may lead to a strike-slip movement, if the shear strength of the fracture is exceeded. The use of a three-dimensional numerical modelling has the advantage that several fracture zones, with arbitrary orientation, can be analysed in the same model.

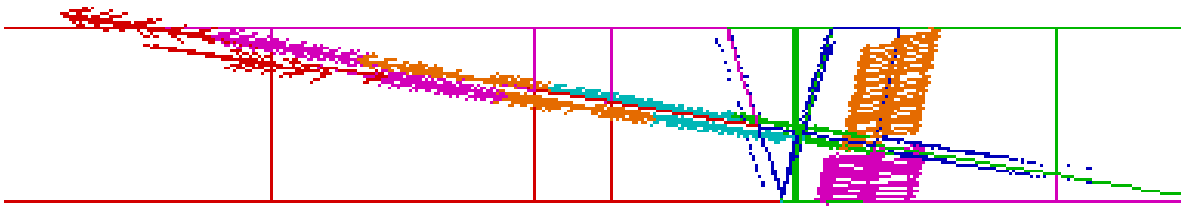

Figure 6-4. *Shear displacement arrows projected on a vertical plane through the mode (the colours of arrows represent different amount of displacements). Both a steep and gently dipping fracture zones has been sheared but in different directions. For the gently dipping fracture that enters the ground surface the displacement is largest closest to the surface.*

6.3.2 Fracture zone strength

The shear strength of a zone will obviously be decisive for the calculated displacements and stress changes. Any material model used for a fracture zones is a strong simplification, because the actual shear behaviour is very complex for most fracture zones. However, accepting a “Coulomb slip” model as a reasonable simplification of the overall behaviour, the strength is determined by the cohesion (c) and the friction angle (ϕ) (see also Section 3.5).

An example of this influence in a numerical model is given in Figure 6-5 (a 3DEC model of the Test Case which will be described further in Chapter 8). In the model TC12, where the friction angle of the fracture planes (representing fracture zones) is lower than in model TC11, all the three principal stresses are influenced at the horizontal scanline intersection with fracture zones. In the model with higher friction the stresses are the same along the scanline, because a fracture zone that does not slip will be able to transfer the shear stress to the surrounding rock mass.

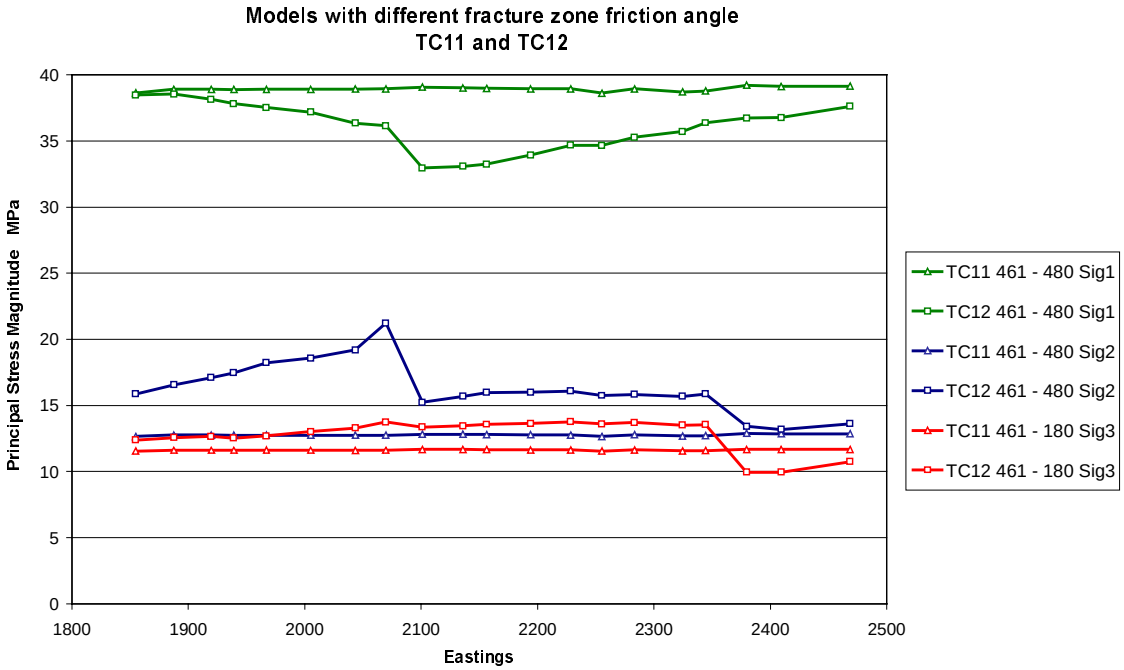

Figure 6-5. *The two models TC11 and TC12 (3DEC models of the Test Case, see Chapter 8) are identical apart from that the friction angles of the fracture zones are 25° and 15°, respectively. The diagram shows calculated principal stress magnitudes along horizontal lines inside the two models. For TC12 it can be seen that slip on the fractures (at about 2080 and 2360) gives influence on the stress field, whereas no influence is seen for TC11.*

6.3.3 Fracture zone size

The magnitude of the shear displacement of a facture (or fracture zone) at slip will depend also on the size of the fracture (with size is here meant extension). The displacement will be largest at the mid distance from the edges. The influence on the stress, however, will depend on where the stress is observed in the model. If for example the interesting point is close to fracture ends, certainly the stress will be different compared to if the fracture end was located at a greater distance from the observation point. In the Test Case, however, the area of interest is smaller than the fracture zones, and the effect of fracture ends on the stress distribution was small, see Figure 6-6. It is thus important that the geometrical features in the area is captured as well as possible but different parts of the geometrical (geological) models will be of larger importance. If a certain zone is intersecting (or inside) the area of interest then naturally the different properties, such as size (the extension), of this particular zone will be the most critical.

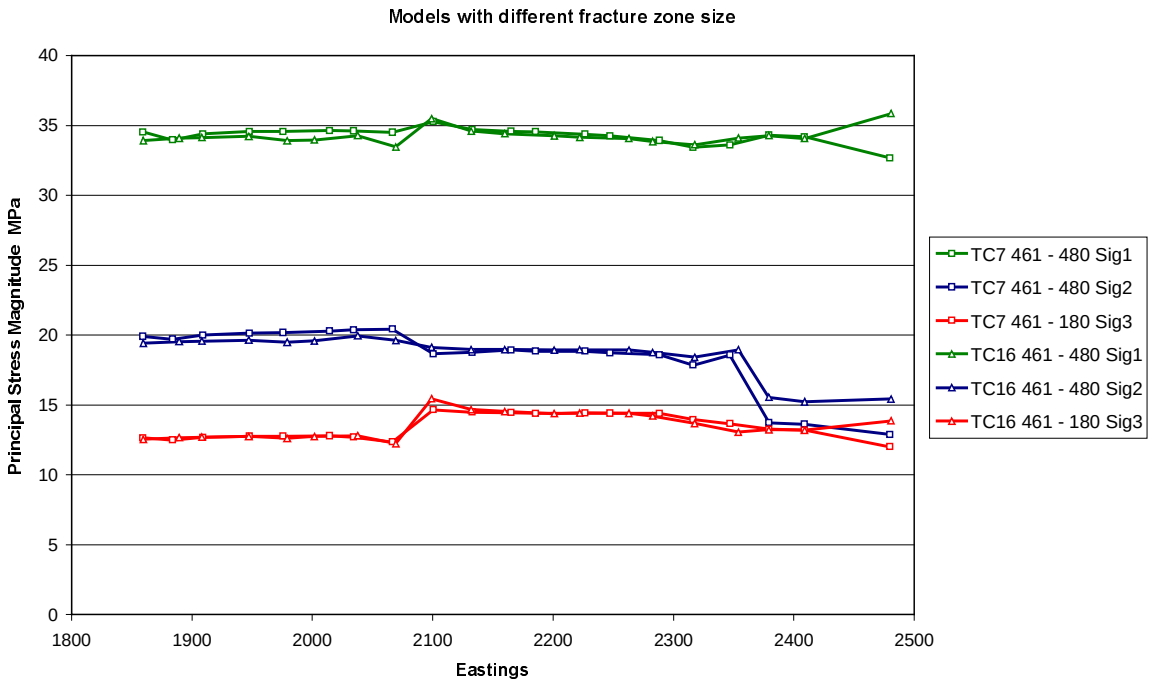

Figure 6-6. *Comparison between results in two models where the region outside the prediction block, which determines the size of the three largest fracture zones, are different. In model TC16 the zone NE1 is about 50% longer, compared to in model TC7. The scanline intersect zone NE1 Easting coordinate around 2350. The intersection with NE2 is at about 2080, but this zone terminates against other zones and its size is therefore not changed. It can be noted that the stresses calculated are fairly similar between the models in this area.*

6.3.4 Fracture zone stiffness

The fracture zone stiffness determines how much the zone deforms elastically due to stress change. If the modelling is performed with boundary displacement (compression or extension of the block), differences in stiffness inside the model will give rise to corresponding stress differences. Therefore it may be worthwhile to consider if there are any reasons to believe that different parts of a zone or different zones are expected to have different stiffness.

It is obviously very difficult to estimate the "equivalent" stiffness of a fracture zone (assuming the properties are smeared out equally over the whole zone width), because the sizes of the structures prevent actual *in situ* testing. Therefore, the selected model stiffness suffers from a large uncertainty and must be based on reasoning and laboratory information from fractures of different scale. This uncertainty makes consequently absolute values off calculated displacements (depending on both stiffness and strength) in large-scale numerical models less interesting than the qualitative pattern.

By selecting stiffness parameters according to the geological description of the fracture zone (and the rock mass between them), the numerical model is expected to get a stress pattern more close to the actual. A fracture zone with a large width and thick core of soft material should be given a lower stiffness, both in normal and shear direction, than a thin zone with fractures with stronger infillings. Also, information about fracture frequency, persistency and connectivity could be used as a basis for the selection of stiffness and strength parameters. If, for example, a zone is expected to have a significantly different stiffness character close to the ground compared to at depth this may be simulated in the numerical model and will give a different stress profile with depth.

7 In situ stress measurement data

In the site investigation program for the future repository several different measurement methods may be applied. The two main methods that have been suggested for the planned measurement program are hydraulic fracturing method and overcoring method /SKB, 2001/. In the following sections these two methods will therefore be briefly commented on to indicate the achievable accuracy in the indata for stress modelling#. For further description and details on stress measurements methods see for example Amadei and Stephansson /1997/.

7.1 Hydraulic fracturing method

One common way of measuring the magnitude and orientation of *in situ* stresses in rocks is to use the "hydraulic fracturing method". With this method a section of a borehole is pressurized with water until a fracture is created in the surrounding rock. The pressure and inflow to the section is continuously measured during the pressurization. Assuming that the *in situ* stress determines at what fluid pressure the rock around the borehole fractures, the stress is determined from the flow-pressure registrations. The method is used to determine the stresses in the plane perpendicular to the borehole axis, normally in the horizontal plane because most holes are vertical, and it must be assumed that the borehole is parallel to a principal stress direction.

This method directly measures the shut-in (when fracture closes) and reopening (when fracture reopens) pressures, which are related to the stress normal to the induced fracture. If the fracture is oriented perpendicular to the minimum horizontal stress, the normal stress of the fracture is a direct measure of the minimum horizontal stress. The weakness of the tradition interpretation of this method is that the *maximum* horizontal stress must be inferred from the minimum stress value based on a simplified concept of the geometry, a circular hole in intact rock. In reality, during the test the geometry changes to circular hole *and* the induced fracture. The water flows into the induced fracture and the pressure will be applied also from inside the propagating fracture. The stiffness of the fracture will be different from the surrounding intact rock.

Rutqvist et al. /2000/ have analysed this complicated hydraulic fracturing loading situation with coupled hydro-mechanical numerical models. They have shown that for most practical situations there is actually no correlation between the apparent reopening pressure (pressure measured in the borehole) and the maximum principal stress around the hole. The performed modelling also showed that there is a clear correlation between apparent reopening pressure and the *minimum* principal stress.

The explanation to this result is the fact that the fracture itself will make the stress situation deviate from that assumed in the equations that are normally used to determine the maximum horizontal stress. Rutqvist et al. /2000/ showed that for a numerical model with a minimum horizontal stress of 10 MPa and maximum horizontal stress 10 MPa, the calculated reopening pressure was 11 MPa. For an identical case but with the

maximum horizontal stress changed to 30 MPa, the reopening pressure was also 11 MPa, i.e. the measured pressure was not influenced.

In another numerical model where both the 'minimum' and 'maximum' horizontal stresses were 50 MPa, the calculated reopening pressure was 62 MPa. It was found that if the maximum horizontal stress was increased three times to 150 MPa the reopening pressure was slightly lowered to 60 MPa. If a very low well-bore storage was assumed (corresponding to the storage produced by the compressibility of water in a half-a-meter long packed of section of the borehole) the corresponding reopening pressures (50 and 150 MPa applied maximum stress) became 40 MPa and 30 MPa, respectively. Thus the reopening pressure for this case actually decreases for an increase in maximum horizontal stress. This is contrary to what is normally assumed.

Similar observations, based on results from field tests, which argue against the use of hydraulic fracturing for *maximum* horizontal stress determination, have also been reported by other researchers /Cheung and Haimson, 1989; Lee and Haimson, 1989/. However they did establish that the hydraulic fracturing method is able to predict the *minimum* principal stress to within an accuracy of 25%. The results from Rutqvist et al. /2000, op. cit./ are also supported by theoretical studies by Morita et al. /1996/, Gou et al. /1993/ and Ratigan /1992/.

Because of the arguments presented above, the *maximum* horizontal stress values determined in the traditional way from the hydraulic fracturing method are considered very unreliable. The results from hydraulic fracturing on maximum stress magnitudes are expected to have systematic errors and could therefore be misleading in a site investigation. The advantages and drawbacks of the different stress measurement methods should be considered when the measurement program for the sites is established.

7.2 Overcoring method

The overcoring technique to determine *in situ* stresses utilizes the principle of stress relief. The method involves measurements of the strains in a piece of rock when it is released from the surrounding rock. Strain gauges are glued inside a small diameter borehole at the desired depth and a hollow core is obtained when a larger diameter core is drilled around the first hole. During this "overcoring" the strains in the gauges of the relieved core is measured continuously. The *in situ* stresses are then calculated by using the measured strains and by assuming elastic behaviour of the rock. The elastic properties of the rock are determined by performing a biaxial loading test on the hollow core. The different steps in the overcoring measurement procedure are explained in more detail in for example Amadei and Stephansson /1997/ or Klasson et al. /2001/.

Using the overcoring method all three principal stresses can be determined because strain gauges are glued to the core in different direction. Therefore overcoring is a method that can be used also to determine the vertical stress magnitude. This an advantage with overcoring methods compared to hydraulic fracturing.

The weakness of overcoring lies in the determination of the elastic properties (Young's modulus and Poisson's ratio), that is required in the interpretation of data. The biaxial testing on the hollow core is normally made up to a stress level that may be different

from the actual stress level at the measurement point /Klasson et al., 2001/. In cases when the core does not have a linear response to the biaxial loading the determination of the Young's modulus is ambiguous and introduces an uncertainty, because the whole method is based on purely elastic and isotropic behaviour. At high stress levels the stress release when overcoring may introduce microcracking in the core around the gauges such that a correct interpretation of the measurement results of this reason becomes difficult /Martin and Christiansson, 1991/. Also some cores do show some degree of anisotropy and this will give an additional source of error in the results.

If the rock is very weak or fractured no reliable measurements can be performed at this point. For both hydraulic fracturing and overcoring methods some bias in the results may therefore arise if the quality of the rock in the area is very heterogeneous. However, the results would still reflect correctly the stresses at the measurement locations.

The volume of rock involved in the overcoring measurements is small ($\approx 1\ dm^3$). Since actual stresses will vary from point to point the scatter in the result will be larger for a method that averages over a smaller volume. Unfortunately, there are no stress measurement techniques that can measure stresses at considerably large scales. However, there is no scale effect in the stress as such, i.e. the average result from a small scale measurement method can be used to determine the mean stress in an area, if the number and spread of measurements in studied area is large enough. Therefore overcoring measurements should be performed at several points, fairly close to each other, to provide a sufficient base for the determination of a mean value at this level. How many reliable measurements that need to be carried out depend on the accuracy desired, the site geology and the difficulties encountered when conducting the measurements /Amadei and Stephansson, 1997/.

8 The Test Case

The methodology for developing a rock mechanics descriptive model was tested in an exercise called the "Test Case". The Test Case included an attempt to make a "property model" (empirical and theoretical approaches) and a "stress model" using the methodologies that was developed under the course of the project. A detailed description of the Test Case exercise is given in Hudson et al. /2002/ and the results are summarized in Andersson et al. /2002/. In this chapter the work performed in the stress model part of the Test Case is presented. The work includes the following parts:

- An initial stress prediction of state of stress, based on data density corresponding to that would prevail *before* a Site Investigation.
- Analysis of stress measurement data and other information provided from the Test Case area, which is the area around the Äspö Hard Rock Laboratory. The information was limited to mimic the type and amount of information available *at* a Site Investigation.
- Numerical models (3DEC) of the study area were built and the potential influence on the *in situ* stress field from the geological structural elements was analysed.
- Comparison between different numerical models and the measurements.
- An updated prediction based on measurements, modelling and site specific information, including an estimation of uncertainty and spatial variability of the *in situ* stress.

8.1 Initial stress prediction based on common data base

8.1.1 Stress magnitudes

The initial stress prediction is based on a Swedish stress measurement database /Martin et al., 2001/ and on data extracted from relevant literature.

Figure 8-1, Figure 8-2 and Figure 8-3 show the data from Martin et al. /2001/ for the horizontal and vertical stresses, respectively. Note that all data that were from Äspö Hard Rock Laboratory were removed from the database, because at this stage the estimation should correspond to the stage before site investigations. Further, only the data in the database collected from depths between 50–600 m were included. (The type of measurement and the quality of measurement in the provided database was not investigated within this project but such investigation could be part of a general approach.)

The reason why the very shallow and very deep data were not included was that the aim in this case was a prediction in "the 550 m block" (a cube with 550 m sides around the ÄHRL), and thus this prediction should be based on the most relevant data. There is no reason to believe that the stresses should be linearly depth-dependent to very great depths, but more realistic is to expect the depth-dependency to change with depth.

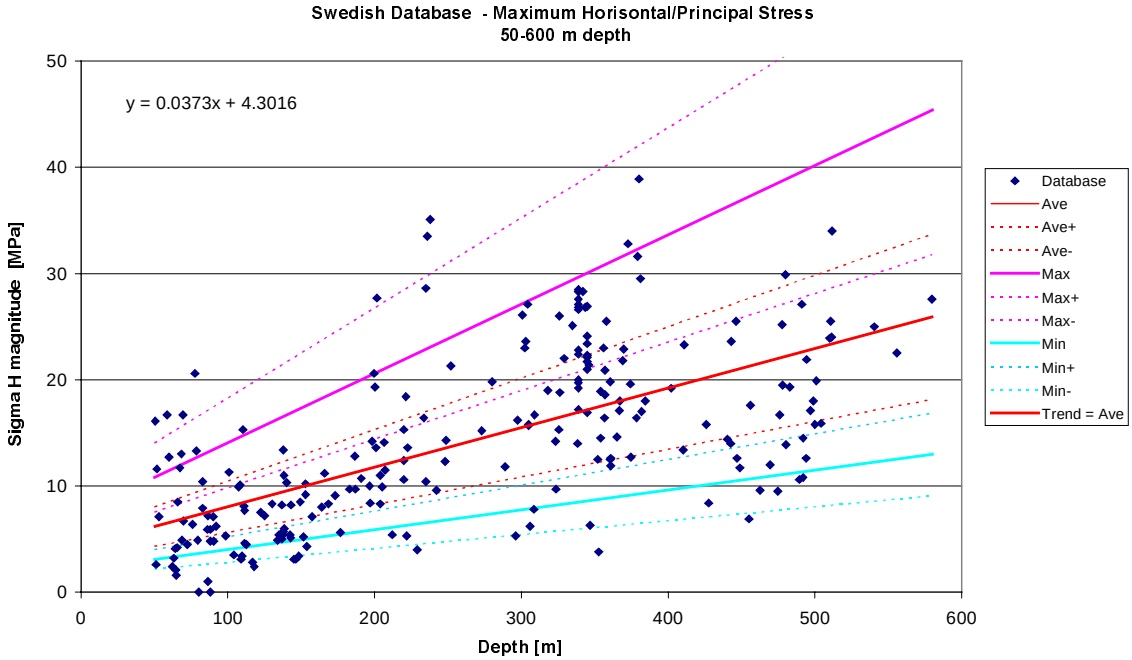

Figure 8-1. *Maximum horizontal stress vs. depth. Data from measurements in gneiss, granite and diorite, performed at 50–600 m depth in 27 different boreholes at different locations in Sweden /based on Martin et al., 2001/. The lines correspond to the selected stress model with the uncertainty span (solid lines) and spatial variability around the mean (dotted lines), see Section 8.1.3. The red line is the centre value for the predicted span in the model for the mean σ_1, which is identical to the best-fit linear trend of the data (equation in corner).*

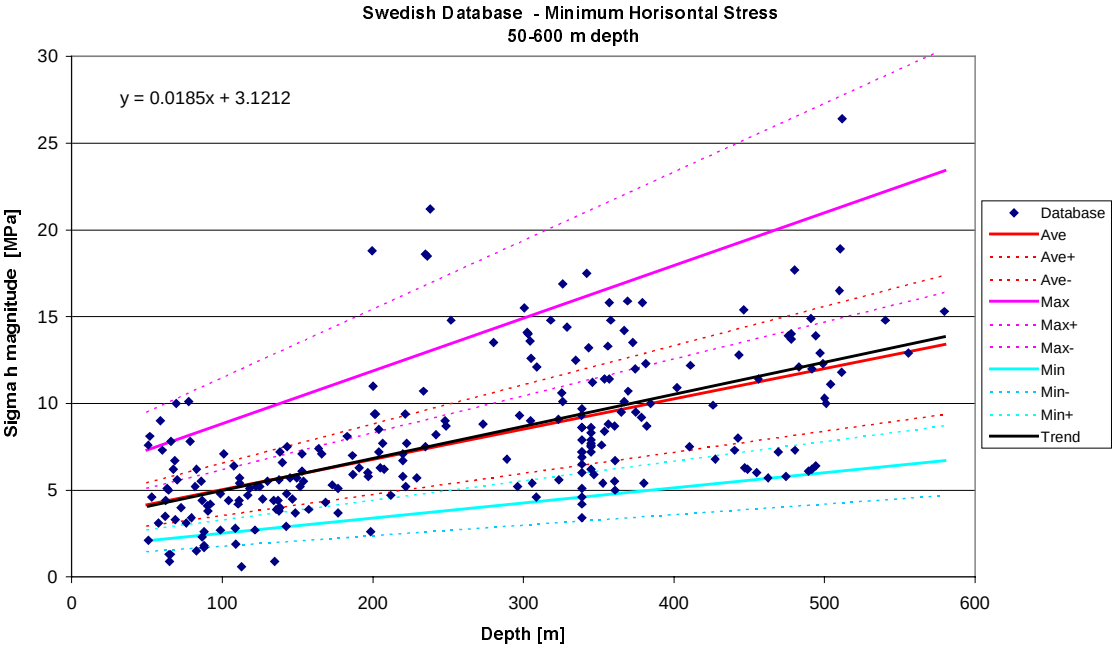

Figure 8-2. *Minimum horizontal stress vs. depth. Data from measurements in gneiss, granite and diorite, performed 50-600 m depth in 8 different boreholes at different locations in Sweden /based on Martin et al., 2001/. The black line is the calculated best-fit linear trend (equation in corner). The other lines illustrate the selected stress model including the uncertainty span and the spatial variability span, see Section 8.1.3)*

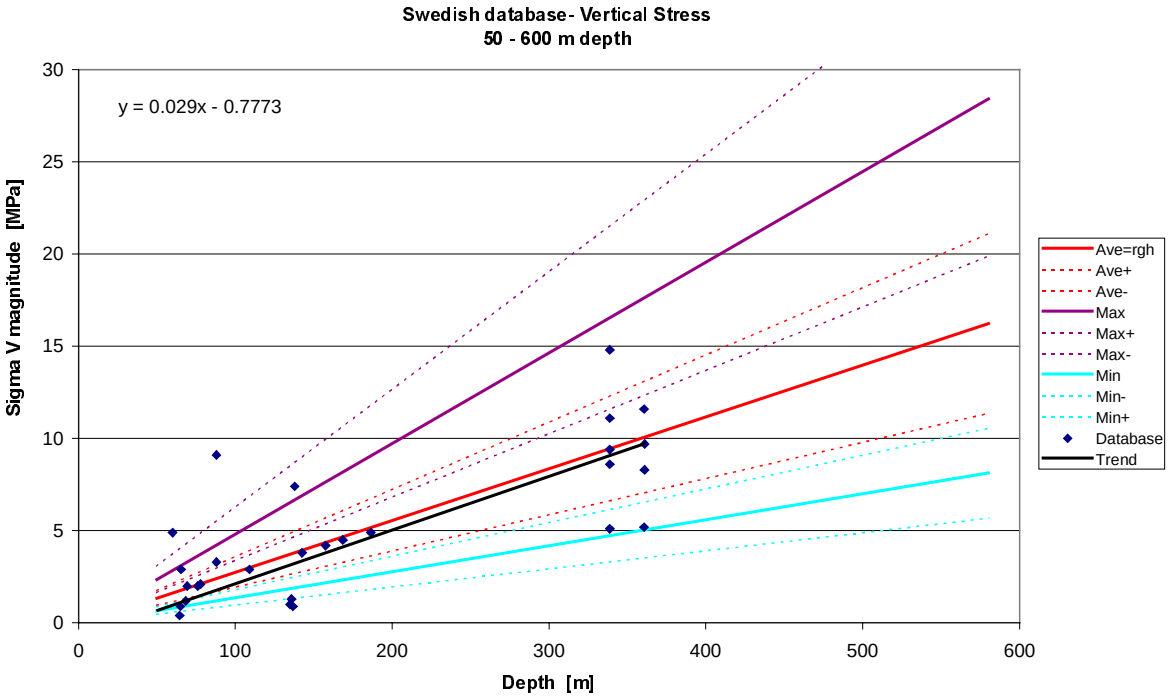

Figure 8-3. *Vertical stress vs. depth. Data from measurements in gneiss, granite and diorite, performed at 50–600 m depth in 17 different boreholes at different locations in Sweden /based on Martin et al., 2001/. Black line is the best-fit linear trend for the data (equation in corner) The coloured lines correspond to the initial model for* σ_2 *for the Test Case which is equal to the calculated overburden, (see Section 8.1.3 and 8.1.4.)*

At very shallow depth the stresses measured are more likely affected by topography and excavations. Also, the large amount of shallow data would have dominated the calculation of best-fit functions. In the absence of any other clear trend, a linear equation based on the data between 50–600 m depth was here judged to be the most appropriate to use.

In the diagrams (Figure 8-1, Figure 8-2 and Figure 8-3) the best-fit linear trend-line for the data are shown with a solid line. Assuming that the database is representative for the whole Sweden, and thus also for the Äspö area, this line was chosen as the most probable estimate (denoted Ave.) for the mean stress magnitude as a function of depth in the 550 m block (at this stage when data from site is not "available"). The pink and light blue lines correspond to the estimated uncertainty span, i.e. it is judged that the *mean* stress at a certain depth at this site will lie within the span from the pink to the blue line. *Around* this mean value the stress is expected to vary from point to point within the block, at the same depth level, due to the natural (actual) stress variation caused by structural influences at different scales. The prediction of this local spatial variation on a smaller depicted in the diagram with dashed lines in the same colour as for the mean.

The "first initial model", based on no site-specific data, for the stress magnitude has an "uncertainty and variability span" such that 95% of the selected measurements from the database are covered by the total span. For further description of the reasoning behind the chosen uncertainty and variability parameters, see Section 8.1.3.

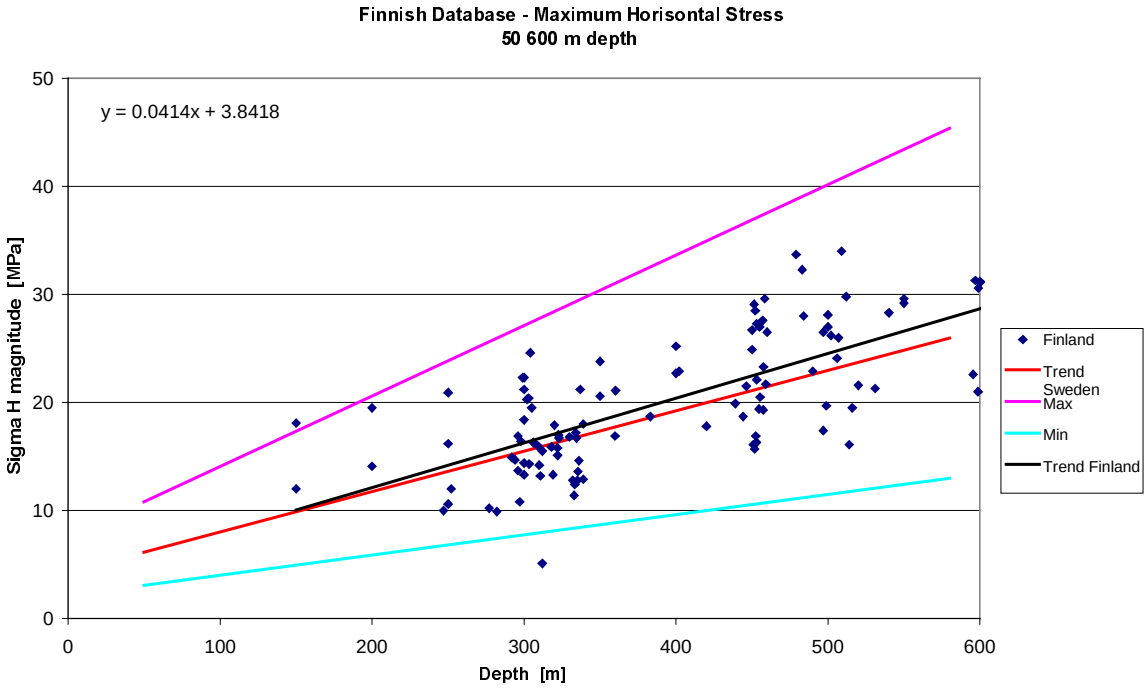

Figure 8-4. *Maximum horizontal stress vs. depth. Data from measurements in 15 different boreholes in Finland /based on Martin et al., 2001/. The solid black line is the calculated best-fit linear trend for the Finnish data (equation in corner). The solid red line is the calculated best-fit linear trend for the Swedish data, selected as a model for the average predicted value. The pink and blue lines represented predicted maximum and minimum values for the mean stress selected based on judgement, see Section 8.1.3 and 8.1.4.*

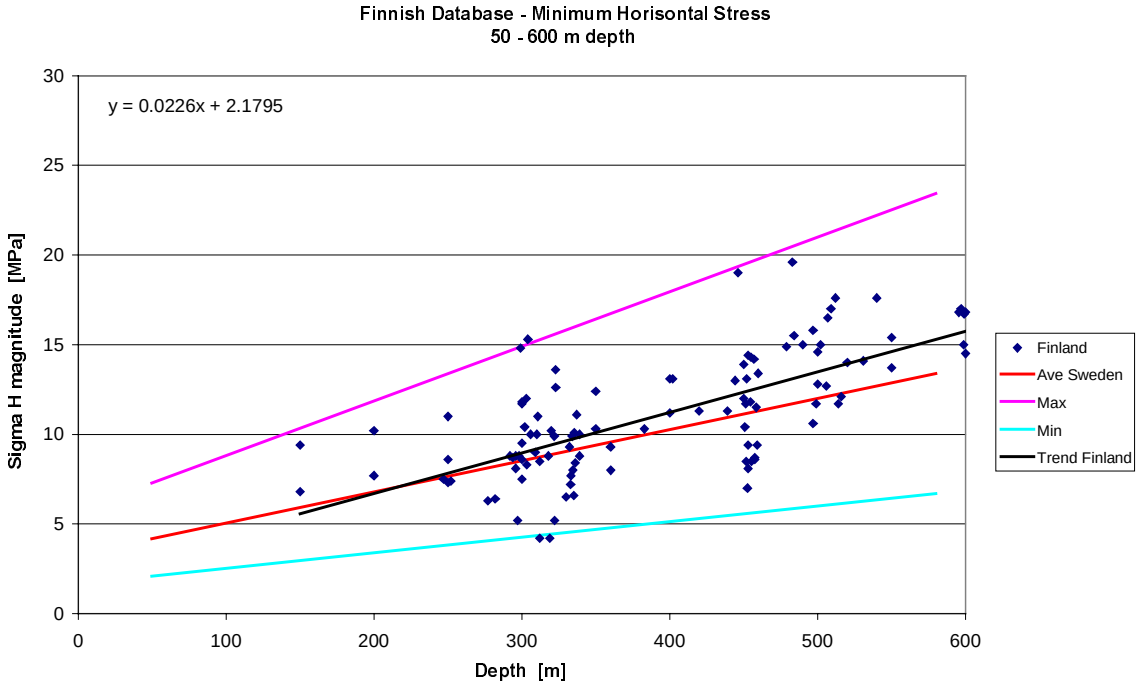

Figure 8-5. *Minimum horizontal stress vs. depth. Data from measurements in 15 different boreholes in Finland /based on Martin et al., 2001/. The colour lines correspond to the initial stress model selected for the Test Case area, see Section 8.1.3 and 8.1.4*

Another source of information is a stress measurement database from Finland. Since Finland and Sweden are both located in the geological unit of Fennoscandia, they are expected to have similar *in situ* stress conditions. In Figure 8-4 and Figure 8-5, Finnish data on maximum and minimum horizontal stresses are shown, from Martin et al. /2001/. Both the best-fit linear trend lines for these Finnish data and the best-fit linear trends from Swedish data are given in the diagrams. The comparison indicates that the differences are fairly small, and this supports the assumption that a general database is appropriate to be used as a first prediction for the area of interest.

8.1.2 Stress orientations

As the database used in Section 8.1 did not contain any information about stress orientation, the orientation for the maximum principal stress has been estimated from a database published by Stephansson et al. /1991/. The orientation was measured on a map, at a few points presented for the southeast of Sweden. The orientation for maximum horizontal stress varied between 119° and 136° (clockwise from magnetic north), corresponding to 131° and 148° in Äspö local coordinate system. This direction also coincides with the general NW-SE stress direction for the southern and central Fennoscandia as observed from stress measurements. Also, focal mechanisms data from Sweden, Norway and Denmark indicate a NW-SE orientation of the maximum horizontal stress /e.g. Slunga et al., 1984; Bungum et al., 1991; Gregersen et al., 1991; Müller et al., 1992, cited in Ask, 1996/.

Another approach to estimate the most probable stress orientation, without stress measurement from site, is to relate the stresses to the orientation of water conducting fractures. It may be hypothesised that the maximum principal stress should be oriented parallel to such fractures, because the lesser normal stress on those fractures would then be an explanation for the higher conductivity observed.

Water conductive fractures have been identified in boreholes KAS02 and KAS06, based on borehole logs. The results are reported by Sehlstedt and Stråhle /1991/. They classified the observed fractures in confidence classes 1–4. Only certain (class 4) water conducting fractures were used, which were 5 fractures, only found in KAS06 at 400 and 560 m depth. The average trend of these conductive fractures was 120° (assuming that this orientation is related to the true magnetic north). The Äspö local north is 12° west of magnetic north, and the corresponding orientation for the conductive fractures in the local system is thus 132°. The estimation on the average trend of maximum horizontal stress is taken as the mean value 136° (note that this is in Äspö local coordinate system).

8.1.3 Description of uncertainty and spatial variability parameters

The uncertainty and the spatial variability in the stress prediction will be described using two “spans” for each prediction, ± u and ± v, respectively.

The u (uncertainty) parameter should correspond to the uncertainty in the estimation of the *mean* stress in a rock unit. It was judged relevant that the uncertainty be calculated as a fixed percentage of the prediction value (mean value). The mean value should correspond to the most probable (expected) value. The reason for this was that, at least for overcoring measurements, the errors are dependent on the magnitude, i.e. the absolute measurement accuracy is less at large stress levels than at lower.

The choice of an uncertainty span that is proportional to the predicted mean value also corresponds to the idea of having a depth dependency in the predicted stress magnitude. If the depth-dependency factor were slightly wrongly estimated, this would cause a much larger absolute error for points at depth compared to the error at shallower depths.

The second span, v, corresponds to the expected spatial variability of *in situ* stress around the mean (magnitude and orientation). The cause of a local variability of both stress magnitude and orientation is the inhomogeneous character of rock mass at all scales. Even the most competent rock will include fracture of some size and differences in the rock type.

The v-parameter is not meant to reflect the lack of knowledge or lack of data, but should reflect the expected actual variation in the parameter from point to point inside the volume it represents. Therefore, the value of the v-parameter will be dependent on the scale considered, i.e. how large rock volume that relates to each value. In a very large rock unit the distance between different points may be larger and also the mechanical properties of the rock mass inside may be expected to vary more.

Based on the measurement database from different locations in Sweden it was concluded that the single stress values might deviate fairly much from the average trend (see Figure 8-1). In particular it seems that the value can be larger than that of the best-fit trend. It was judged reasonable that most of the Swedish database values should fall inside the total uncertainty and variability span and a minimum of 95% of the data was selected as a reasonable criterion. (Remember that the data behind the database was, of time limitation reasons, not studied closer such that it was detected which data came from the same region, borehole, same method etc.)

Based on the different considerations mentioned above the u and v parameters were estimated (not calculated). For prediction of magnitude, the u-parameter was in *the initial stage* selected to be 75% on the maximum side and 50% on the minimum side, for all principal stresses. The v parameter, for the initial stage, was selected to be 30%. Less than 5% of the data points in Figure 8-1 lie outside the total (uncertainty and variability) span of the selected model.

Since the two trend indications, from the database and from the core logs, fit fairly well to each other, the u-parameter was selected to ±15° for prediction of trend. Since the trend of the maximum principal seems from the database to be fairly stable this also indicate that the dominating factor behind the stress field is the tectonic compression, and this in turn implies that the plunge of the maximum principal stress should, in a large-scale perspective, be more or less horizontal. The uncertainty for the plunge is therefore estimated to be small, ±10°.

Locally, i.e. comparing different single measurement points within the 550-m block, the orientation (both trend and plunge) is expected to vary around the mean value within ±15°. This variation is expected because of influence from fractures of different sizes and the heterogeneity in mechanical properties within the block. This particular number was not selected based on any strict calculation; rather it was judged that a span of 30° would cover most of the variation seen in the stress databases.

8.1.4 Initial prediction for the 550 m block

For the initial prediction linear depth dependence was chosen for the stress magnitude, because there was no general knowledge at this stage of some mechanism that would suggest a different distribution. Also, the uncertainty estimations between different parts of the block were not varied at this stage.

The initial prediction includes a linear variation with depth for all principal stresses (see Figure 8-1 to Figure 8-5). The prediction equations apply to the whole 550 m block of the Test Case. With "initial" is referred to prediction made at a stage where no measurement results from the site are available and no geological geometrical model is established. Thus, this prediction would be the same for any site in Sweden (but will depend on the databases available at the time for prediction).

The initial stress prediction for 50–550 m depth is as follows:

$\sigma_1 = 0.0373(-z)+4.3$ [MPa] $u_{upper} = 75\%$, $u_{lower} = 50\%$, and $v = 30\%$ (8-1)

$\sigma_2 = 0.027(-z)$ [MPa] $u_{upper} = 75\%$, $u_{lower} = 50\%$, and $v = 30\%$ * (8-2)

$\sigma_3 = 0.0174(-z) +3.3$ [MPa] $u_{upper} = 75\%$, $u_{lower} = 50\%$, and $v = 30\%$ * (8-3)

where z is the depth coordinate (negative downwards), compressive stresses are positive, u_{upper} and u_{lower} are the estimated uncertainties at upper and lower sides of the prediction, respectively, and v is the local spatial variability span. (*Due to the depth-dependence and uncertainty in the estimation, the intermediate and minimum stress may change in orientation with depth, i.e., the equation for σ_2 may give a lower value than the equation for σ_3 and vice versa).

8.1.5 Initial prediction for the Target block

The stress prediction model presented above for the 550 m block has been applied on the "Target volume" for the Test Case. The Target volume consists of a number of smaller "cubes" (30x30x30 m) inside the 550 m block chosen to enable comparison between the description model from the Test Case project and a description model based on more data. The Target volume is located at the experimental level of the Äspö Hard Rock Laboratory /refer to Andersson et al., 2002/ for more detail on this). The initial result for the stress magnitudes inside the Target volume are given in Table 8-1. Since the stress magnitudes are only dependent on the z-coordinate in this model, the predictions are given for four "cube groups" corresponding to the four different cube levels in the target block.

In Table 8-2 the orientations of the estimated stresses in the target volume are presented. Since the three principal stresses are orthogonal in each point, only three parameters are needed to define the orientation. It was chosen to give trend, β, and plunge, α, for the maximum principal stress, σ_1, and the plunge of σ_2. From these values the trend of σ_2 and the trend and plunge for σ_3 may be determined. The values u and v correspond to the uncertainty and variability estimates described in Section 8.1.3.

Table 8-1. Stress magnitudes according to initial stress model in Target area.

Cube ID	Rock Unit	Cube Centre z	σ_1	Min-Max (u)	±v	σ_2 *	Min-Max (u)	±v	σ_3 *	Min-Max (u)	±v
		(m)	(MPa)	(Mpa)	(%)	(MPa)	(Mpa)	(%)	(MPa)	(Mpa)	(%)
1–120	Any	-395	19.0	9.5–33.2	30	10.2	5.1–17.9	30	10.7	5.4–18.7	30
121–240	Any	-425	20.2	10.1–35.4	30	10.7	5.4–18.7	30	11.5	5.8–20.1	30
241–360	Any	-455	21.3	10.7–37.3	30	11.2	5.6–19.6	30	12.3	6.2–21.5	30
361–480	Any	-485	22.4	11.2–39.2	30	11.7	5.9–20.5	30	13.1	6.6–22.9	30

* The principal stress in this direction may in some cases be σ_3 instead of σ_2.

Table 8-2. Stress orientations according to initial stress model in Target area.

Cube ID	Rock Unit	Cube centre β_1 (m)	σ_1 Trend β_1 (°)	±u (°)	±v (°)	σ_1 Plunge α_1 (°)	±u (°)	±v (°)	σ_2 Plunge α_2 (°)	±u * (°)	±v (°)
1–120	Any	-395	136	15	15	0	10	15	0	45	15
121–240	Any	-425	136	15	15	0	10	15	0	45	15
241–360	Any	-455	136	15	15	0	10	15	0	45	15
361–480	Any	-485	136	15	15	0	10	15	0	45	15

* The principal stress in this direction may in some cases be σ_3 instead of σ_2.

8.2 Site specific information

8.2.1 Geological information from Test Case site

The geological model provided for the Test Case includes five major fracture zones inside the study volume /Hudson (ed.), 2002/. Relating the geological model and the RVS geometrically simplified model to the so called “550-m block” (a cube around the ÄHRL with 550 m side length) it may be noted that:

- Totally five fracture zones intersects the 550 m-block, dipping 70°–90°.
- The 550 m-block in RVS consists of six “rock mass units” and five “units” corresponding to the fracture zones.
- The so-called “Target block” (a part of the 550 block situated around the experimental level at the laboratory) is intersected by one fracture zone in the centre (NE2). Also, fracture zones EW1 and NE1 cut two opposite corners of the target block.

These fracture zones are all steeply oriented. Pre-investigations performed by Talbot and Riad /1988/ conclude that the fracture zones in the Simpevarp area (including Äspö) have experienced several reactivations of pre-existing faults. Both left and right-handed

(dextral) strike-slips and dip and oblique slip faults has been observed. They further conclude that this indicates that such reactivations involved major changes in the direction of the stress field.

The description of the geological model of the Test Case refers to a report by Munier /1995/ stating that the latest detectable brittle movements in EW1appears to be strike-slip dextral. The same information is given in Nisca /1987/ and Gustafson et al. /1989/, where it is written: “Once the steep EW penetrative fabric was established at least 1400 Ma ago, its anisotropy appears to have influenced all subsequent deformation of the rocks on Äspö. The bulk kinematics of the first ductile shears through the younger semi-ductile vein systems and still younger brittle fracture zones appear to have been remarkably similar in general location and geometry. Left-handed ductile shear movements changed to right-handed faults and fracture zones, but all regional displacements appear to have occurred along the same planar zones.”

The description of the geological model gives indication of the fracture zone thickness. EW1a and EW1b are the widest, 45 and 50 m, and NE1 and NE2 are given widths of 28 and 25 m, respectively. Fracture zone EW3 is assigned with 14 m width. It should, however, be noted that these width are differently related to the actually expected width of the zones. The fracture zone NE2 is strongly undulating and the 25 m are here referring to a span within which the zone is expected to be located. The actual zone itself is observed to be 0.6 – 6 m wide. For the other zones the model unit width has been given the same width as that of the actual zone at the points where they have been observed (tunnels, outcrops, boreholes).

The fracture zone NE1 in the model is in fact only the north part of a wide zone with two strands. Of further importance for the estimation of the mechanical properties of this zone is the information that an approximately 8 m wide part of NE1 has open centimetre wide fractures and cavities and partly clay-altered rock. The central 1 m wide section is completely clay altered /Rhén et al., 1997/.

Since the model does not include any gently dipping structure it was initially not expected to have any major abrupt stress magnitude changes with depth, but the zones may still influence the stress field.

8.2.2 Stress measurement from Test Case site

Stress magnitude data

Within the Test Case exercise stress measurement data were available from boreholes KAS02, KAS05 and KA3579G.

Figure 8-6 shows the stress magnitudes for the maximum principal stress, from these three boreholes, as a function of the z-coordinate in the local coordinate system. Figure 8-7 show corresponding diagrams for the intermediate and minimum principal stress. To be able to judge whether these site-specific data conform to the overall stress pattern in Sweden, the best-fit linear trend (from Figure 8-1, Figure 8-2 and Figure 8-3) and the estimated uncertainty spans (according to the *initial* prediction) are also added in the diagrams.

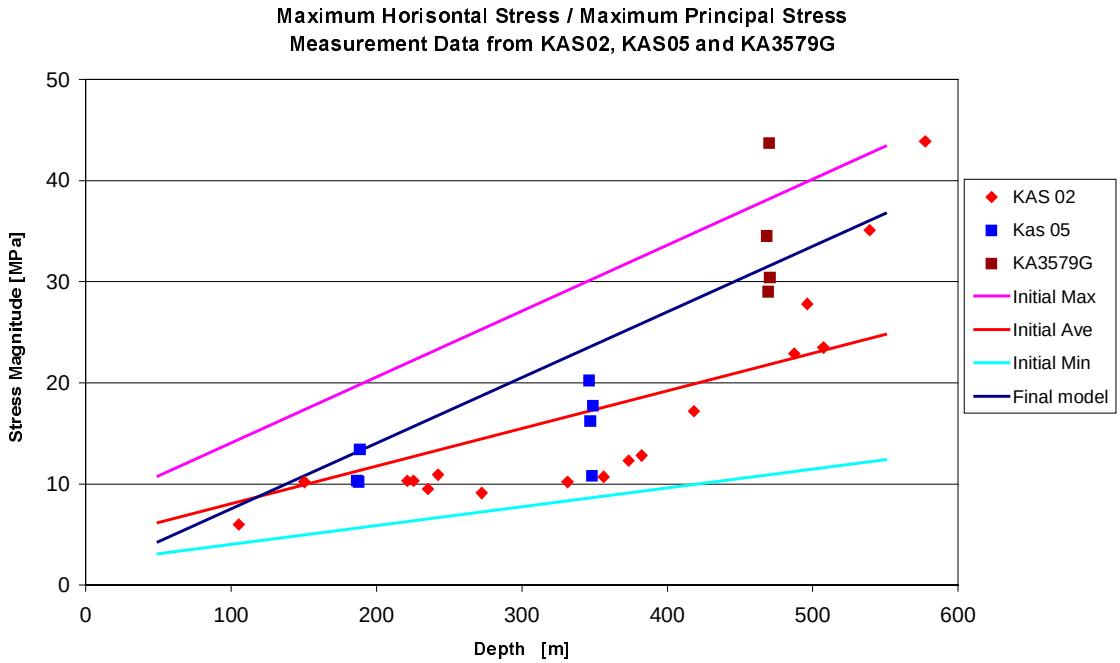

Figure 8-6. *Maximum principal stress, σ_1, vs. depth. Data from measurements in three boreholes at ÄHRL. In KAS02 the measurement method was hydraulic fracturing and in KAS05 and KA3579G the method was overcoring. For KAS02 the maximum horizontal stress is assumed to correspond to the maximum principal stress. Final prediction (will be presented in section 8.5).*

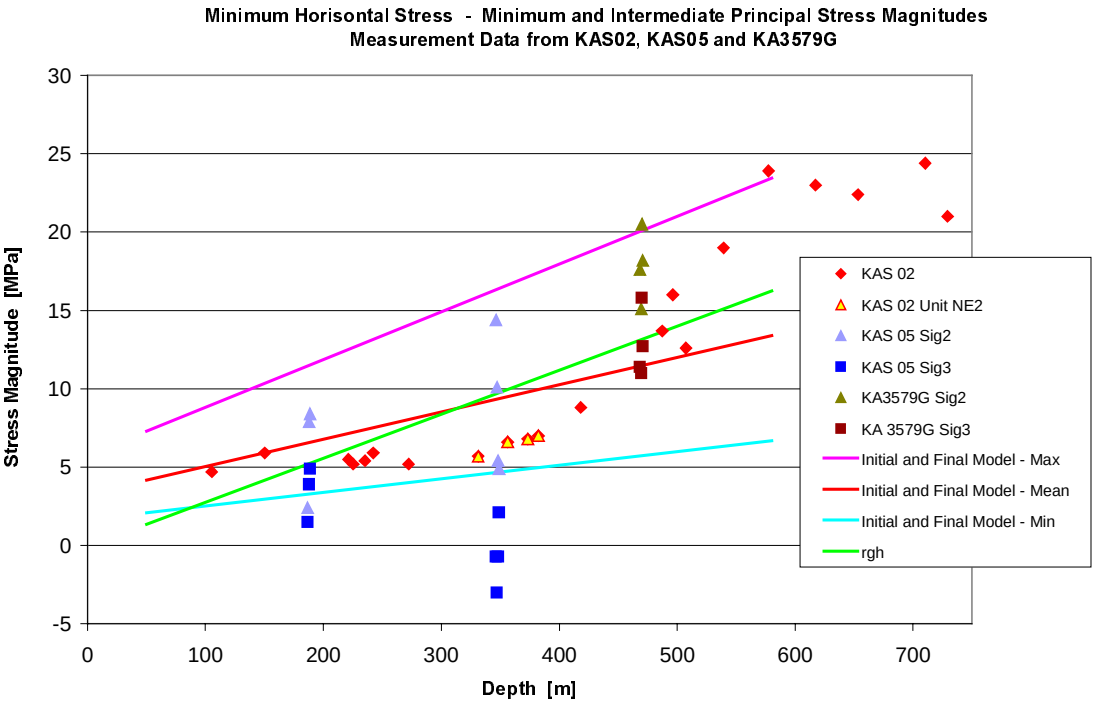

Figure 8-7. *Minimum and intermediate principal stress vs. depth. Data from measurements in boreholes at ÄHRL. In KAS02 the measurement method was hydraulic fracturing and in KAS05 and KA3579G the method was overcoring. Using the hydraulic fracturing method the minimum horizontal stress is here assumed to correspond to be the minimum principal stress, but the method gives no information on actual stress direction. The lines show the initial stress model (see section 8.1.4) and the final prediction (will be presented in section 8.5).*

It can be noted that most measurement data, for all three principal stresses, fall within the total span of the initial estimate, i.e. the measurements are not remarkably different from what has been seen at other locations in Sweden. In this sense the site-specific data supports the suggested initial model.

It may further be seen in Figure 8-6 that the measurements in KAS02 gives lower stress values than the other measurements. The measurements in KAS02 are performed with hydraulic fracturing methods and the other measurements with the overcoring method /Bjarnason et al., 1989; Klasson et al., 2001).

Overcoring measurements are usually taken in groups with several data close to each other in the borehole. Such data can be used as a rough measure of the spatial (local) variation in stress, although some of the spread may be due to other factors. For the Test Case data a summary is given in Table 8-3. As may also be seen in the figures there are data from three depth levels out of which the middle level is located in what is interpreted as the fracture zone NE2 (rock unit J). The number of data from each level is only 3 and 4, and this cannot be considered as a sufficient number for good quality statistics but, nevertheless, the standard deviation of the magnitudes at each level was calculated, also shown in the Table 8-3. Remember here that stress in a point is a tensor and that a simple calculation of average for the principal components separately, as performed here, may be less meaningful if the spread in magnitudes and orientation is large. Therefore the figures should be interpreted carefully and together with the orientation data.

Table 8-3. Spread in overcoring results for stress magnitudes.

Borehole Overcoring measurements	KAS05 Depth Ca 190 m	KAS05 Depth Ca 350 m	KA3579G Depth Ca 470 m
Number of data points	3	4	4
Mean σ_1 Magnitude	11.3 MPa	16.2 MPa	33.4 MPa
Mean σ_2 Magnitude	6.2 MPa	8.7 MPa	17.8 MPa
Mean σ_3 Magnitude	3.4 MPa	-0.6 MPa	12.7 MPa
St. Dev. σ_1 Magnitude	1.8 MPa	4.0 MPa	6.6 MPa
St. Dev. σ_2 Magnitude	3.3 MPa	4.5 MPa	2.2 MPa
St. Dev. σ_3 Magnitude	1.7 MPa	2.1 MPa	2.2 MPa
St. Dev. / Mean ,σ_1	16%	24%	19%
St. Dev. / Mean ,σ_2	53%	51%	12%
St. Dev. / Mean ,σ_3	51%	(-363%)	17%

Stress orientation data

In Figure 8-8 the orientation of the maximum horizontal stress and the maximum principal stress are presented. The direction is given in the local Äspö coordinate system. Since a subhorizontal stress may have some slight variation in plunge this means that a trend can be 180 degrees apart, such as the measurements in KAS05 at 350 m level. The plunge of the maximum principal stress, can be determined when using overcoring techniques, but is only assumed to be perfectly horizontal with hydraulic fracturing. Figure 8-9 shows measurement data on the plunge of the maximum principal stress.

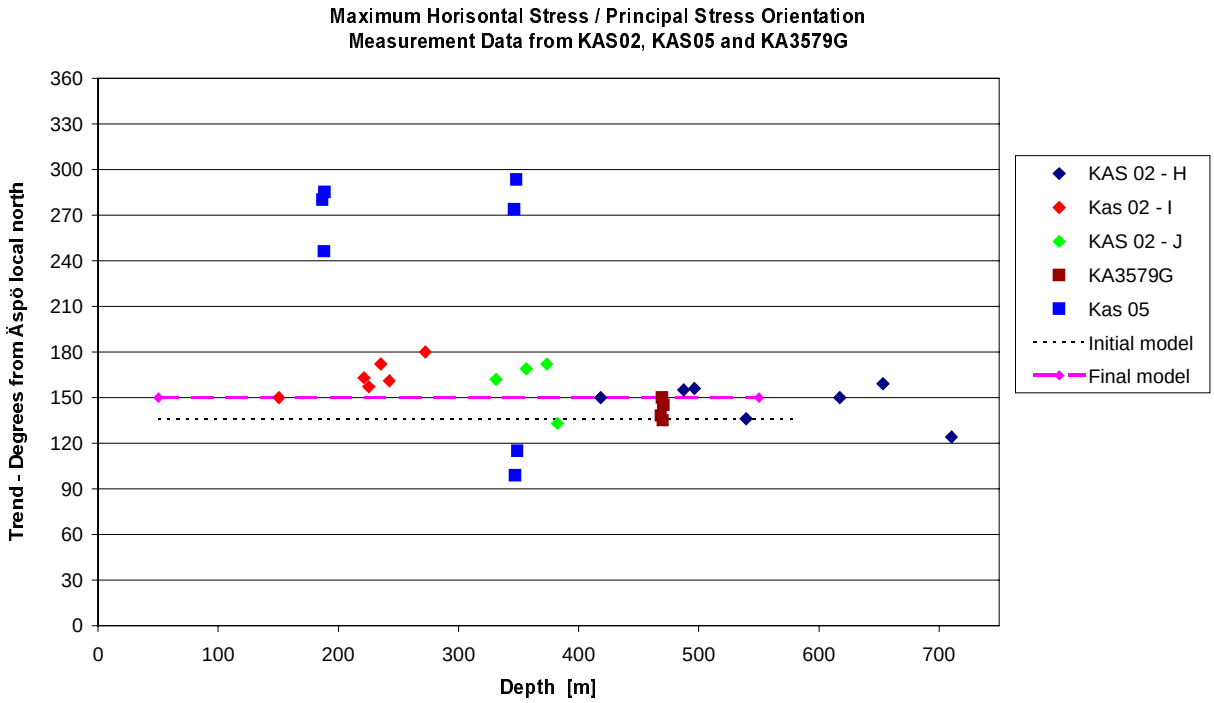

Figure 8-8. *Trend of the maximum horizontal stress as determined from measurements from the Test Case site. I, J and H refers to the rock units in the geological model of the 550 m block.*

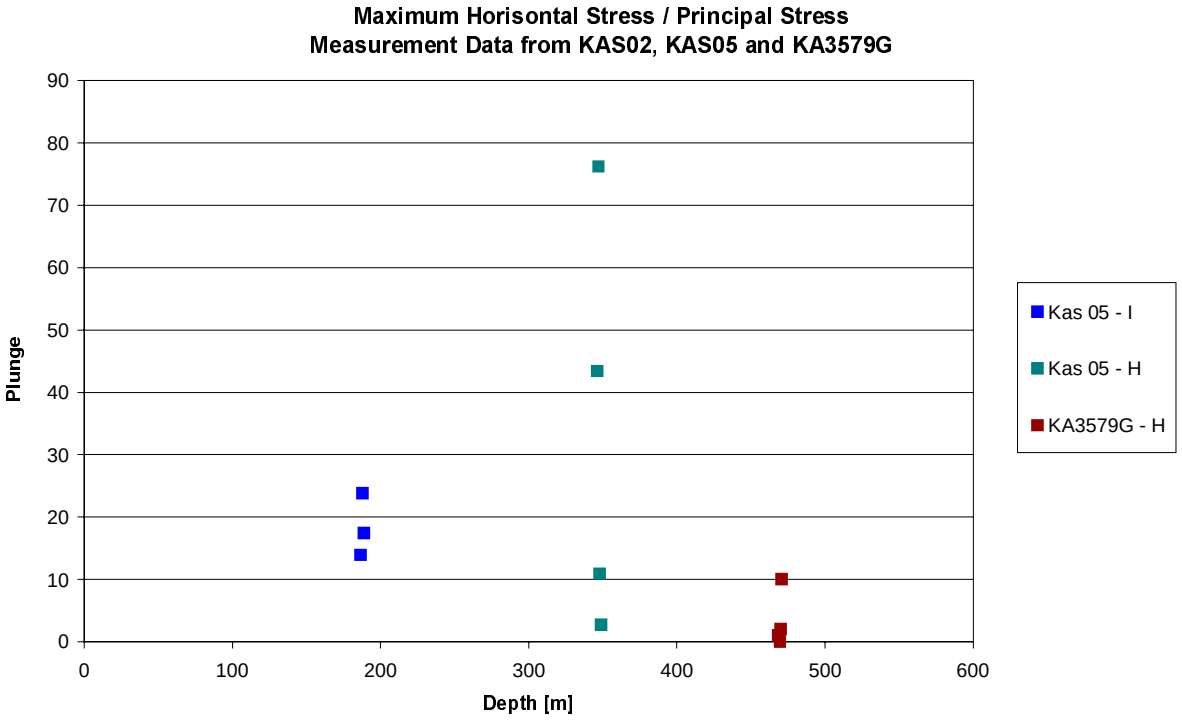

Figure 8-9. *Plunge of the maximum horizontal stress data as determined from overcoring measurements in boreholes at the Test Case site.*

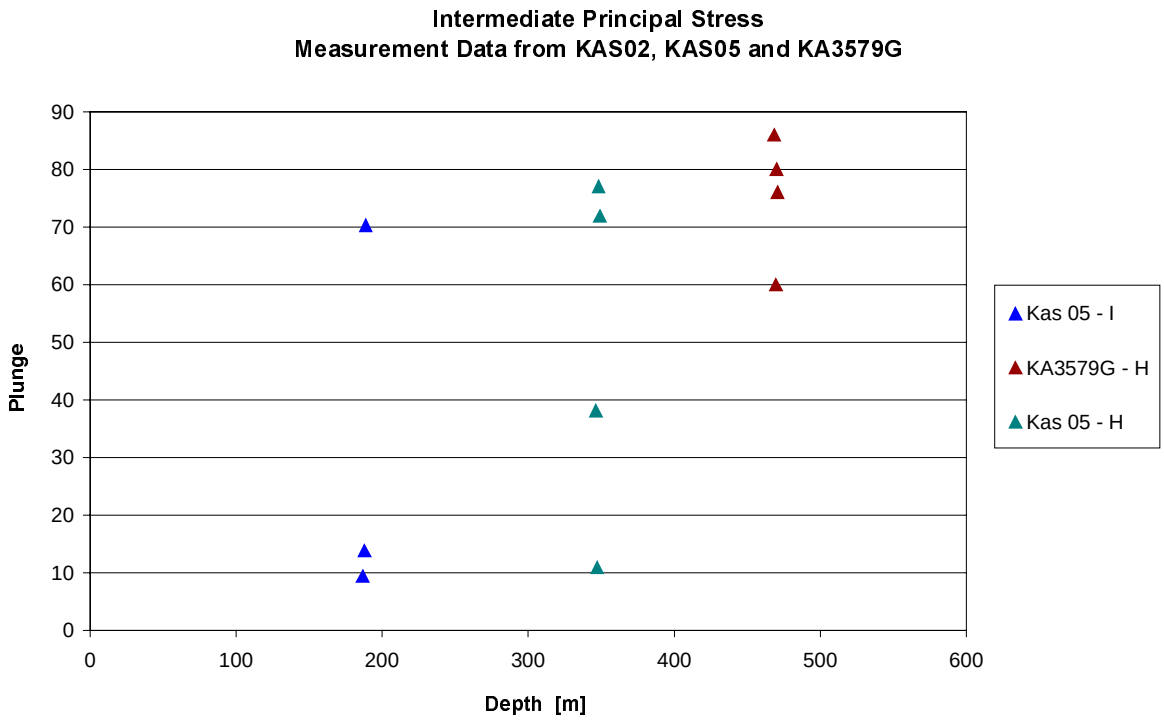

Figure 8-10. *Plunge of the intermediate principal stress as determined from overcoring measurements at the Test Case site.*

The orientation of the intermediate and minimum stress is by definition in the plane perpendicular to the maximum principal stress. The plunge of the highest and smallest stress in this plane may however vary. In Figure 8-10 and Figure 8-11 the plunge determined at each overcoring measurement point are presented for the intermediate and the minimum stress, respectively.

It can be noted that the maximum horizontal stress seems to be fairly horizontal according to measurement in units H and I but the measurements from the unit representing the fracture zone NE2 (unit J) give a large spread in the orientation results. This result may be explained by that the fact that inside a fracture zone the stresses should be expected to vary more than in the homogenous blocks. Also, at these depths the magnitudes of σ_2 and σ_3 are of the same order, thus giving large differences in calculated stress orientation (Figure 8-11).

For the intermediate and minimum principal stresses the orientation is not consistent for the two upper overcoring measurement levels but for the lower level the data indicates that the minimum principal stress is horizontal.

The spread in the orientation data from the overcoring measurements are summarized in Table 8-4 in the same way as for the magnitudes. Note that the trend direction is given with respect to the Äspö local north (which gives 12° higher values than against magnetic north). Note that the stress is a tensor and that the three principal stresses in each point thus are orthogonal to each other. If the magnitude of two principal stresses are the same the orientation of them are not defined. From the figures and tables it can

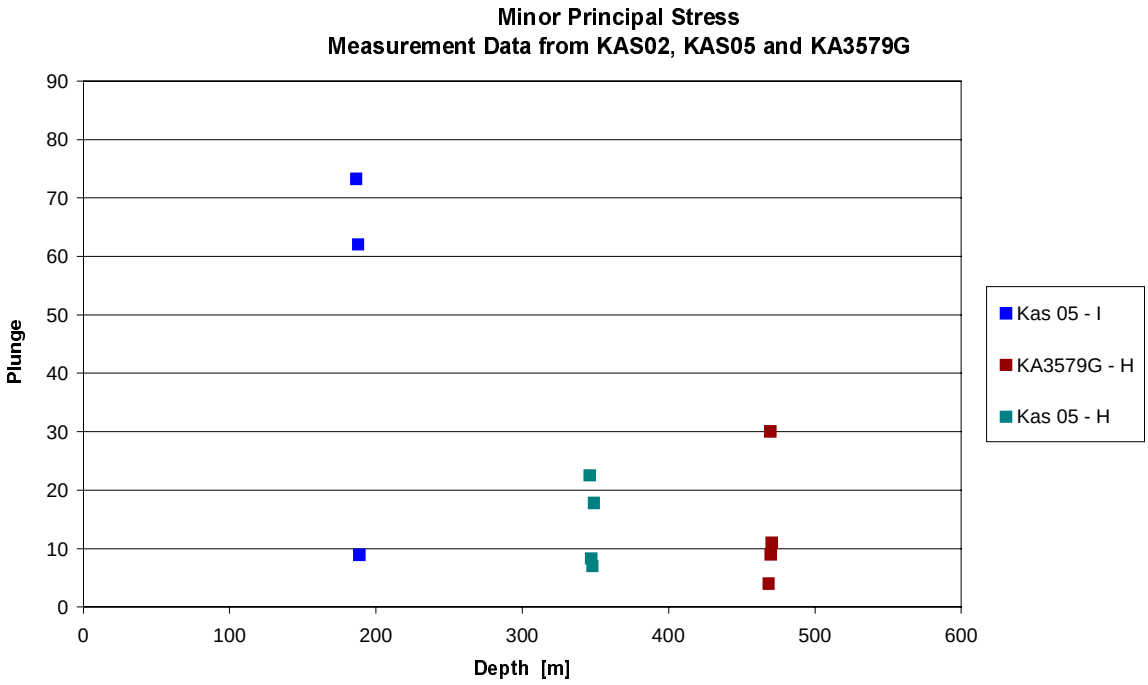

Figure 8-11. *Plunge of the minimum principal stress as determined from overcoring measurements at the Test Case site.*

Table 8-4. Spread in overcoring results for stress orientation.

Borehole Overcoring Measurements	KAS05 Depth Ca 190 m	KAS05 Depth Ca 350 m	KA3579G Depth Ca 470 m
Number of data points	3	4	4
Mean Trend σ_1	153°	127°	142°
St. Dev. Trend σ_1	8°	77°	7°
Mean Plunge σ_1	18.4°	33.3°	3.3°
St. Dev. Plunge σ_1	5.0°	33.6°	4.6°
Mean Plunge σ_2	31.2°	49.5°	75.5°
St. Dev. Plunge σ_2	34.0°	31.0°	11.1°
Mean Plunge σ_3	48.0°	13.9°	13.5°
St. Dev. Plunge σ_3	34.4°	7.5°	11.4°

be seen that the stress situation is most clear at the deepest level. The reason for this may be several. The stress state at depth has a clearer anisotropy (larger difference in stress magnitude in different direction) such that the determined orientations of the three principal stresses may become consistently measured of this reason. Also, these measurements are performed more recently in a shorter hole (measured from the Prototype Repository tunnel in the ÄHRL) and the quality of these measurements could possibly be better. The data from the middle level are located in the rock unit associated with fracture zone NE2, and at this level the minimum stresses are very spread both in terms of magnitudes and orientation, the minimum stress is even determined to be tensile. These results could be result of difficult measurement conditions at the zones or

result of actual strong variation in the in situ stress. (It has not been inside the scope of this project to look into the raw data interpretation of the stress measurements.)

8.3 Numerical analysis of in situ stress

An attempt to model the *in situ* stress situation at the Test Case site has been made following the sequence outlined in section 6.2.2. The decisions made in the modelling for each step are described in the following sections.

8.3.1 Geometry of the 3DEC model

Model size

The size of a numerical model in general should be selected to match the size of problem to be studied. The issue for this particular modelling is not very common, since normally the *in situ* stress field is assumed and the effects of different changes in the model, e.g. excavations and loading, are studied. In this project the aim was to analyse what type of *in situ* stress variation in the Test Case region that could be a result of mechanical response to regional loading of the rock. This means that the problem as such had an infinite size. Therefore it was necessary to simplify the question clearly by making a number of assumptions concerning the volume.

Firstly is was assumed that, inside the 550 m block, the effects from the closest fracture zones would dominate the stress variation, and that the fracture zones far from this volume was not included specifically. It was further assumed that the area with the surrounding rock was located in the same regional stress field, and thus having the same stress levels in general.

Further looking at a regional map of the Äspö region it could be noted that the EW1 and NE1 seemed to have an extension in the order of 5 km, and that the 550 m block was also surrounded by fracture zones of even larger regional size. This was taken as an indication on that that a block of side length in the order of 4 km might be regarded as a block with similar boundary conditions. The model size (the side length is 10 km) was selected because it gave a total size of the model that was about double the size of the largest structures (see below). It was judged that the possible stress effects around the ends of zones would then not reach the boundaries of the model itself.

Fracture zone geometry

Based on the idealized structure geological model of Äspö (the model in the Rock Visualization System, RVS) a number of five fracture zones were incorporated into the 3DEC model block. The natural fracture zones are geometrically modelled as thick plates in the RVS model. Such a plate has a thickness, which encompasses a natural fracture zone that undulates along its stretch. In 3DEC, a fracture zone was modelled as a single planar surface with supposedly equivalent properties. The planar surfaces were placed in the 3DEC model as if they ran along the centre lines of the fracture zones included in RVS-model.

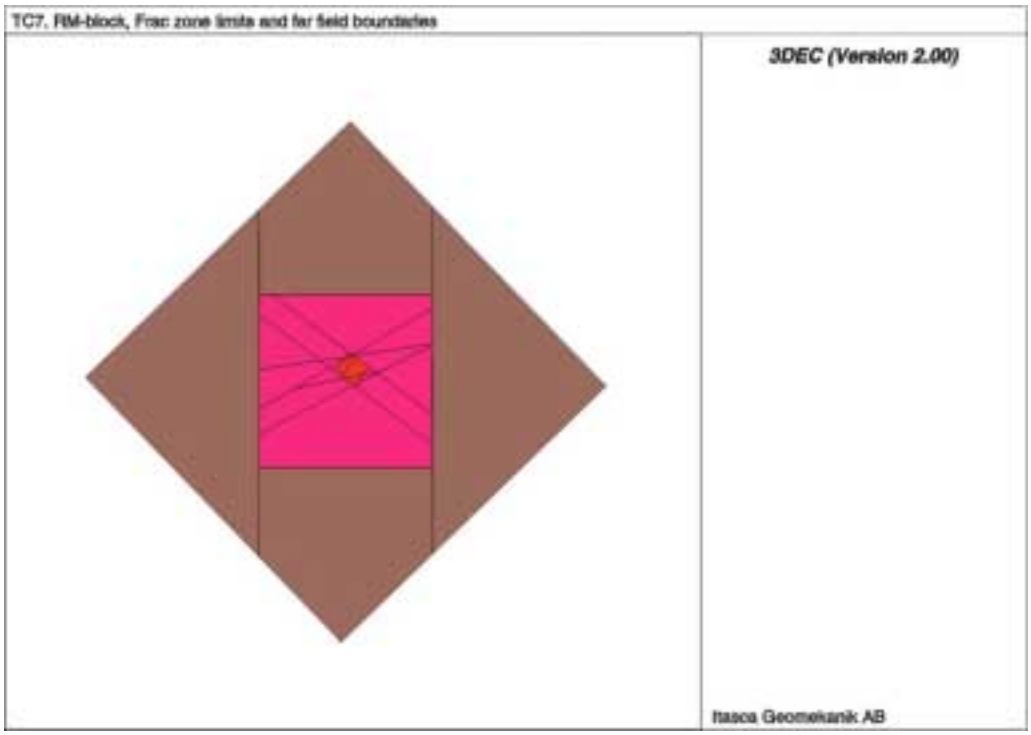

a)

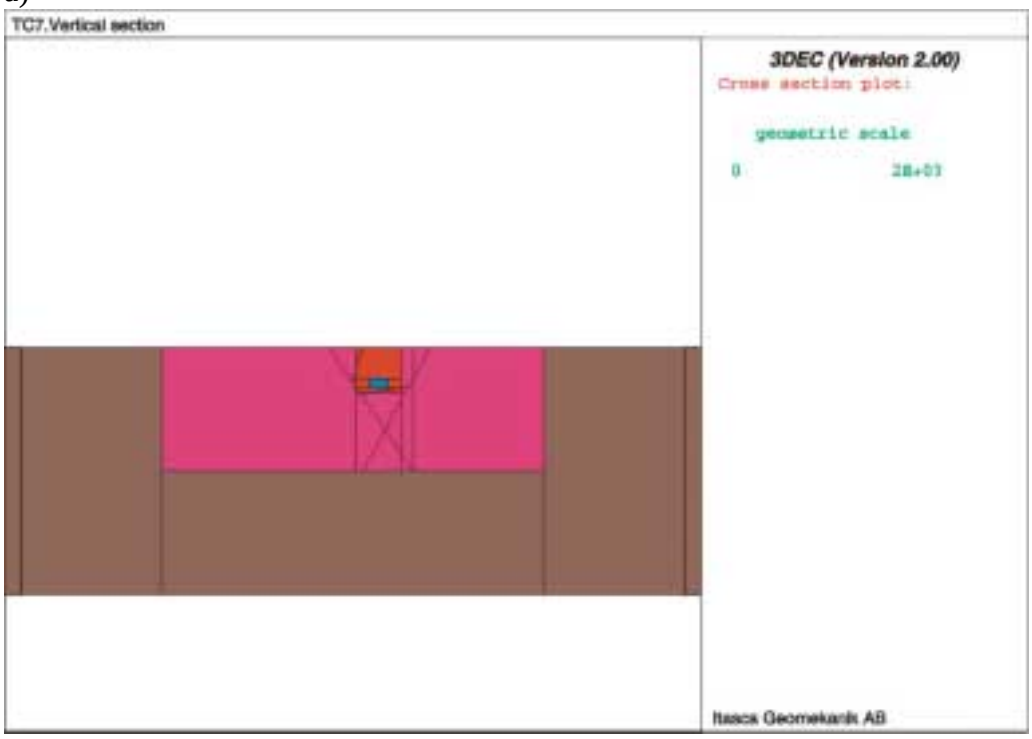

b)

Figure 8-12. *a) Horizontal view of the 3DEC model of the Test Case area. Side length 10 km. Lower: Vertical section through the model. The thickness of the model is 3 km. The red area is the intersection with the "550 m block" and the blue area lies in the "Target volume" at 380-500 m depth.*

Figure 8-12a and Figure 8-12b show a horizontal and a vertical section of the model block respectively. The sides of the outer brown regions in the figures represent the far-field boundaries of the model, across which the boundary conditions were imposed. The next square represents a region of the model block, which delimits the extent of the large fracture zones. For the first series of parallel runs, the side length of this region was chosen to be 4 kilometres. The red square represents the so-called 550 m block, having a side length of 550 m, in which the *in situ* stress variations were to be studied. The rectangular in blue on the vertical section (Figure 8-12b) represents the Target volume, in which more details from the *in situ* stress numerical predictions were to be given.

Figure 8-13 shows how the fracture zones (in the 3DEC model) are oriented and related to each other. The zones NE2 and EW3 are smaller and terminate towards larger zones. The larger zones are in the model assumed to terminate as shown in the figure. Figure 8-14 gives a view of the 550-m block, again looking in the east direction. Each fracture zone volume and each volume between the fracture zones were given a separate "names" (A to N) within the Test Case project to facilitate the presentation of measurement and model data. In the 3DEC model the fracture zones does not have any actual thickness, because the fracture zone is modelled as behaving as a single plane.

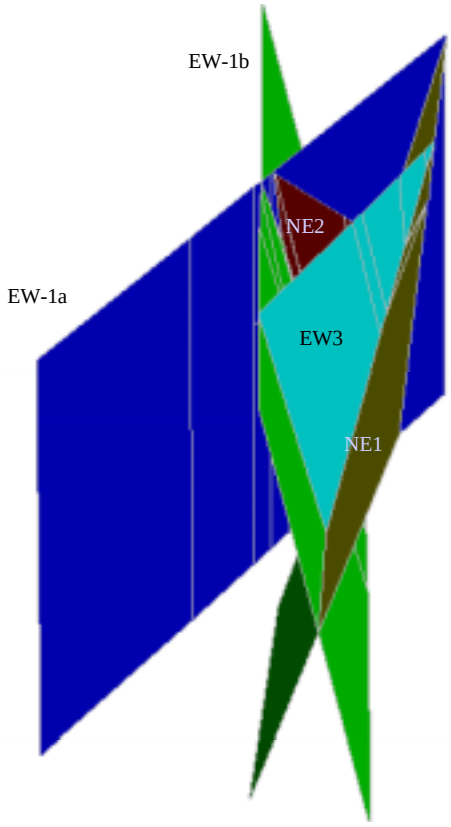

Figure 8-13. *Fracture planes, representing the five major fracture zones, in the 3DEC models of the Test Case area.*

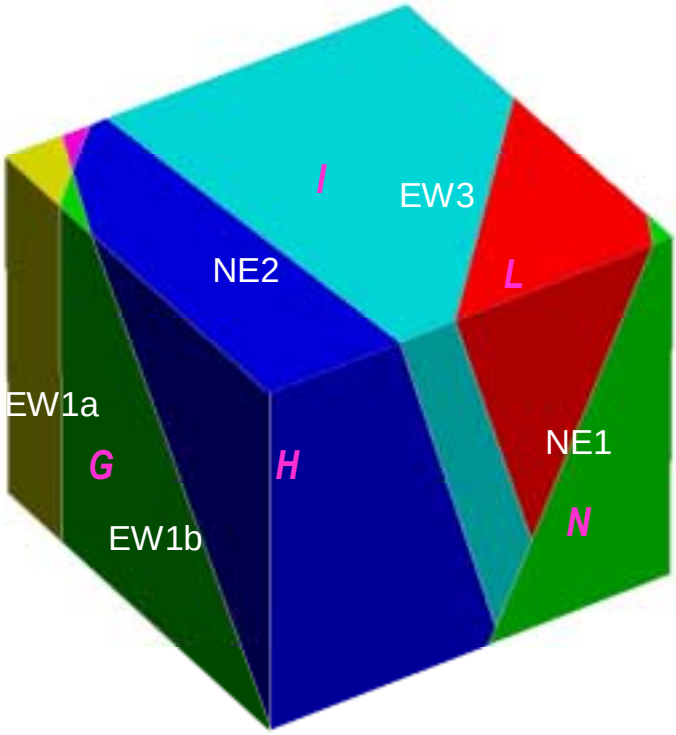

Figure 8-14. *Fracture planes, representing the five major fracture zones, in the 3DEC models of the Test Case area (white letters). The names for the "rock units" between the zones are given (pink letters).*

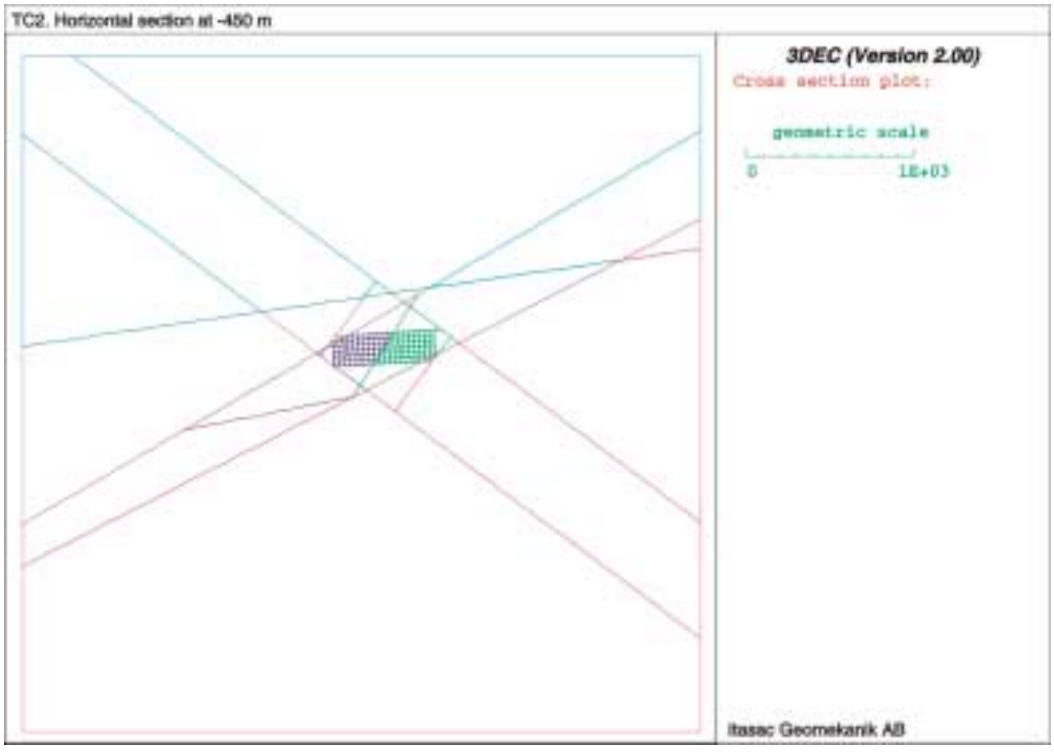

Figure 8-15. *Horizontal section through models, showing the location of the Target volume and the fracture zones. Note that some of the lines are just "artificial" fractures used for the construction of the 3DEC model. These fractures are given high strength properties to be "invisible" in the rock mass. The cubes were not modelled specifically as blocks in models but are included here to illustrate the scale and location.*

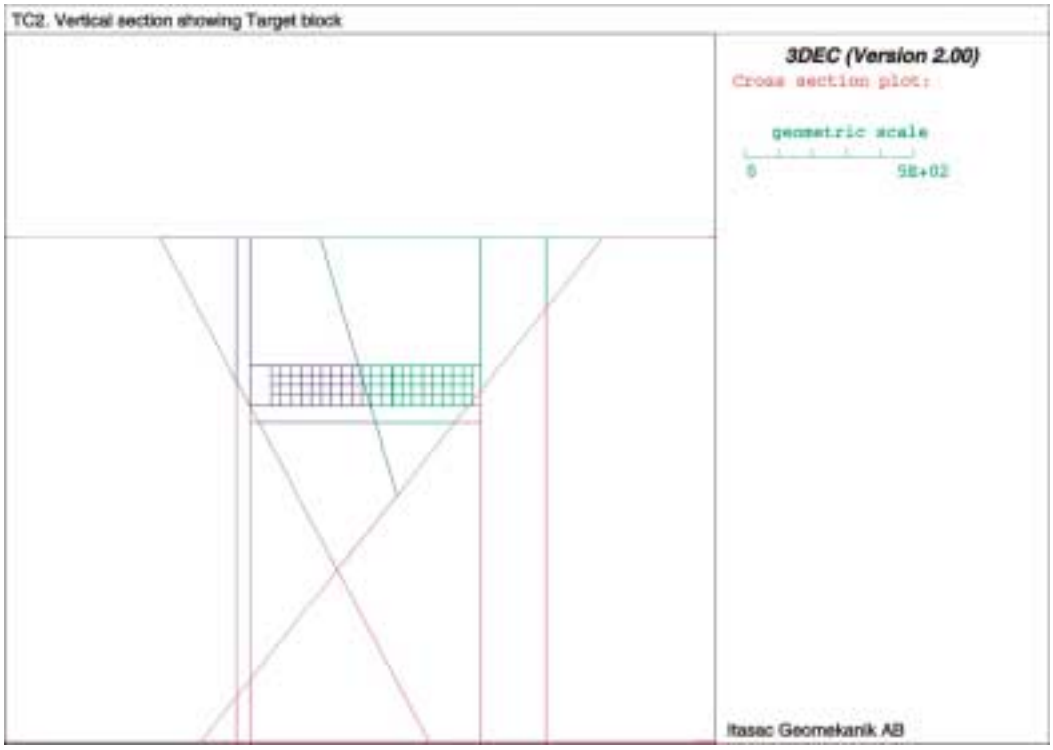

Figure 8-16. *D:o, Figure 8-15, in vertical section in central part of model. The lines show the fracture intersections with the plane and some lines represent boundaries of different model regions: the Target area "cells" are 30x30x30 m in size. (The cell blocks are just included here in this model for illustration purposes and not used in the model for calculations (apart from TC2).*

Figure 8-15 and Figure 8-16 are close-up views showing the location of the Target volume, in relation to the 550 m-block and the zones. The Target volume was divided into 480 cubes, where each cube, 30 x 30 x 30 m, was the smallest unit of the rock mass in which *in situ* stress magnitudes were to be assigned.

Zone discretization size

The zone discretization was, for most models, selected as follows:

- In the outer region (region 4, see Figure 8-12) the longest allowed zone (calculation element) edge length was set to 500 m.
- In the region around the larger fracture zones the maximum "edge length" was set to 200 m.
- In the region that corresponds to the 550 m block the maximum "edge length" was set to 80.
- In the region inside the Target, the maximum "edge length" was set to 20 m.

This discretization level was selected (by judgement) such that the computation should take a reasonable time and still give a reasonable result considering the scale of the study and the accuracy of input data. There is no exact way to determine the ideal mesh size, but this has to be determined for each modelling. For the Test Case, in the sensitivity analysis one model with a finer zoning was included to enable comparison. The accuracy should be selected in the light of other uncertainties in the analysis, and depending on what type of conclusion to be drawn from the results. In this case the

scale of blocks in the “Target Cells” was 30 m and therefore the discretization zones should be selected smaller than this.

8.3.2 Modelling approach

Geological setting

As described in more detail in Chapter 2, the causes for stress variation in the earth crust are many. It was also discussed what was the most probable cause in this region, namely stress redistribution due to movements along pre-existing zones of weakness. Also the site specific information provided for the Test Case /Hudson (ed.), 2002/ indicated that there were no major mechanical differences between the rock types, and there was therefore no reason to believe that stiffness differences in the intact rock would be the cause of significant stress variations.

From the geological description in Hudson /ed., 2002/, Talbot and Riad /1988/ and Stille and Olsson /1990/, it was concluded that on a large scale the rock in he area, from a mechanical point of view, could be described as consisting of only two types of material, rock mass between the fracture zones and the fracture zones themselves. This simplification involves the assumption that the material properties are constant inside all the large rock mass blocks and across the fracture zones, respectively.

This assumption is supported by the observation that many reactivations have taken place along the same fracture zone and that no new fracture zones have been created during the youngest geological periods /Talbot and Riad, 1988/. The stress and deformation pattern should thus be controlled by elastic deformation in the rock mass blocks and by slip deformation on the fracture zone planes. The stress changes with time relates to changes in magnitude and direction of the regional stress field.

Geological mechanism modelled

By changing the direction and magnitude of initiated stresses in the 3DEC model, the local changes due to the response along existing fracture zones has been studied. The differences in pattern that could be observed, between models, are due to the different angle and thus stress/strength situation that each fracture zone (modelled as a single fracture plane) obtained for different loading situation.

In the modelling it has been assumed that the *current* stress is only dependent on a boundary stress field that coincides with the general stress field of today. In reality, previous loadings slip failures and, deformations could also influence the stress pattern of later loading situations. However, it should be remembered that in this exercise the attempt was not to describe the whole history of the Äspö area, and not to actually calculate the regional stress *magnitude level* from the knowledge of geological history, because there is no possibility to do this. (The only way to estimate stress magnitudes is to rely on measurements, from a general database and/or site specific). But it was attempted to explain relative stress *pattern* in the area, in the light of the existing fracture zone pattern. Such “pattern understanding” would be valuable because the aim was to predict the stress in a large volume of rock, also in areas where no measurement data exists. The amount of site-specific stress measurement data was limited to mimic the situation during actual site investigation for repository localization.

Note also that because of many assumption and parameters in the calculations, there could be no single model being "The correct model". Many different combination of loading cases and property parameters could give similar model results. Therefore the 3DEC analysis was used together with the results from other analyses, using empirical and theoretical approaches and engineering judgement to judge what stress model to prefer before others. The attempt was to use 3DEC as help in understanding the current pattern for the *in situ* stress in the area.

8.3.3 Initiated stresses and boundary conditions

Based on the uncertainty spans estimated, the *in situ* stresses initiated were different in different models. In most cases, however, the stress field was identical with the field referred to as the "initial stress model" that was presented in Section 8.1. The average value for the prediction of the maximum horizontal stress was used in some of the models and the high value was used in other cases. Table 8-5 lists what was the stress level for each model, "Average" and "Higher" respectively. The minimum horizontal stress was always given the same value, similar to the average value of the initial prediction (Section 8.1). A vertical stress corresponding to the weight of the overlying rocks was also initiated to the model.

The stresses initiated increase linearly with depth, with a different gradient for each principal stress. The stresses are initiated in the coordinate system of 3DEC, which has the same orientations as for the Äspö local system. The components in xx, yy and zz plane and the shear components are calculated such that the orientation of the principal stresses remains constant from surface down to the bottom of the model. It may be noted that the initiated σ_1 is always oriented horizontally while σ_2 and σ_3 exchange directions with depth, according to the assumed stress field. In the upper part, the vertical stress is the least principal stress whereas at greater depths it becomes the intermediate principal stress. After the stresses are initiated the model is "run" to equilibrium, i.e. the deformation and stress changes needed to reach equilibrium is calculated. It is the equilibrium state that, with this approach, is assumed to represent the actual stress field.

8.3.4 Mechanical properties of the 3DEC models

Rock mass material properties

The rock mass properties used in the models were selected based on the preliminary information submitted by the two other investigation teams of the Test Case and also using our own judgement. The material model used for the rock mass blocks was chosen to be elastic in most models and following Mohr-Coulomb failure criterion (elasto-plastic model) for one model as a comparison. The material parameters used for each model analysed are given in the Table 8-5.

Fracture zone properties

The geological setting of the Äspö area strongly suggests that the deformation and strength properties of the fracture zones should differ from the surrounding rock. The major fracture zones have been reactivated many times and have been moving in different directions. In fact, the underlying hypothesis of this numerical analysis is based on the presumption that the fracture zones have slipped to some extent. Therefore

Table 8-5. Properties for different 3DEC models analysed.

Model	Initiated stress level	Rock mass Young's modulus (GPa/m)	Poisson's ratio	σ_1 trend (°)	Fracture zone Friction angle, ϕ (°)	Normal stiffness Kn (GPa/m)	Shear stiffness Ks (GPa/m)	Notes
TC1	Average	40	0.25	136	30	0.1	0.05	
TC2	Average	90	0.30	121	30	0.1	0.05	1), 2)
TC3	Average	40	0.25	151	30	0.1	0.05	
TC4	Average	40	0.25	136	30	0.1	0.05	
TC5	Average	40	0.25	136	27	0.1	0.05	
TC6	Average	90	0.30	121	30	0.1	0.05	1)
TC7	Higher	40	0.25	136	15	0.1	0.05	
TC8	Average	40	0.25	136	15	0.1	0.05	
TC9	Average	40	0.25	136	25	0.1	0.05	
TC10	Higher	90	0.30	121	25	0.1	0.05	1)
TC11	Higher	40	0.25	151	25	0.1	0.05	
TC12	Higher	40	0.25	151	15	0.1	0.05	
TC13	Higher	90	0.30	121	15	0.1	0.05	1)
TC14	Higher	40	0.25	151	15, 25	0.1	0.05	
TC15	Higher	40	0.25	151	15	0.1	0.05	5)
TC16	Higher	40	0.25	136	15	0.1	0.05	4)
TC18	Higher	90	0.30	121	25	0.1	0.05	1)
TC20	Higher	40	0.25	136	15	0.1	0.05	
TC22	Higher	40	0.25	151	15	0.1	0.05	
TC23	Higher	40	0.25	121	15	0.1	0.05	
TC30	Moving Bound.	40	0.25	136	30	0.1	0.05	3)
TC31	Moving Bound.	40	0.25	151	30	0.1	0.05	
TC32	Moving Bound.	40	0.25	151	30	0.1	0.05	6)
TC33	Moving Bound.	40	0.25	151	15	0.003–40	0.0015–20	7)
TC34	Moving Bound.	Varies	0.25	151	15	0.1	0.05	8)

1) The high E-modulus and Poisson's ratio were originally used by mistake but are kept in the table since it gives a possibility to study the influence of these. Model T23, which is similar to TC13, was run to correct for the mistake.
2) This model has a different grid where every 30x30 cell in the Target area is a 3DEC block (with "invisible fractures" between them). The grid was good only for illustration purposes but the grid without the cell blocks was better for the mechanical calculations.
3) To be compared with TC1. The difference lies in the loading sequence (see text).
4) This model has a larger region 3, i.e. the fracture zones EW1a and b and NE1 are longer. Compare with TC7.
5) This model has a Mohr-Coulomb material model for the rock mass (ϕ=45, c= 5 MPa, Tensile strength 5 MPa). Compare with TC12.
6) Different loading rate, otherwise like TC31.
7) The Stiffness varies with depth (see text). The friction angle is the same for the whole fracture surface. The same properties are given to all fractures.
8) The rock mass Young's modulus varies with depth, from 11 GPa/m at shallow depth to 40 GPa/m from 700 m depth and deeper.

fairly low strength properties are also considered. The influence of some of the fracture zone properties was studied specifically.

The fracture zones are simulated as single deformation planes and the Coulomb slip model is used. The fracture parameter values used for the analysed models are given in Table 8-5. In most of the models the stiffness has been the same over the whole fracture surface, and this may be argued to be unrealistic. In nature it is more probable that the fracture zone stiffness and strength would vary from point to point and also from part to part. For example it should be expected that, in general, the properties are weaker close to ground surface than towards depth and also weaker in the central parts compared to parts close to the fracture ends. (The values were for this modelling selected based on preliminary judgement from the project group. Ideally the values should be selected based on the final results from "property group", i.e. from the rock mechanics site descriptive model of rock mass and deformation zone properties.)

Simulating such variation in fracture zone properties would of course make the model more complex and, while the information about the actual geometry and composition of the fracture zones were very limited, it was therefore chosen to simplify the fracture behaviour and to give single parameter values for all fracture surfaces. The exception is model T33 where the stiffness of the fracture zones is increasing with depth, simulating an assumed change in mechanical properties.

Similar objections against all the parameters used could be raised, i.e. they could have been stress-dependent and have spatial variability etc. One could also have studied influence of cohesion, tensile stress, strength criterion and many other things. However, for the purposes of this project it was considered that the type of analysis performed and the variation of parameters was enough to illustrate the methodology.

Input from other Test Case modelling teams

The work done in this project has been performed independently from the "Geology Group" of ÄHRL. However, a discussion with "geology group" has taken place during a workshop. Information from the geologists concerning observed deformation pattern, i.e. slip indicators for the major fracture zones also can give support to a selection of a specific stress model before others.

Information about the geological (mineralogical) and mechanical characters of the different major fracture zones could be valuable when one wants to argue for certain strength parameter value and parameter uncertainty (e.g. a zone which is expected to have extensive clay must be considered different from a zone with only increase fracture frequency). This type of useful characterization would also come out as a result from the work by the "empirical group" and "theoretical group", aiming at estimations of mechanical property parameters. However, it is expected that the uncertainty in mechanical property parameters to represent the fracture zones will remain fairly uncertain /see Leijon, 1996; Staub et al., 2002; Röshoff et al., 2002).

More interaction with the geology group in discussing the regional geology and regional tectonics of the area may have been useful for the stress group, because it could have given support to (or questioned) the selected initiated stresses, fracture zone sizes and/or the loading sequence of the model. Depending on the amount and type of additional site-specific information available it may (or may not) have changed the stress model.

8.3.5 Examples of results from 3DEC models

Figure 8-17 shows the same type of shear displacement plots for two different models where TC1 has a higher fraction angle, 30°, on the fracture zones compared to model TC8 that has 15° friction angle. The arrows correspond to the shear displacements that have occurred on the model at a certain depth (-450 m). The largest shear in the section is about 0.6 mm in TC1 and in TC8 about 20 mm (see legends of the plots). It is only in TC8 that the zones will reach the shear stress limit for slip and the two figures illustrate this difference.

Note that the lengths of the arrows in the figures correspond to the projected displacement vectors on the actual plane of the plot (with different scales), but the colouring code corresponds to the total shear displacement at the contact, independent of direction (see legend).

The same kind of shear displacement plot in a vertical section through the models TC22 and TC33 are shown in Figure 8-18 and Figure 8-19. There are two differences between these two models. One is that the fracture normal and shear stiffness are constant with depth (and the same for all zones) in TC22. In TC33 the fracture stiffness is much lower at shallow depth (the block was divided into layers with different properties in the block contacts, i.e. different stiffness at different contact points). The other difference is that the boundary condition for TC22 was fixed and the stress was initiated before calculation to equilibrium. The boundary condition for TC33 was a moving boundary inwards (compression) for the NW and SW boundary, such that a large stress is built up in this direction. The boundaries in the other direction were fixed. The difference in displacements calculated for the two models reflect the difference in properties such that the largest displacements for TC33 occur at the surface and decrease dramatically towards depth.

The stress direction in the models can be illustrated with stress trajectory plot in sections of the models in a similar way; Figure 8-20 shows the horizontal section and Figure 8-21a vertical section. For each finite difference element centroid a “stress cross” is drawn, where the length of the three arms are proportional to the stress magnitudes. The lines have to be projected to the plane of the plot and should therefore be interpreted with care. It can be noted in the horizontal section that the longest lines, the maximum principal stress, have the same direction in all points and this is the direction 136°. Small changes in the direction of the intermediate and minimum principal stress can be noted in a few points, but this is not strange because they are of the same order of magnitude.

In the vertical section the “stress crosses” has different colour corresponding to the different stress levels with depth. It can be noted that the principal stresses are horizontal and vertical, as was desired when stresses were initiated. The small movements on the fractures in TC1 (ϕ=30° and stress level “Average”) have not caused any “disturbance” of the initiated stress field, i.e. in this case not so much happened with stresses in the model when the fracture properties were set and the calculations steps continued to reach the new equilibrium.

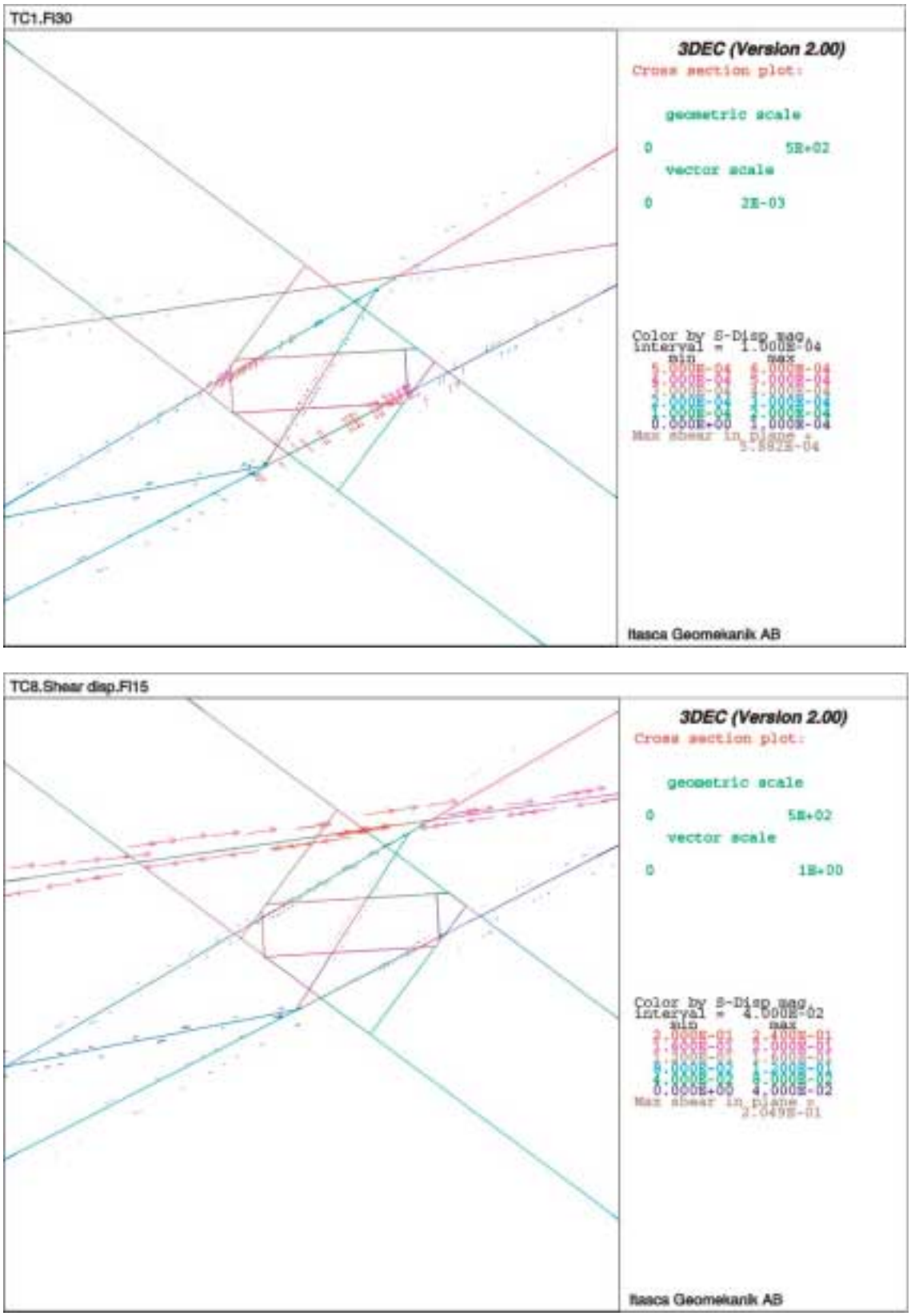

Figure 8-17. *Shear displacement along fractures zones in model TC1 (upper) and TC8 (lower). TC8 has a low friction angle on the fracture zones, 15°. The section is horizontal and north is upwards. Only the central part o the model is inside the plot. (Some lines are just edged of different model regions and do not have fracture properties. Refer to Figure 8-13 for geometry and names.) The inner area is the Target area. The arrows are the components in the plane of the plot but the colour coding in the legend is the total shear displacement. The maximum shear displacement of TC1 and TC8 is 0.6 mm and 0.2 m, respectively.*

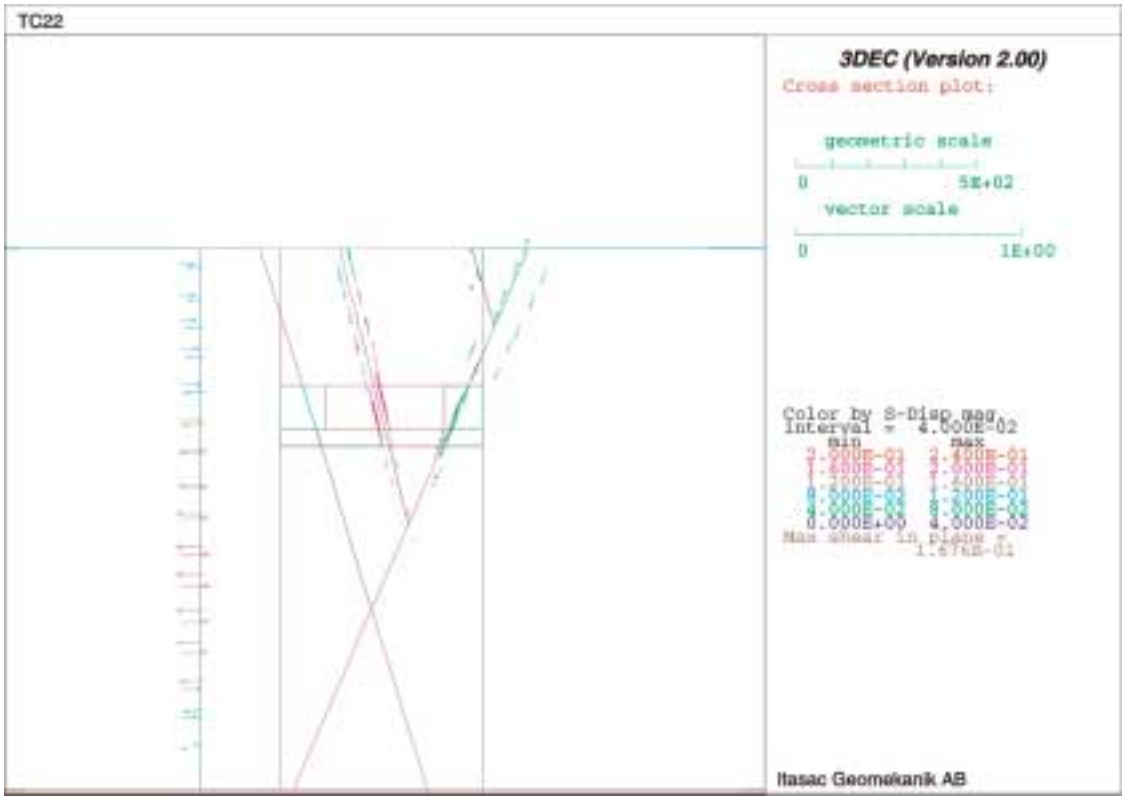

Figure 8-18. *Shear displacement along fractures in a vertical section through model TC22. TC22 has friction angle 15° on the fracture planes. Looking into the section is towards east and he fracture zones are from leftEW1a, EW1b, NE2 EW3 and NE1.*

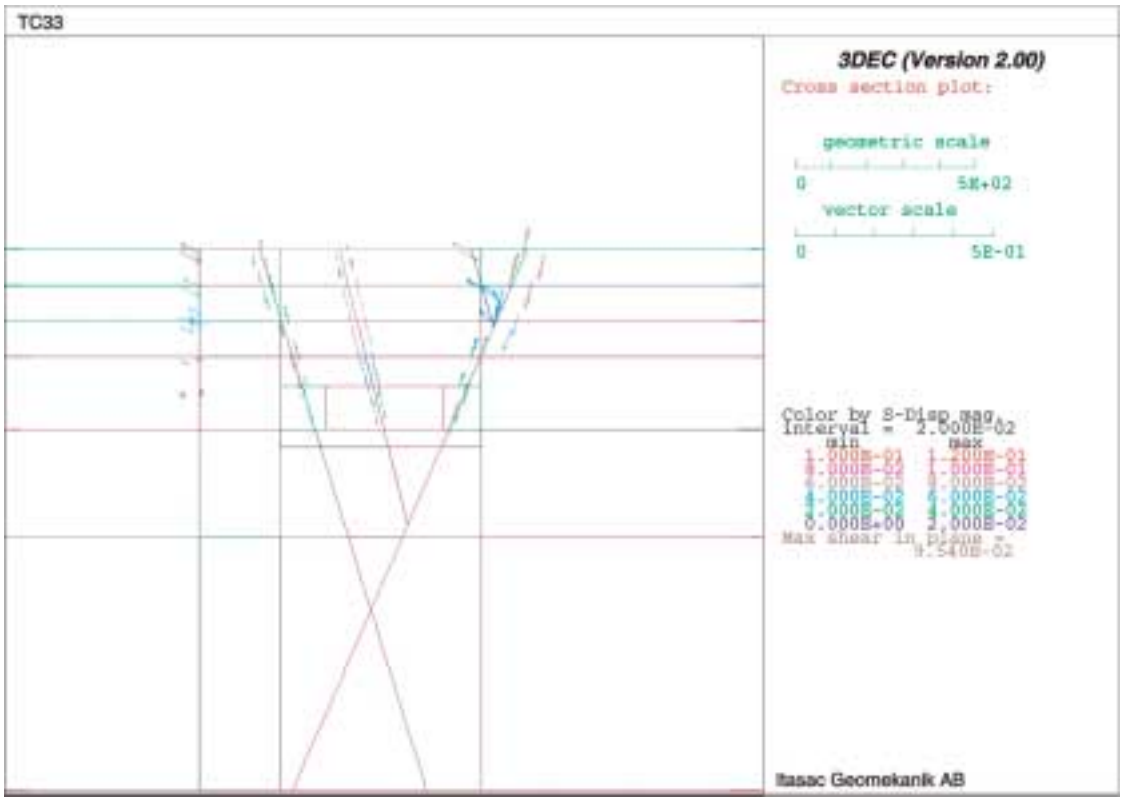

Figure 8-19. *The same vertical section as in Figure 8-18, but for model TC33. The relative movements of the rock mass blocks can be noted from the arrows. (In this model the properties of the fracture is different depending on the depth and therefore the blocks were divided horizontally).*

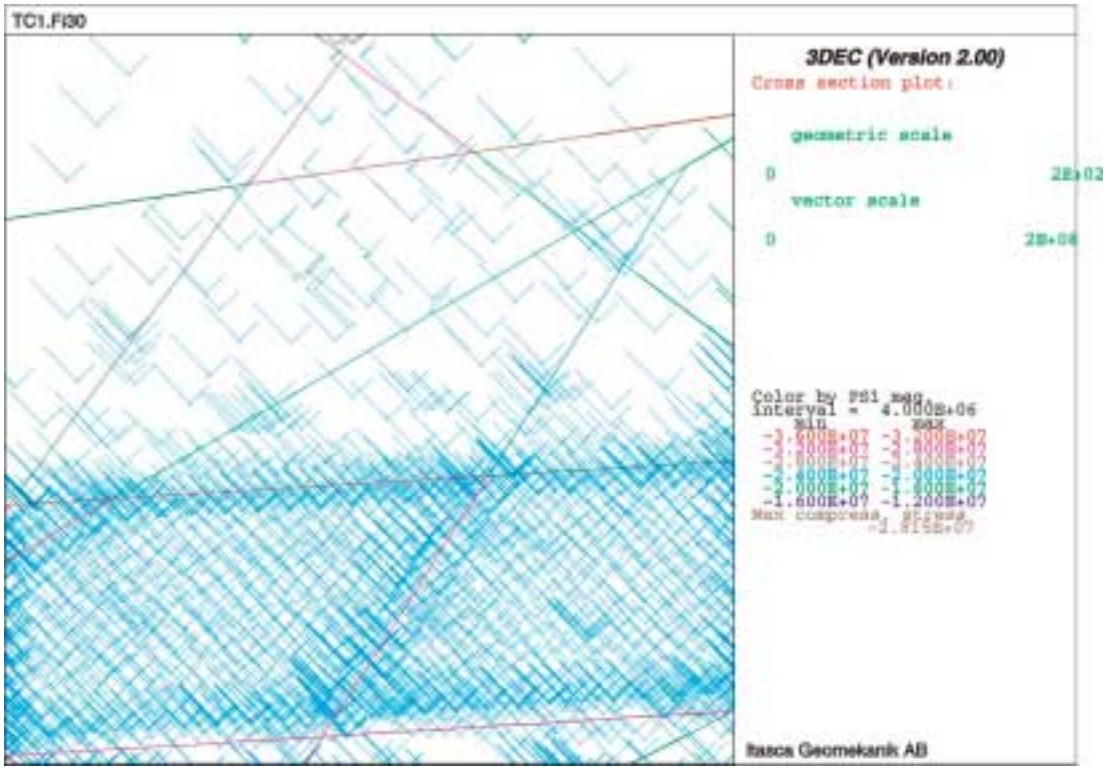

Figure 8-20. *Stress trajectories in a horizontal plane, level –460, through model TC1. The lines are trajectories projected to the plane of the plot. The colour is in this case the same because σ_1 has the same magnitude at the same depth.*

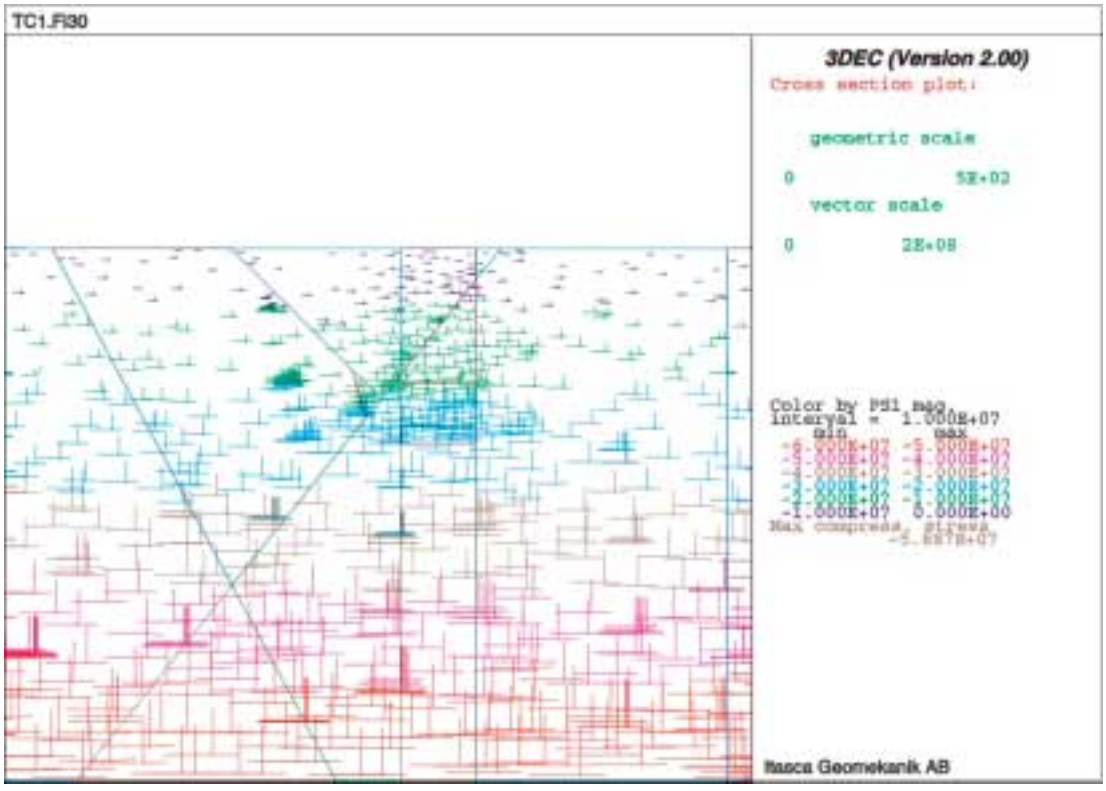

Figure 8-21. *Stress trajectory plot in a vertical section, looking north, of model TC1. The colour coding is for the maximum principal stress. At the depth of the Target area the magnitude is in this case about 20–25MPa. The stresses increase linearly with depth according to what has been initiated in the model. No influence from the fracture zones can be seen in the model TC1.*

8.4 Comparisons between models and measurements

8.4.1 Stress magnitude

The Figure 8-22, Figure 8-23 and Figure 8-24 show how the principal stresses calculated for some of the models compare with the measurements data provided for the Test Case. The data are taken out of the 3DEC model along a line of similar location as borehole KAS02. The overcoring data are not taken exactly along this line but the data was still put into the figure for comparison. KAS05 is not located very far from KAS02.

It can be noted that σ_1 and σ_3 does not change other than almost linearly with depth. The σ_2 changes slightly in the models in connection to the fracture zone NE2 (which in the model is without width but in reality is 1–6 m wide).

It should be remembered that this borehole does not intersect any of the other fracture zones. Unfortunately there were no measurement data from boreholes that intersect any of the other fracture zones in the area. If such data were available there would have been a better chance to see if any model was to prefer. Also it may be remembered that the fracture zone NE2 is not the largest fracture zone in the area, and thus its influence could be less than the influence at other zones.

In Figure 8-22 it may be noted that the difference between the models and the data from hydraulic fracturing measurements are quite large. However, this difference is of less importance since the estimates of maximum horizontal stress using this method are not reliable /e.g. Rutqvist et al., 2000/. Hydraulic fracturing is much more certain in predicting the minimum horizontal stress. The maximum horizontal stress is in this method derived as a simple function of the minimum horizontal stress, see Section 7.1.

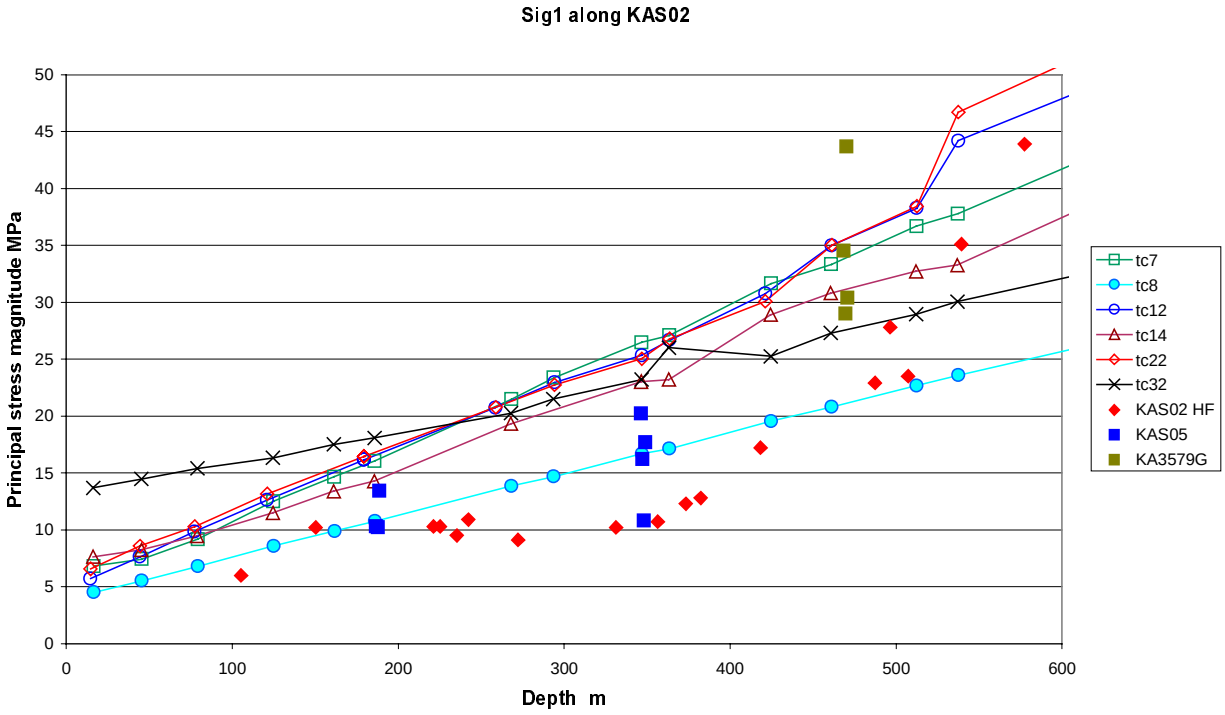

Figure 8-22. *Calculated and measured maximum principal stress. Maximum horizontal stress from hydraulic stress measurements are given for comparison, and σ_1 results from overcoring.*

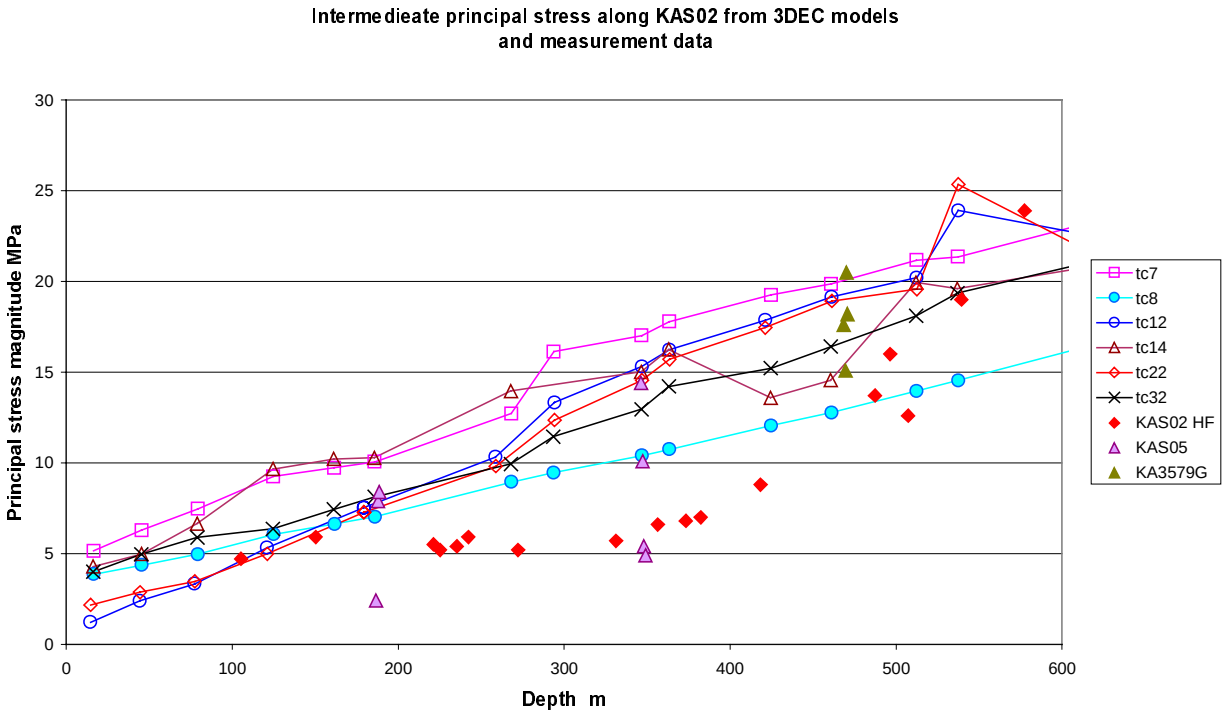

Figure 8-23. *Calculated and measured intermediate principal stress. Minimum horizontal stress from hydraulic stress measurements are given for comparison, and σ_2 results from overcoring.*

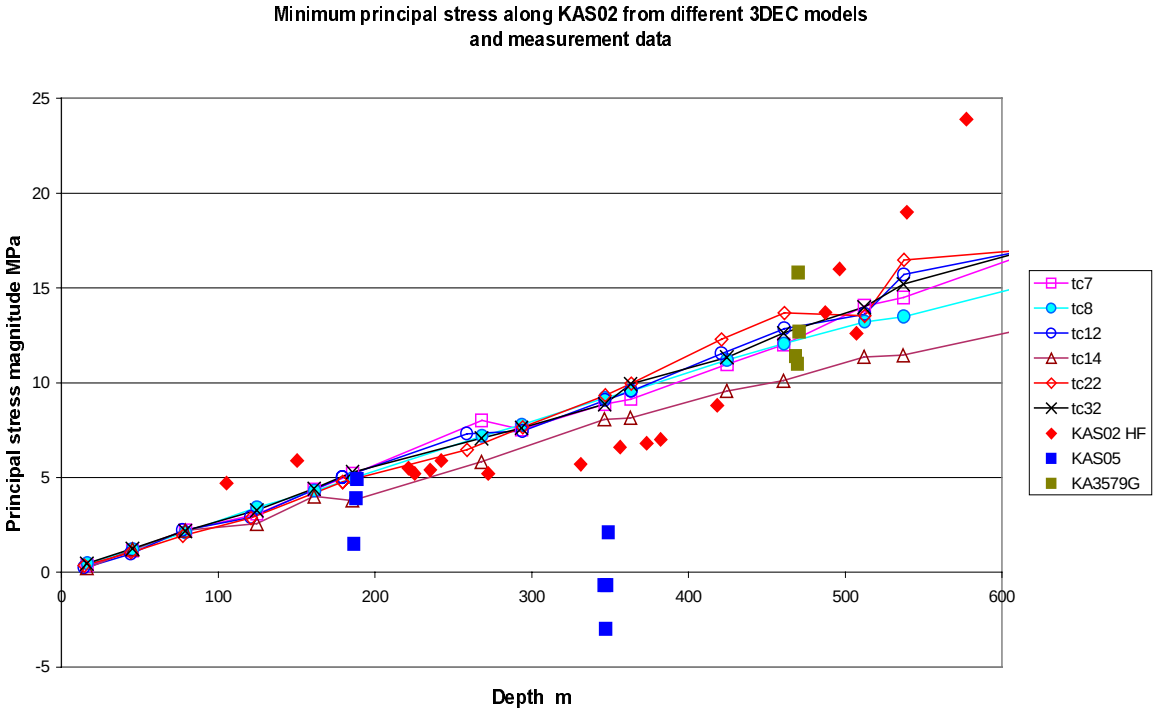

Figure 8-24. *Calculated and measured minimum principal stress. Minimum horizontal stress from hydraulic stress measurements are given for comparison, and σ_3 results from overcoring.*

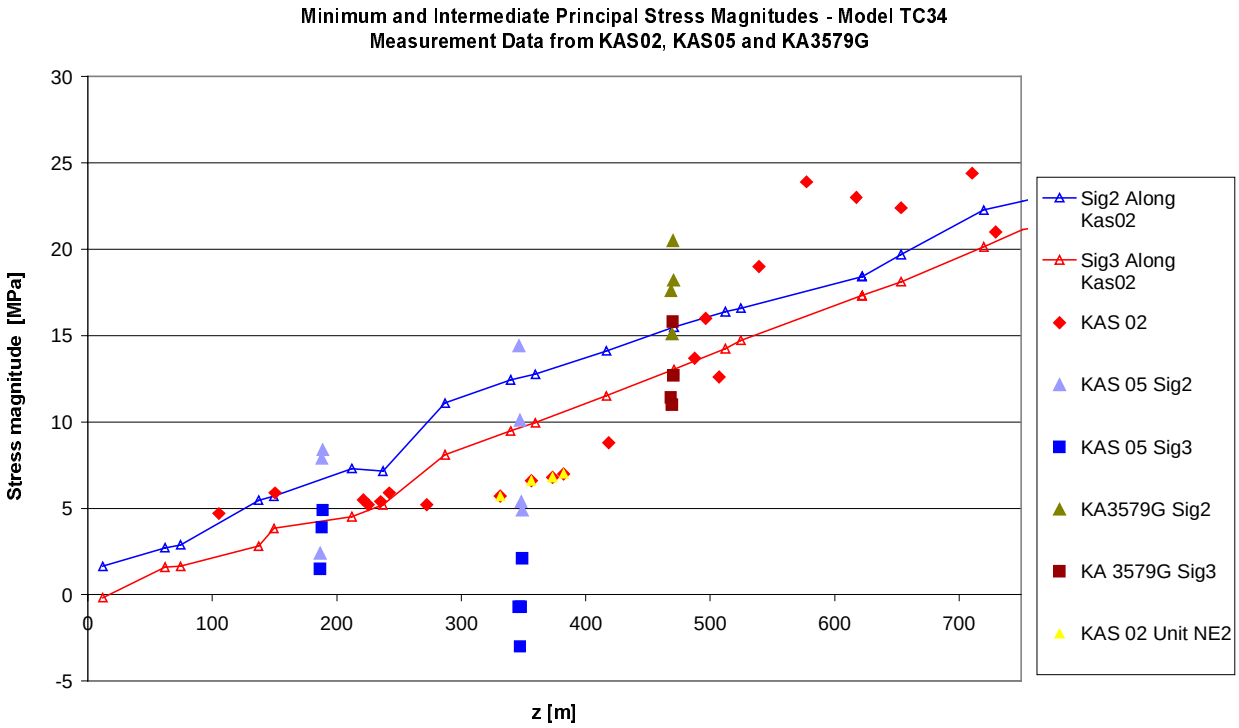

Figure 8-25. *Intermediate minimum principal stress from model TC32. Minimum horizontal stress from hydraulic stress measurements are given for comparison, and σ_2 and σ_3 results from overcoring. Data inside the fracture zone NE2 in KAS02 are marked.*

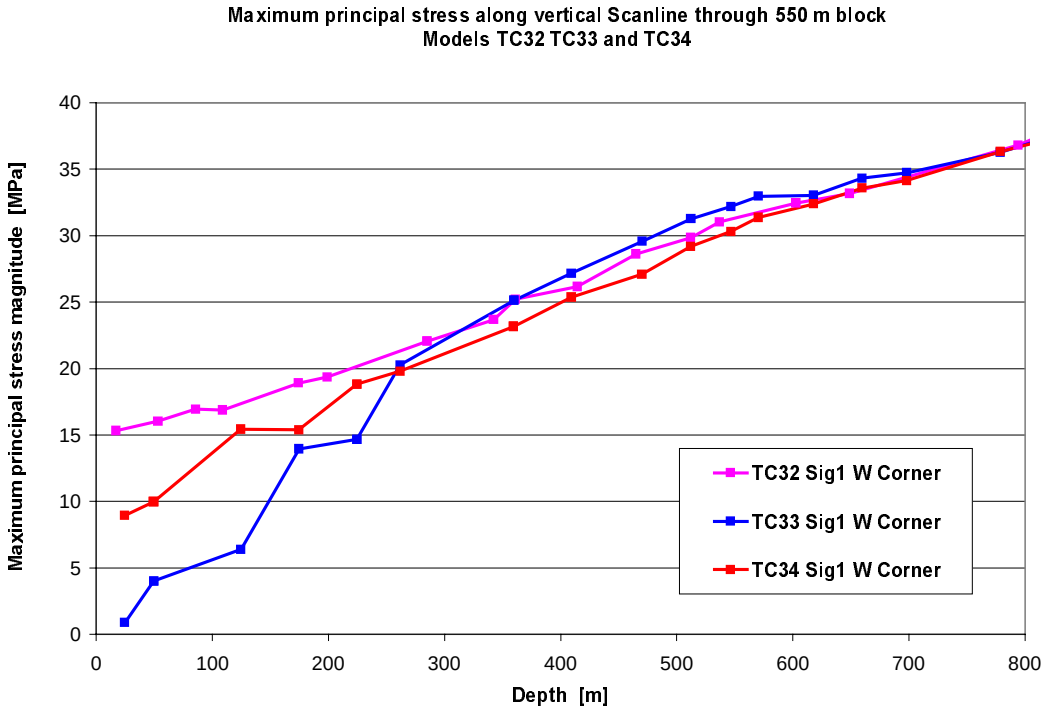

Figure 8-26. *Models with different stiffness properties (see Table 8-5). If the stress seems to have lower values close to ground surface this may be explained by lower stiffness either in zones or in the rock mass. The measurement data close to surface are not sufficient to judge if this type of effect prevails at Äspö or not.*

In Figure 8-26 the results of the maximum principal stress along a vertical line through the models are compared for the three models TC32, TC33 and TC34. These three models have been compressed in a similar way but the stiffness properties were different (see Table 8-5). For models TC33 and TC34 the non-linear increase in stiffness will result in a corresponding non-linear increase in stress width depth.

This modelling is useful to illustrate the phenomenon as such, but it is difficult to judge which model is more representative for the situation at Äspö without some support from the geological and the property models. The stress data are thus not enough to give any support for a certain selection. The general slope of the stress curve will be different depending on the Poisson's ratio chosen for the model. The influence of this parameter on the models with moving boundary condition has not been studied in the project but it is expected possible to find a set (or several sets) of parameters giving a reasonable fit to the measurement data.

It seems that models with the "average" assumption for the maximum principal stress level have too small values compared to measured maximum values. The minimum stress level in the 3DEC models (mainly determined by the initial assumption) seems to fit reasonably well with the measurements of minimum stress at the site. The models with orientation 151° (Äspö local north) are preferred because of the fairly clear indication on orientation in borehole KAS02 measurements. This direction is also within the estimation span of the initial model (Section 8.1.2).

Inside the Target volume the result were taken out along lines corresponding to the centre of cube rows with similar depth (see Fihure 8-15). The principal stresses along the four corner rows are given in Figure 8-27, Figure 8-28 and Figure 8-29, for model TC12, TC33 and TC34, respectively. The points where a jump in values can be observed correspond to the move from a block to another, i.e. to the intersection of a fracture zone (this will be different for the different cube rows). The clearest effect is seen for the intermediate principal stress.

For models TC32, TC33 and TC34 the stresses were applied by moving the boundaries in NW and SE towards each other such that the block was compresses ("moving boundary" condition). The general stress magnitudes of models TC33 and 34 are just a result of how long the models were run. If the boundaries were let to move a little more inwards, i.e. the model was a little further compressed, the levels would naturally been higher. The selection of a certain level must be based on measurement data.

The model TC12 is an example of the modelling sequence with *initiated* stresses (not moving boundaries) and this explains the difference in stress magnitude compared to TC33 and TC34. Other models, not shown here, give more or less similar results as the three examples shown. The magnitude and shape of the curves will vary slightly with changing parameters. It can be noted in Figure 8-27 that a change in magnitude can be seen before and after the intersection of a zone but the stress levels away from intersections will be the same. In models were fracture zones are strong, such as TC1, the corresponding plot of stress magnitudes show almost constant levels (some small variation is due to the fact that the values are not picked at exactly the same depth), see Figure 8-30. The models illustrate the expected influence on stress at a fracture zone, but the models are of course strong idealizations of the real more complex geometries at the zone.

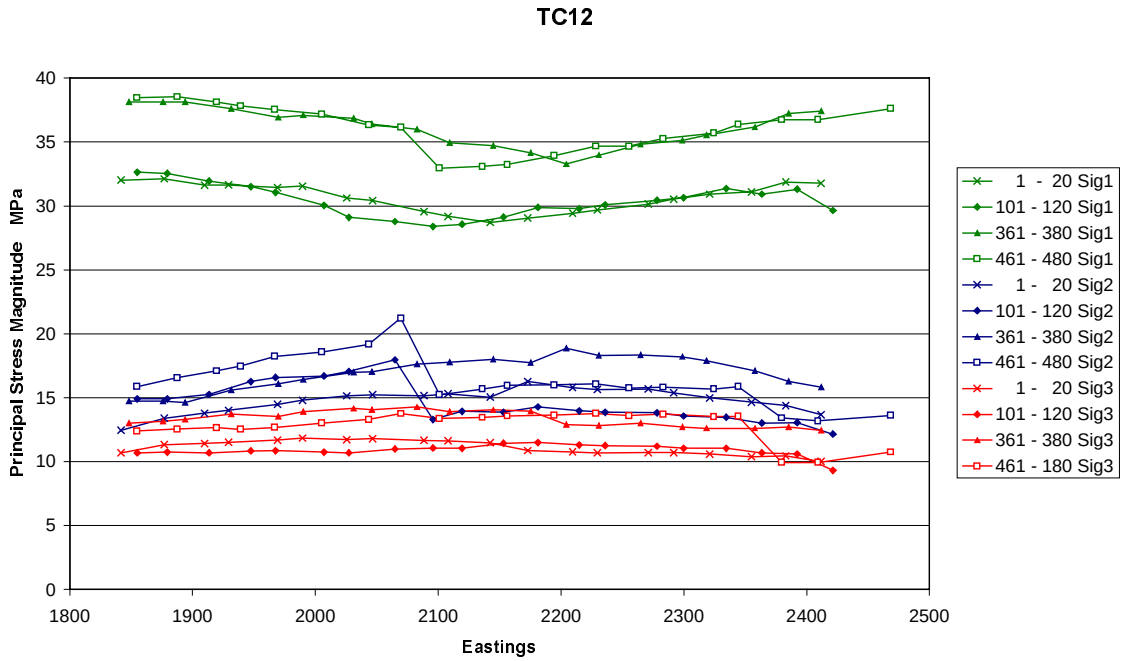

Figure 8-27. *Calculated principal stresses for model TC12 inside the Target volume of the Test Case. Eastings is the x-coordinate of the ÄSPÖ96 local coordinate system. (The numbers of the legend refer to the Target volume cube numbers.)*

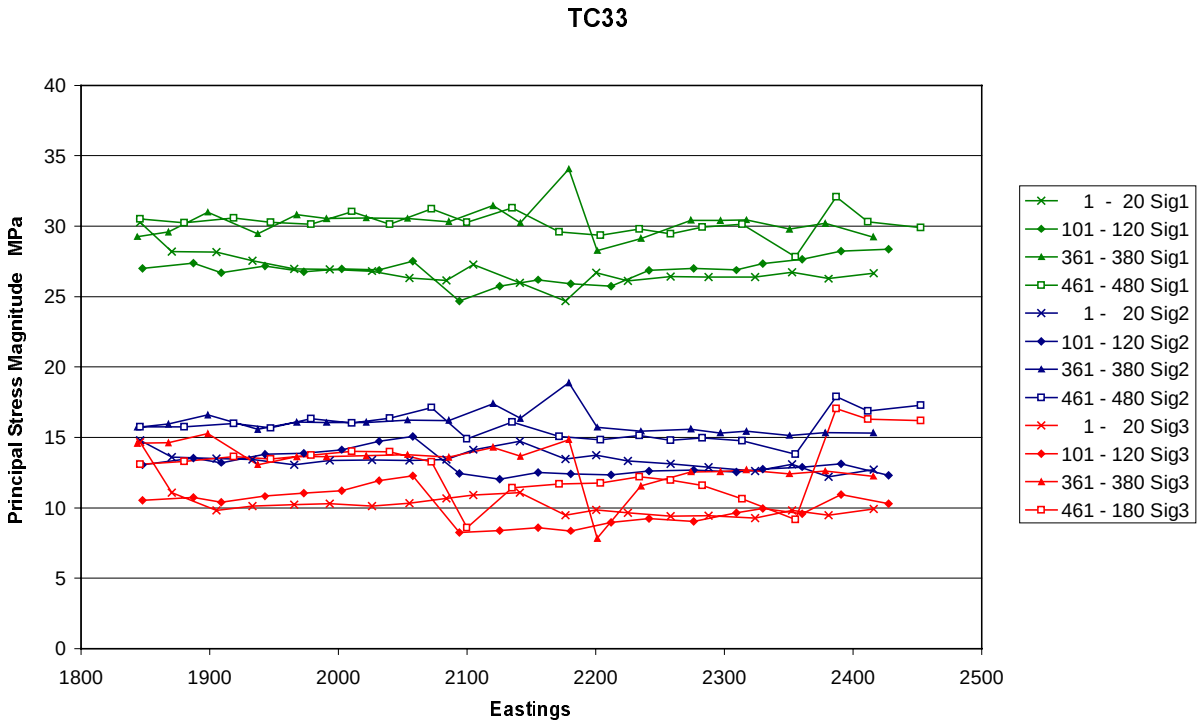

Figure 8-28. *Calculated principal stresses for model TC33 inside the Target volume of the Test Case. (The numbers of the legend refer to the cube numbers). The row 461–480 intersects the zone NE1 at about Easting 2370.*

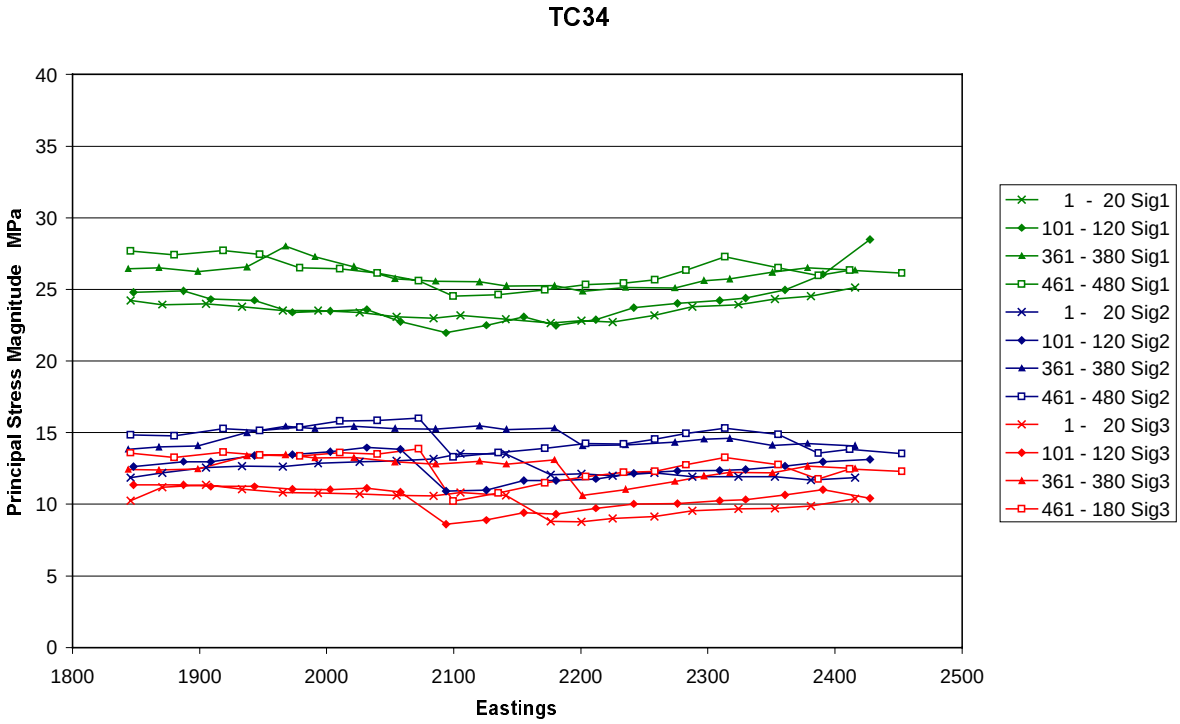

Figure 8-29. *Calculated principal stresses for model TC34 inside the Target volume of the Test Case. (The numbers of the legend refer to the cube numbers). The row 461–480 intersects the zone NE1 at about Easting 2370.*

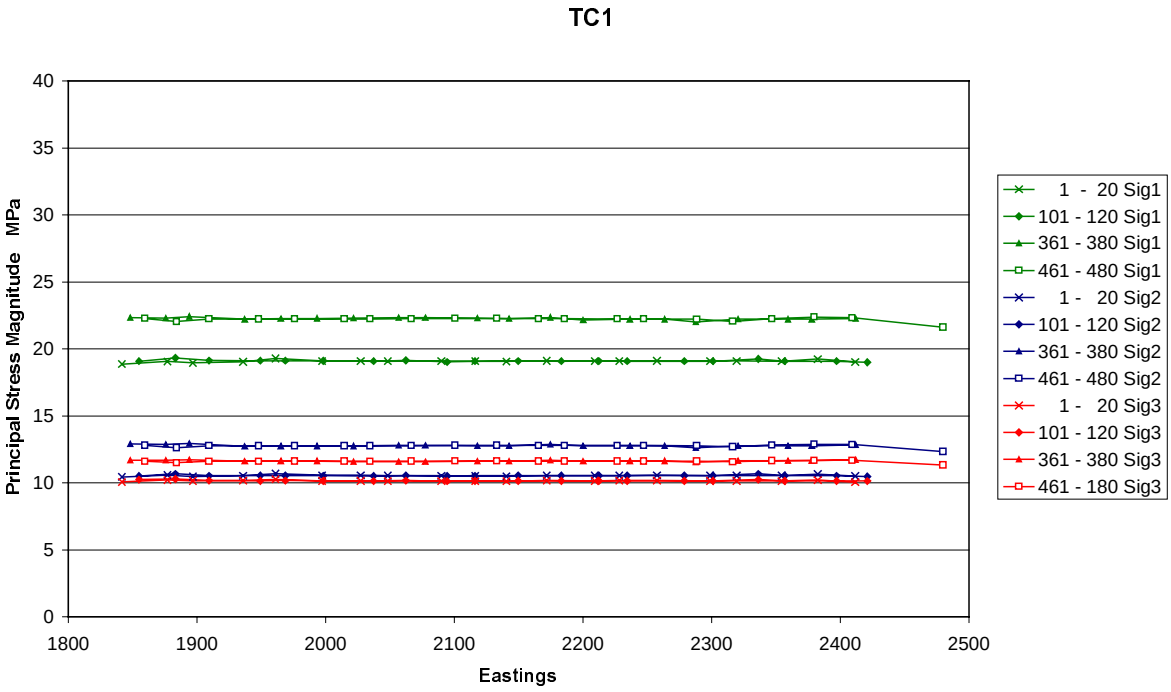

Figure 8-30. *Calculated principal stresses for model TC1 inside the Target volume of the Test Case. Eastings is the x-coordinate of the ÄSPÖ96 local coordinate system. (The numbers of the legend refer to the Target volume cube numbers.)*

In the Target volume, in particular at lower levels, the intermediate and minimum stresses are of similar magnitude and this makes a determination of orientation of them quite meaningless. However, the orientation of the *maximum* principal stress should be possible to interpret in such areas, which also the information desired with respect to design needs.

A possible alternative modelling sequence could have included also movement (e.g. relaxation) of the boundaries perpendicular to the minimum stress (boundaries in SW and NE). Other possible alternative models include simulation of the overlying rock erosion for example. However, it is believed that more models, without additional input on stresses or on geological/mechanical properties would not result in much different conclusion for this test.

8.4.2 Stress orientation

Figure 8-31, Figure 8-32 and Figure 8-33 show the calculated plunge along four horizontal lines in the corner of the Target volume. The results from the different models are not identical, but qualitatively they are similar. The orientation of σ2 and σ3 is influenced by the intersection of fractures and, since their magnitudes are not very different they may change plunge from subhorizontal, inclined to subvertical. The plunge of the major principal stress is stable and mot influences by the fracture zones.

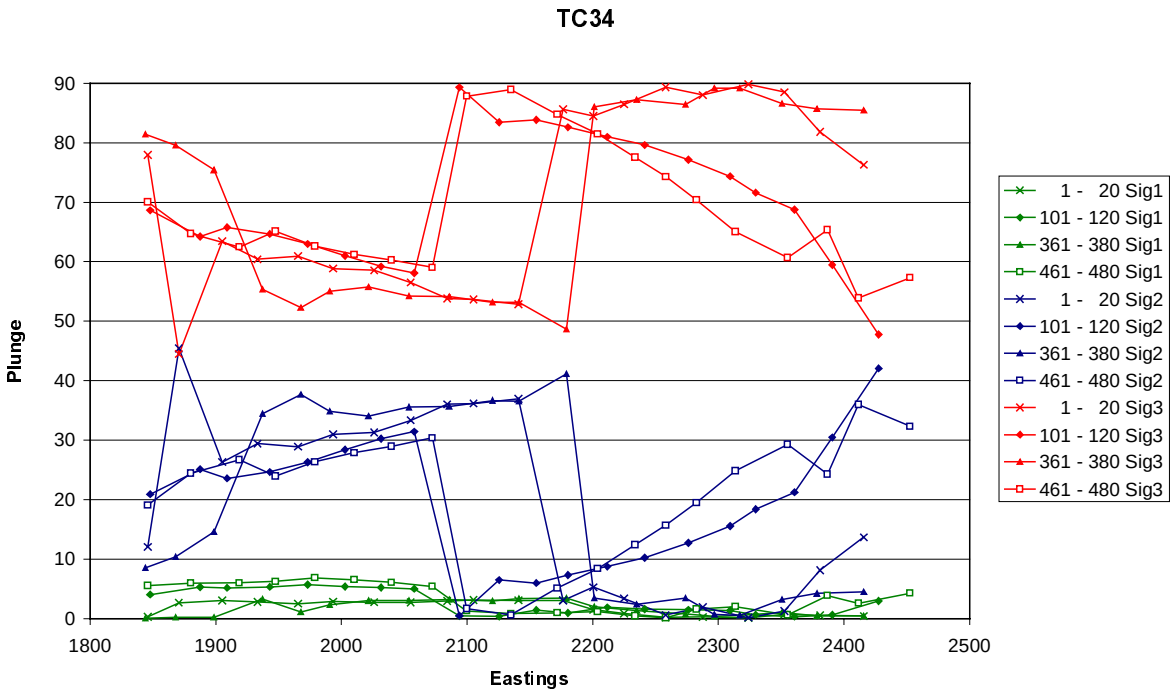

Figure 8-31. *Calculated plunge of the principal stresses along horizontal scanlines in the Target volume for model TC34 (cf. Figure 8-29). It can be noted that the determined plunge change a lot for $\bullet_2$ and $\bullet_3$ at the fracture zone. They are fairly similar in magnitude and therefore a relatively small change in magnitude is sufficient to rotate the field. The maximum stress is stable and subhorizontal.*

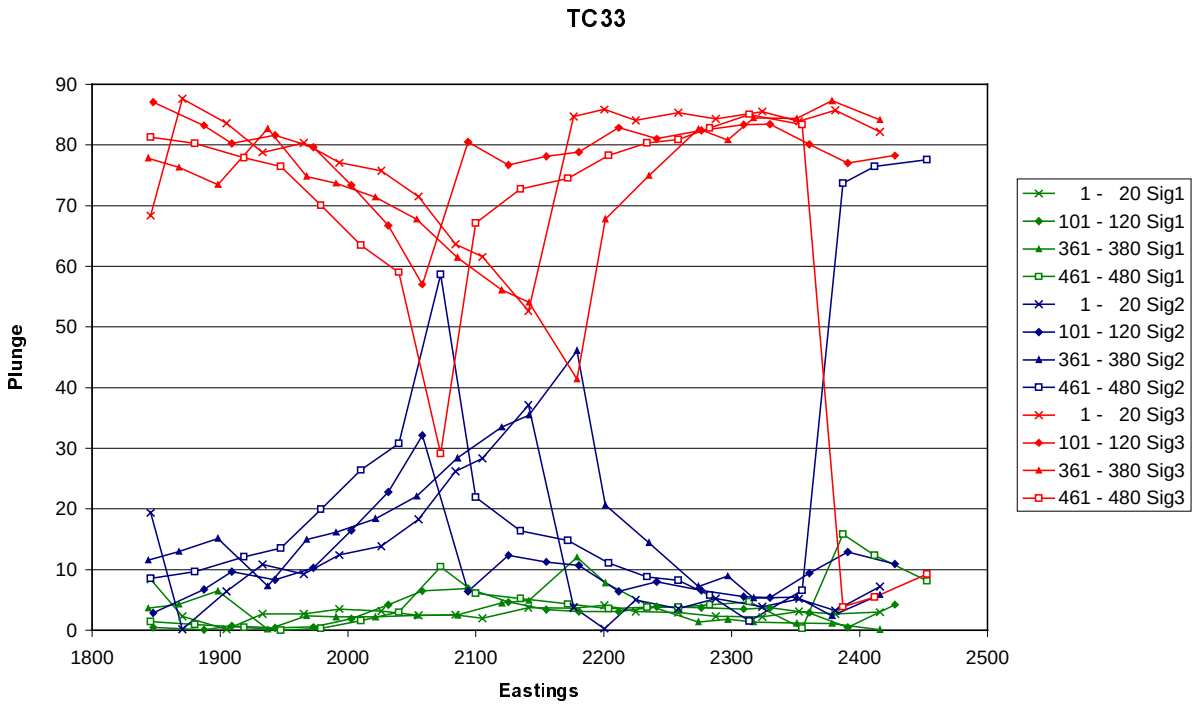

Figure 8-32. *Calculated plunge of the principal stresses along horizontal scanlines in the Target volume for model TC33.*

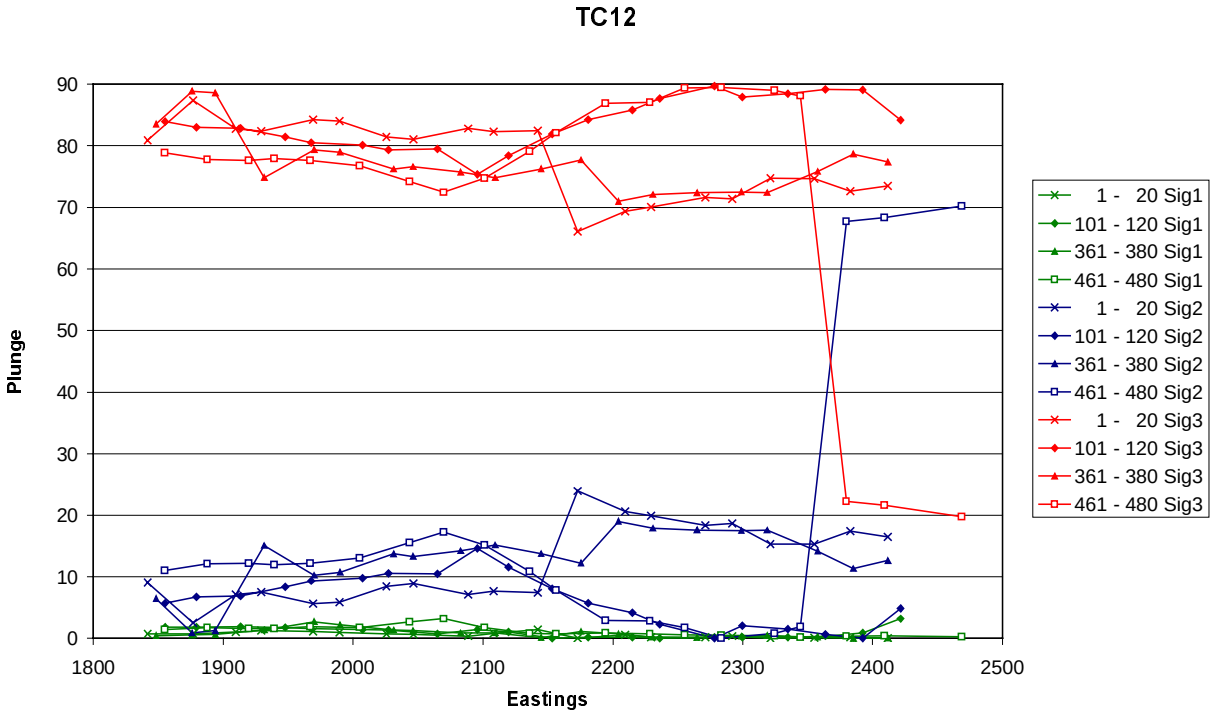

Figure 8-33. *Calculated plunge of the principal stresses along horizontal scanlines in the Target volume for model TC12.*

8.5 Final in situ stress prediction

8.5.1 Prediction of stress field in 550 m block

Principal stress magnitudes

The initial stress model has been adjusted based on the site-specific information and on the numerical modelling results. The final prediction concerning principal stress magnitudes in the 550 m block is presented in Table 8-6 to Table 8-11. (The word 'rock unit' here refers to the geometrical units in the RVS model of the 550 m block of the Test Case, see Figure 8-14). As can be noted the prediction for the mean is the same in the whole domain but the uncertainty span and the variability are different for points in the more intact blocks and in the fracture zone units, respectively.

The uncertainty values (25% and 30%) were selected based on three considerations:

1) Amadei and Stephansson /1997/ report figures from the literature about uncertainty and measurement accuracy. They present accuracy estimates in the range ± 10–20% for overcoring measurements, when the rock is fairly homogeneous and elastic. They further report from different field experiences that with the use of hydraulic fracturing the determination of the minimum principal stress should have an accuracy of ± 10–30%, the vertical stress ± 5–10% and the maximum horizontal stress ± 25–50%. When comparing hydraulic fracturing data with overcoring data the discrepancy has shown to be largest for the maximum principal stress, up to 50%. (But within this exercise is was chosen not to use the hydraulic fracturing data for σ_1 and therefore the uncertainty range for overcoring and for determining the minimum horizontal stress with HF are the most relevant in our case). Generally it is felt that it is difficult to compare the different types of figures (uncertainty/ accuracy/ scatter/variability/error/confidence) reported in the literature because their meaning is vague. In particular, there is often no attempt made to distinguish between the expected *actual* variation and the measurement accuracy as such. Also, the geological conditions at the measurement sites and the measurement equipment used are different, which further complicates the comparison of results. According to laboratory studies reported in /Amadei and Stephansson, 1997/ the accuracy of the overcoring instruments in ideal materials should be < 10%. If rock is anisotropic the stress determination can differ by as much as 25% in magnitude. However, the rock at Äspö is not expected to be strongly anisotropic.

2) The site-specific data for the Test Case was limited and therefore the uncertainty of the stress magnitude prediction should not be low. Measurements have note been made in several units of the studied domain and there exists major structures within the domain that could possibly be influencing the stress field. The modelling has indicated that the fracture zone slip may cause stress magnitude change, mainly for σ_2 and σ_3. Therefore the values in fracture zones and in rock units N (south of NE1) were also selected slightly higher.

3) The measurement report from Klasson et al. /2001/, concerning overcoring data, discusses the sources of errors and data confidence. They make the general judgement that the (possibly systematic) measurement error, introduced by the fact that the rock does not fulfil the assumption of homogeneity and linear elastic behaviour (which is a *part* of what is here called uncertainty), should not exceed 15%.

Table 8-6. Final prediction of σ1 stress magnitudes for Test Case 550 m block.

Rock Unit	FZ Name	Mean σ_1 (Mpa) at z –500	Function of depth	Uncertainty u % of mean	Variability v % of mean
A		33.5	$\sigma_{1=}$ 0.065(-z)+1	25	15
B C D E F	EW1	33.5	$\sigma_{1=}$ 0.065(-z)+1	25	50
G		33.5	$\sigma_{1=}$ 0.065(-z)+1	25	15
H		33.5	$\sigma_{1=}$ 0.065(-z)+1	25	15
I		33.5	$\sigma_{1=}$ 0.065(-z)+1	25	15
J	NE2	33.5	$\sigma_{1=}$ 0.065(-z)+1	25	50
K	EW3	33.5	$\sigma_{1=}$ 0.065(-z)+1	25	50
L		33.5	$\sigma_{1=}$ 0.065(-z)+1	25	15
M	NE1	33.5	$\sigma_{1=}$ 0.065(-z)+1	25	50
N		33.5	$\sigma_{1=}$ 0.065(-z)+1	25	50

Table 8-7. Final prediction of σ2 stress magnitudes for Test Case 550 m block.

Rock Unit	FZ Name	Mean σ_2 (Mpa) at z = -500	Function of depth	Uncertainty u, % of mean	Variability v, % of mean
A		13.5	$\sigma_{2=}$ 0.027(-z)	25	15
B C D E F	EW1	13.5	$\sigma_{2=}$ 0.027(-z)	30	50
G		13.5	$\sigma_{2=}$ 0.027(-z)	25	15
H		13.5	$\sigma_{2=}$ 0.027(-z)	25	15
I		13.5	$\sigma_{2=}$ 0.027(-z)	25	15
J	NE2	13.5	$\sigma_{2=}$ 0.027(-z)	30	50
K	EW3	13.5	$\sigma_{2=}$ 0.027(-z)	30	50
L		13.5	$\sigma_{2=}$ 0.027(-z)	25	15
M	NE1	13.5	$\sigma_{2=}$ 0.027(-z)	30	50
N		13.5	$\sigma_{2=}$ 0.027(-z)	30	50

Table 8-8. Final prediction of σ3 stress magnitudes for Test Case 550 m block.

Rock Unit	FZ Name	Mean σ_3 (Mpa) at z = -500	Function of depth	Uncertainty u, % of mean	Variability v, % of mean
A		12.0	$\sigma_{3=}$ 0.0174(-z)+ 3.3	25	15
B C D E F	EW1	12.0	$\sigma_{3=}$ 0.0174(-z)+ 3.3	30	50
G		12.0	$\sigma_{3=}$ 0.0174(-z)+ 3.3	25	15
H		12.0	$\sigma_{3=}$ 0.0174(-z)+ 3.3	25	15
I		12.0	$\sigma_{3=}$ 0.0174(-z)+ 3.3	25	15
J	NE2	12.0	$\sigma_{3=}$ 0.0174(-z)+ 3.3	30	50
K	EW3	12.0	$\sigma_{3=}$ 0.0174(-z)+ 3.3	30	50
L		12.0	$\sigma_{3=}$ 0.0174(-z)+ 3.3	25	15
M	NE1	12.0	$\sigma_{3=}$ 0.0174(-z)+3.3	30	50
N		12.0	$\sigma_{3=}$ 0.0174(-z)+3.3	30	50

The local spatial variability (v) values for the stress magnitudes of 15% and 50%, respectively, were selected based on the following considerations:

1) The overcoring measurement results from points close to each other (see Table 8-3), indicated that the spread may be larger in the fracture zone compared to the more intact rock units. These site-specific data further indicate that the spread in stress magnitude data from the same depth may be in the order of (assuming that a span of ± the data standard deviation would cover most of the actual variation). It should, however, be noted that the indication is fairly weak since the number of data behind the figures are few.

2) The discrepancy in v values between rock units for rock mass between and inside fracture zones was considered realistic based on the conceptual model of a fracture (or deformation) zone. It is known that fracture zones may change in appearance from point to point, sometimes being wider and sometimes consisting of several branches etc. A rock unit including a larger variation in fracturing and material deformation properties, compared to surrounding rock, must be considered to also have a larger variation in stress magnitudes.

3) The measurement report from Klasson et al., /2001/ also makes an estimate of the "total" measurement error. They estimate that the measurement scatter for a group of measurement to be 1–3 MPa for magnitudes of 15–25 MPa. The scatter was regarded as an estimate of the non-systematic errors. (This estimate was here judged to mostly reflect the expected spatial variability.)

For further discussion about issues with relevance to the selection of the parameters u and v refer also to Section 8.1.3, Section 9.8 and Chapter 7.

Principal stress orientations

The prediction of the stress orientation in the different rock units is presented in Table 8-9, in the same way as for the magnitudes. The orientation of the minimum principal stress may be derived from the maximum and intermediate principal stress orientations, since the principal stresses are by definition perpendicular to each other. As was mentioned earlier the uncertainty in the magnitude makes it not possible to definitely give a certain notation concerning which principal stress to be the intermediate and the minimum (the indexes 2 and 3 might be interchanged to be correct). At many sites in Sweden the two smallest principal stresses may have the same magnitude, at least at some depths. However, this prediction says that, in areas where magnitudes are dissimilar, the three principal stresses are expected to lie parallel or subparallel to the horizontal and vertical directions.

Table 8-9. Final prediction of principal stress orientations in the 550 m block.

Rock	FZ	σ_1 Trend (Äspö local north) (°)			σ_1 Plunge (°)			σ_2 Plunge (°)		
Unit	Name	β	u	v	α_1	u	v	α_2	u *	v
A		150	15	15	0	10	15	0	10–45	15
B C D E F	EW1	150	30	25	0	20	30	0	10–45	30
G		150	10	15	0	10	15	0	10–45	15
H		150	10	15	0	10	15	0	10–45	15
I		150	10	15	0	10	15	0	10–45	15
J	NE2	150	30	25	0	30	30	0	10–45	30
K	EW3	150	30	25	0	30	30	0	10–45	30
L		150	10	15	0	10	15	0	10–45	15
M	NE1	150	30	25	0	20	30	0	10–45	30
N		150	15	15	0	10	15	0	10–45	15

* Depending on depth. For z = 0– -100 u = 10, for z = -100– -400 u = 45 and for z < -500 u = 10.

The uncertainty (*u*) values for the orientation (10°, 15° and 30°) were selected based on the following considerations:

1) The hydraulic fracturing results and the results from the few overcoring measurements see Figure 8-8, give a fairly consistent direction for the maximum horizontal stress (coinciding here with the major principal stress). No systematic changes in orientation with respect to the different units or different depths can be identified based on the available data. The exception to this is the KAX05 data.

2) The orientation seen for maximum horizontal stress in the database from stress measurements in Sweden gives a picture of a fairly stable orientation.

3) The orientation of the intermediate and minor principal stresses are not independent of the major principal stress (they are always perpendicular). The uncertainty figure rather reflects how large the ‘risk’ is that the magnitude of the minor and intermediate stresses are the same, because it is obvious that if they are of the same magnitude it will not be meaningful to determine their direction and the expected variation in measured plunge should be large. This is behind the footnote of the table.

The local spatial variability (*v*) values for the orientation (15°, 25° and 30°) were selected based on the following:

1) The standard deviation for groups of overcoring data (Table 8-4) is 7° and 8° for the trend of the major principal stress, (measured in rock unit above and below the fracture zone NE2) and about 5° for the plunge. The standard deviation for the plunge of the intermediate and minor stress is lower at the deepest measurement level (about 11° compared to 34°). This may be explained by the larger difference in magnitude of the intermediate and minor stresses at depth. A larger difference (clearer stress anisotropy in the vertical plane perpendicular to the major principal stress) would make the (actual) orientation more stable, and less influenced by minor local changes in magnitudes.

2) The discrepancy in *v* values between rock units for rock mass between and inside fracture zones was considered realistic based on the conceptual model of a fracture (or deformation) zone. The complex nature of a fracture zone is expected to give more local deflections and local stress redistributions resulting in a higher local spatial variability in the stress orientation, compared to the averagely fractures rock units.

3) According to the measurement report from Klasson et al. /2001/ the measurement work (borehole KA3579G) went on smoothly and an overall good rock quality was noticed. Only a few intended measurement points were discarded. They did mention about any particular problems concerning the determination of fracture orientation.

8.5.2 Stress prediction in Target block

Principal stress magnitudes

The final stress prediction model presented above (in Section 8.5.1) for the 550 m block has been applied on the Target volume of the Test Case. The result for the stress magnitudes is given in Table 8-10. Since the stress magnitudes are only dependent on the z-coordinate in this model, the predictions are given for four "cube groups" corresponding to the four different cube levels in the Target volume.

Table 8-10. Final predictions of principal stress magnitudes in the Target volume of the Test Case.

Cube ID	Rock Unit	Cube Centre z (m)	σ_1 (Mpa)	Min-Max (u) (Mpa)	±v (%)	σ_2 * (Mpa)	Min-Max (u) (Mpa)	±v (%)	σ_3 * (Mpa)	Min-Max (u) (Mpa)	±v (%)
1–120	H	-395	26.7	18.7–34.7	15	10.7	8,0–13,3	15	10.2	7,6–12.7	15
1–120	I	-395	26.7	18.7–34.7	15	10.7	8,0–13,3	15	10,2	7,6–12,7	15
1–120	J	-395	26.7	18,7–34,7	50	10.7	7,5–13,9	50	10,2	7,1–13,2	50
121–240	H	-425	28.6	21.5–35.8	15	11.5	8,6–14,4	15	10.7	8,0–13,4	15
121–240	I	-425	28.6	21.5–35.8	15	11.5	8,6–14,4	15	10,7	8,0–13,4	15
121–240	J	-425	28.6	21.5–35.8	50	11.5	8,4–14,9	50	10,7	7,5–13,9	50
241–360	H	-455	30.6	22.9–38.2	15	12.3	9,2–15,4	15	11.2	8,4–14,0	15
241–360	I	-455	30.6	22.9–38.2	15	12.3	8,6–16,0	15	11,2	8,4–14,0	15
241–360	J	-455	30.6	22.9–38.2	50	12.3	9,2–15,4	50	11,2	7,9–14,6	50
361–480	H	-485	32.5	24.4–40.7	15	13.1	9,8–16,4	15	11.7	8,8–14,7	15
361–480	I	-485	32.5	24.4–40.7	15	13.1	9,8–16,4	15	11,7	8,8–14,7	15
361–480	J	-485	32.5	24.4–40.7	50	13.1	9,2–17,0	50	11,7	8,2–15,3	50

* The principal stress in this direction may in some cases be σ_3 instead of σ_2.

Principal stress orientations

In Table 8-11 the orientations of the estimated stresses in the target volume are presented. Since the three principal stresses are orthogonal in each point, only three parameters are needed to define the orientation. It was chosen to give trend, β, and plunge, α, for the maximum principal stress, σ_1, and the plunge of σ_2. From these values the trend of σ_2 and the trend and plunge for σ_3 may be determined. The values u and v correspond to the uncertainty and variability estimates described in Section 8.5.1.

Table 8-11. Final predictions of principal stress orientations in the Target volume of the Test Case.

Cube ID	Rock Unit	Cube Centre z	σ_1 Trend β_1	±u	±v °	σ_1 Plunge α_1	±u	±v °	σ_2 Plunge α_2	±u *	±v
1–120	H	-395	150°	10°	15°	0°	10°	15°	0°	45°	15°
1–120	I	-395	150°	10°	15°	0°	10°	15°	0°	45°	15°
1–120	J	-395	150°	10°	15°	0°	10	45	0°	45°	45
121–240	H	-425	150°	10°	15°	0°	10°	15°	0°	45°	15°
121–240	I	-425	150°	10°	15°	0°	10°	15°	0°	45°	15°
121–240	J	-425	150°	10°	15°	0°	10	45	0°	45°	45
241–360	H	-455	150°	10°	15°	0°	10°	15°	0°	45°	15°
241–360	I	-455	150°	10°	15°	0°	10°	15°	0°	45°	15°
241–360	J	-455	150°	10°	15°	0°	10	45	0°	45°	45
361–480	H	-485	150°	10°	15°	0°	10	15°	0°	45°	15°
361–480	I	-485	150°	10°	15°	0°	10	15°	0°	45°	15°
361–480	J	-485	150°	10°	15°	0°	10	45	0°	45°	45

* The principal stress in this direction may in some cases be σ_3 instead of σ_2.

8.6 Conclusions from Test Case

The available stress measurement data were not sufficient too identify a clear pattern in the stress variation at the Test Case site. The reason to this was that there was no obvious consistency between results from different methods and there was a large uncertainty in the interpretation of the data.

Hydraulic fracturing measurement data for the *maximum* principal stress were judged too uncertain to form a basis for the stress prediction. This judgement was founded on theoretical arguments from the literature.

Overcoring measurements were therefore used to predict the *maximum* principal stress. Hydraulic fracturing measurement data were used, together with overcoring measurement data and 3DEC modelling, to make a prediction of the *intermediate and minimum* principal stresses.

Additional overcoring data from the 300 – 400 depth interval, at locations outside fracture zones, would be helpful in supporting/rejecting the final stress model.

The 3DEC modelling indicated a possible explanation to a change in minimum and intermediate stress magnitude when crossing fracture zone NE2 inside the Target volume. This is an upward movement of the blocks H, I and L (between EW1 and NE1)

caused by the horizontal stresses (a horizontal compression) in the region. The 3DEC models further suggest that a change in stresses occurs when passing the fracture zone EW1. This zone has undergone a dextral (sub-horizontal) slip movement.

The mean orientation for the maximum principal stress is predicted with a fairly high degree of certainty because both regional stress pattern and the site-specific measurements indicate the same orientation: 150° ± 10° trend and 0° ± 10° plunge. The local spatial variation around the mean is predicted to be within ± 15° for both trend and plunge. This prediction applies to the whole 550 m block away from the fracture zones. The spatial variability of the principal stress magnitudes inside or close to fracture zones is predicted to be large.

The orientations of σ_2 and σ_3 are lying in the plane perpendicular to σ_1, but plunge and trend in this plane are uncertain of two reasons. Firstly the hydraulic fracturing measurement technique cannot give any information on this matter and therefore the available data are few and also the overcoring data are not very conclusive. Secondly the intermediate and minimum principal stresses are expected to be of the same magnitude at laboratory depth, and in such case the stress level is the same in all direction in the plane perpendicular to the maximum principal stress direction (σ_2 and σ_3 have then no defined direction).

9 Recommended method for the development of a stress model at a repository site

9.1 Introduction

Based on the literature review performed and on the experiences gained from the Test Case exercise a flowchart for the process of developing a stress model at a site has been developed. This flowchart is shown in Figure 9-1 and can be regarded as a short summary of our recommended methodology. In the following sections the different parts of the flowchart are explained.

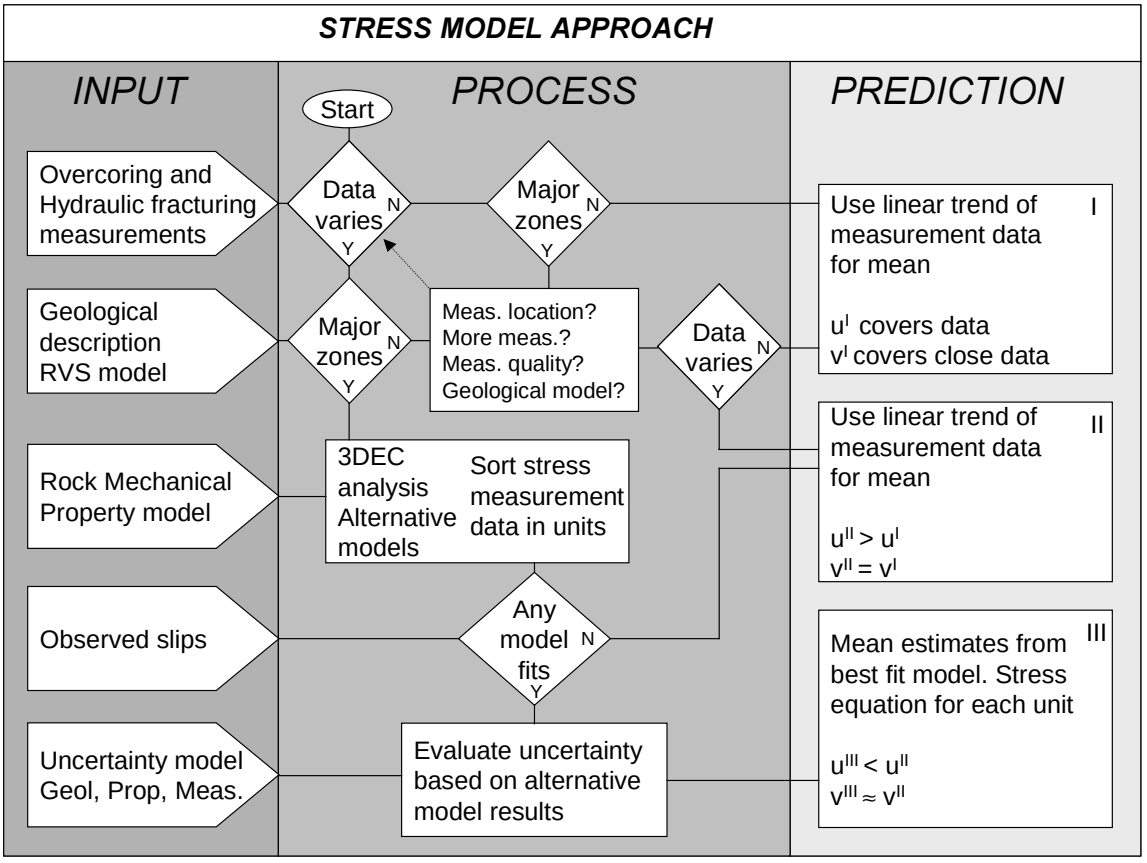

Figure 9-1. *Flow-chart illustrating the steps in the suggested process of building an in situ stress prediction.*

9.2 Input

The information concerning the *in situ* stress level at a specific site may be of different kinds. The most important source of information is from stress measurements made at the site. Measurements can be done using different methods (see Chapter 7). Other information relevant for the development of a stress model can be derived from core discing in drill cores or core discing in connection with stress measurements /Hakala, 2000/. If borehole breakouts ("dog-earing") occur this can also give an indication of stress level and stress orientation.

Another important source of data for use when developing a stress model for a repository site is the input from the "geological model". This relates to geological heterogeneities within the study area (specifically rock type variation and geological structures (fractures etc.)) and the geological history of the site. Of particular importance are geological features that may influence the estimation of the mechanical properties of the rocks.

These include features related to fractures and fracture zones such as any alteration of the rock bounding the fracture caused by the ingress of weathering fluids, the presence of any infilling material, fracture aperture, evidence of shearing along the fractures and evidence of multiple slip events.

It is also valuable if observations are available from both boreholes and the surface. This enables the variation of structures with depth to be determined. This is particularly relevant to fracture frequency, aperture, and occurrence of soft infilling materials. The geological input should also include a description of the uncertainty of the model, i.e. it should be used to determine the level of confidence regarding the location and extension of major fractures and fracture zones with depths.

Clearly, information concerning mechanical differences between different rock units in the region, given by the "property model" is directly relevant to the construction of a numerical model. In addition it is useful to establish the mechanical properties of the major fracture zones, although this may turn out to be a difficult task with large uncertainties involved. The rock mechanics "property model" should also include a description of the uncertainty in any of the parameters. For example, it is valuable to know if a certain fracture zone has estimated property values based on drill cores from bore holes intersecting the zone (and therefore are considered comparatively certain) or if the properties are estimated based on other reasoning such as extrapolation from the surface either inside or outside the site. The methodology to arrive at a "property model" at a site is described and discussed further in Andersson et al. /2002/, Röshoff et al. /2002/ and Staub et al. /2002/.

It should be noted here that a knowledge and understanding of the geology also outside the volume of the study area, for which the stress predictions are required, is of great interest. The structural model should preferably be large enough to include the whole extent of any fracture zones intersecting the area and also show the extent and orientation of the whole of these structures. In addition, if there are other underground activities in the region or if there are stress measurement in the region (but outside the site) they should also be considered. A broad understanding of the geological setting and tectonic framework of the site can provide an invaluable insight into the structures and stress patterns that are likely to occur in the study area.

Further, information about tectonic activity in the region can be used to infer stress direction and should therefore also be provided.

9.3 Do the stress measurement data show variation?

The first step in the suggested approach for developing a stress model for a site is to determine whether the site-specific information indicates a variation in stress within the area of interest. The term "variation" is understood in this context as an *in situ* stress field that has a variation other than a linear increase with depth for the stress magnitude or which has different stress fields in different parts of the site.

To be able to answer this question the measurement data must be evaluated. It is also important at this stage to ensure that the volume within which the prediction is supposed to be made is clearly defined. The measurement data should preferably be located within this volume. If the data are very sparse or if the quality of the data is poor it may be difficult to answer the question (see also Chapter 7).

9.4 Are major fracture zones present in the area?

The next step is to study the geological model of the site and determine if the volume for which the prediction is to be made is intersected by any major fracture zone (or other type of deformation zone). For the design of a future repository a location without major fracture zones will be preferable for both design and safety reasons. However, since the repository will have a large horizontal extent it may not be possible to locate it inside an area that is not cut by at least one major fracture zone.

For the geological conditions pertaining in Sweden the most likely reason for any significant variation in the *in situ* stress field is the occurrence of a fracture zones (see Chapter 4). It should be noted here that gently dipping and sub-horizontal fracture zones, which are much less likely to be detected by surface mapping than sub-vertical zones, are equally likely to generate important stress heterogeneities within the potential repository site. Therefore the geological model at hand should be evaluated carefully, particularly if it relies heavily on surface mapping and should be checked to ensure that sub-surface features have not been overlooked. If there is a significant variation in the stress data from the site and if the site contains any major fracture zones, the stress situation should be analysed further with the help of a three-dimensional analysis tool (Section 9.6).

If there is no variation in the measurement data but there are major fracture zones in the area the location of measurement data should be checked carefully before any prediction is made (Section 9.5).

If there is no variation in stress and no major fracture zone(s) the prediction of the stress regime may be established without further analysis. This prediction should consist of a linearly varying trend for the three principal stresses. The same prediction should in this case be valid for the whole prediction volume. See Section 9.8 for an explanation of the recommended way of describing the uncertainty in the predictions.

9.5 Evaluation of measurement data

The measurement location in relation to the different rock units (geometrical units) in the geological model should be determined. This is easily done by using the RVS system and the SICADA database. By doing so it is possible to judge whether any stress data has a correlation to the geology.

In addition, all information possible from the stress measurement works should be gathered, including the raw data if possible. Raw data, such as strain records during overcoring, biaxial test results and core descriptions are valuable if the uncertainty of a single measurement needs to be examined. If a certain datum deviates much from the overall pattern this measurement could be checked to see of there are any measurement related explanations for the value or if it should be considered as a true stress value. Ideally the stress measurement reports should include a notation on confidence level for each single measurement so that the more uncertain results can readily be identified.

9.6 Three-dimensional modelling

By building a three-dimensional numerical model of the site, including any major fracture zones it may contain, the expected stress distribution can be analysed. The suggested procedure was outlined in Chapter 4 and exemplified in Chapter 6. The main hypothesis behind such analysis is that the current fracture zones are in equilibrium and previous slip on the fracture zone planes is the cause of today's stress variation. The influence of stiffness differences in the area may also be included in the analysis.

The results of the modelling will be much controlled of the applied modelling approach. The loading sequence, and boundary conditions must be selected carefully and with respect to what main factor to be studied, influence from stiffness differences of influence from fracture shear movements. The numerical study should include a sensitivity study, i.e. a comparison of several models with different properties and boundary conditions.

When anticipating a varying *in situ* stress field, a three-dimensional numerical analysis is a means of predicting the stresses in the areas of the site where no stress measurements have been performed or where the measurements are very uncertain.

9.7 Is there any model that fits?

The most difficult step in the development of a stress model for a site is the selection among different potential models having different degree of fit to the input data. The stress field in the models will depend on the loading sequence and the geometrical and strength properties of the zones, and therefore the different assumptions behind each model should be compared with the input information concerning rock mass and fracture zone mechanical and geometrical properties.

The aim of this step is to judge which one of the possible models, i.e. which one of the different combinations of influencing factors (geometry, zone property, boundary conditions) best represents the actual stress field.

In this step one should consider all the site-specific input available, but it is also as important to consider the current knowledge and understanding in the relevant subjects as reported in the scientific literature. This comparison and the judgements to be made may appear to be a somewhat subjective step. However, this is inevitable and acceptable as long as the reasoning is documented properly.

One way to quantify the difference between a certain stress model (for example a particular linear function with depth) and the measurement data could be to calculate the sum of the differences point by point, or to use some other similar statistical method. However, it is recommended that the comparison be made by judgement on the qualitative fit by the investigator. This more subjective method is preferred because there are many different factors to consider in the comparison and some of them may not be correctly incorporated if one uses only a calculated "best-fit-factor". If several models give a similar fit to the measurement data, which could very well be the case, the model that seems most reasonable in terms of the property assumptions made should be selected as the model on which to base predictions. If models with similar fit to the measurements also indicate the similar stress fields in areas outside the measurements then there is actually no need to make any selection between the models (or it does not matter which one is chosen), since the aim of the modelling is support of a certain stress prediction rather than to find a "true model". In this case the stress field is not sensitive to the parameters and conditions varied between models.

Simple models are preferred over more complicated models, i.e. a simple linear function should be used if there is no other model that better explains observed features. It is *not* recommended that non-linear curves (exponential, logarithmic or polynomial) fitted directly to measurement data be used as "models", because in such case there is no mechanical explanation for the observed stress variation. The data obtained in a single borehole should therefore not be used directly, without further analysis, as a prediction in areas away from the measurements. (At the measurement point the measurement result should of course be regarded as representative of the actual stresses in this point, if the data are considered reliable.)

It is important to note clearly within which part of the region and, even more importantly, at which depth a certain prediction is made. A linearly increasing depth-dependant stress magnitude has often been used as a stress prediction /e.g. see Amadei and Stephansson, 1997/. However, there is no reason to think that the stresses should necessarily continue to increase at the same rate beyond a certain depth. The stress models should therefore be used carefully and not for predictions much deeper than the deepest measurement.

9.8 Uncertainty parameter estimation

We have chosen to divide the sources for uncertainty in stress prediction into two categories corresponding to two different parameters, the "u-parameter" (uncertainty parameter) and the "v-parameter" (variability parameter). These uncertainty parameters will determine two "spans" for each prediction ($\pm$ u and $\pm$ v, respectively).

9.8.1 The u–parameter

The first span corresponds to the uncertainty in the estimation of the *average in situ* stress (magnitude, trend and plunge). With "average" is here meant the general stress situation expected within a certain specified rock volume, a "rock unit". For example, one rock unit could be the rock mass consisting of the same rock type and lying between three major deformation zones. In this volume the geological model (a simplified geometry model) of the site states that the condition should be fairly homogeneous. The u-parameter is meant to cover the uncertainties in the geological model, the uncertainty concerning tectonic regimes prevailing, lack of measurements, systematic measurement errors, measurement bias etc.

The rock unit volumes will in the site investigations probably be of very large size (10–100 km^3). The parameter stress existing in any arbitrary "local point" of the rock mass is defined as the load divided by the area over which the load is acting. A scale of the stress parameter must therefore be *chosen* depending on the problem. The "local stress scale" was considered to be the volume of rock that would determine a stress measurement result, i.e. a volume in the order of 0.01–1 m^3. With average stress of a certain rock unit is understood the mean value of all the local stress values, of 1 m^3 size volume, that belongs to this unit. If the prediction of stress is given as an equation with depth the average stress is the mean from volumes having the same depth location in the rock unit.

If there was a perfect measurement method that was actually able to measure stress at large scale (or at a very large amount of points) and with excellent accuracy, then the uncertainty parameter u would have become zero in rock units where such measurements were made. However there are many different sources of uncertainty when performing and interpreting stress measurement results, and the u-parameter is meant to reflect this uncertainty (see Chapter 7). The aim of the process to make a stress model is to minimize the u-parameter, in areas where stresses are important.

9.8.2 The v–parameter

The second span, v, corresponds to the expected spatial variability of *in situ* stress *around* the average (magnitude and orientation). The cause of a local variability of both stress magnitude and orientation is the inhomogeneous character of rock mass at all scales. Even the most competent rock mass will include fractures of some size and rock type heterogeneities, such that a small (< 1 m^3) volume of rock should not be expected to be subjected to exactly the same stress as all the other 1 m^3 volumes in the same rock unit.

In contrary to the u-parameter, the v-parameter is *not* meant to reflect the lack of knowledge or lack of data, but should reflect the expected *actual* variation in the parameter from point to point inside the volume it represents. Therefore, the value of the v-parameter will be dependent on the scale of the rock units, i.e. how large rock volume that relates to each value. In a very large rock unit the distance between different points may be larger and also the mechanical properties of the rock mass inside may be expected to vary more. The chosen definition of "local stress" given above is also important for the expected v-parameter. The larger the definition volume of "local stress" is, the smaller the expected v-parameter becomes (as the local volume size approaches the size of the rock unit v approaches zero).

Also in contrary to the u-parameter the v-parameter is not expected to change in any particular direction with increased knowledge, increased number of measurements or improved measurement techniques. The quality of the stress model is not reflected in the v-parameter.

The v-parameter is also not so interesting for the assessment of the constructability at a site because small-scale stress variation will not influence the design. In the design it is mainly interesting to know the average stress level, such that the overall stability conditions can be predicted.

The problematic thing with the v and u parameters is that it can be impossible to distinguish in measurement data scatter what is the cause of the scatter. If the whole scatter in values (at the same depth) is caused by the local heterogeneity and fractures then the scatter could be used directly to estimate the v-parameter. However, some of the scatter could be due to measurement errors. In particular non-systematic error components in measurements are impossible to separate from spatial variability components. The only way to get insight to this it to rely on measurement research performed under known conditions.

A great portion of judgement must be used when finally selecting the numbers for u and v. They could be expressed either in terms of the actual units (e.g. MPa) or they can be expressed as % of the average. Section 8.5 gives an example of how these parameters were selected for the Test Case.

One example of the suggested way of describing the stress prediction: σ_1 = 20 MPa, with u = 20% and v = 10%, means that the *average* maximum principal stress in the rock unit is expected to lie in the span 16–24 MPa and that the local variation around the *average* is such that the actual local stress inside the unit lies in the span 14.4–17.6 MPa (if the average is as low as 16 MPa, 16±1.6 MPa), *or* in the span 21.6–26.4 MPa (if the average is 24 MPa). The predicted total possible span for a single σ_1 measurement value is thus the interval 14.4–26.4 MPa.

In cases when the rock units for predictions are located such that the stress variation with depth inside the unit cannot be neglected, the prediction of the average stress may be expressed as a *function* of the depth coordinate. In this case the uncertainty and variability, if expressed as percentages of the average stress, will also be depth dependent in absolute values.

10 Conclusions

10.1 Stress influencing factors

The main mechanism controlling the stress magnitudes in Sweden is the Alpine collision and the Mid-Atlantic rifting. These factors cause the stress field to show similarities in most parts of north-western Europe, having a NW-SE trend of the maximum principal stress.

The orientation of the stress field is largely determined by the relative movements of the plates. However, the stress orientation may also be influenced by the presence of large regional weak zones such as the Tornquist deformation zone that lies between Sweden and Denmark. The strike of the Tornquist deformation zone is parallel to the maximum principal stress as observed in central and southern Sweden.

The mechanism determining the magnitude of the stress is more complex but the general pattern is an increase in magnitude with depth at least for the upper kilometres. To determine the stress magnitude at a certain site and depth, with reasonable certainty, stress measurement should be used.

10.2 Stress model methodology

A methodology for building a stress model has been proposed. It involves different steps, starting with a preliminary stress estimation, followed by steps for interpreting site-specific information. If the stress pattern and structural geology of the site is complex, including major fracture zones intersecting the area, numerical analyses of the stress field is recommended.

Different numerical models (i.e. alternative geological concepts) can be analysed to provide possible explanations to observed stress patterns. The orientation of fracture zones with respect to the applied stresses determines the direction of fracture zone deformation. Stress measurement results and observations from the site concerning slip directions must be used in the evaluation of the modelling.

The mean orientation for the maximum principal stress may be predicted with a fairly high degree of certainty because both regional stress pattern and the site-specific measurements can be used. The same general trend, 135°–165°, and 0° ± 10° plunge, is expected for the whole central and southern Sweden, but local deviations could exist. This prediction applies to rock mass blocks away from major fracture zones. The local spatial variation in the orientation may be predicted based on measurement data.

The confidence in the prediction of the stress magnitudes will be dependent on the measurement results and the complexity of the site. Inside, and also in the vicinity of, major fracture zones both the stress magnitudes and stress orientation are expected to vary strongly from point to point. The prediction of the mean stress inside a fracture zone is therefore more uncertain and the predicted local variability will be larger.

The stress prediction should include a quantitative estimation of the uncertainty and the variability. Two parameters, *u* for uncertainty and *v* for local variability, are proposed. The aim of a stress model process is to minimize the u-parameter, in rock units where the stress level is of importance for the design and safety assessment.

10.3 Stress measurements

In the future stress measurement programs, much consideration should be taken to the geological model of the site, such that measurement located inside or close to fracture zone units can be distinguished from measurements taken in more intact rock mass units at a distance from a deformation zone.

The measurements should preferably be performed using overcoring techniques or overcoring supported by hydraulic fracturing and HTPF measurements. Overcoring measurement techniques can be used to predict all three principal stresses and to determine the ratio between the principal stress magnitudes. The ratio may then also be used to estimate maximum principal stresses at from minimum principal stress data.

Hydraulic fracturing measurements can be used to determine the *minimum horizontal* stress, often coinciding with the minimum principal stress. Hydraulic fracturing measurement data should *not* be used to determine the *maximum* horizontal stress. Hydraulic fracturing can be performed in already existing borehole. The orientation of the stress field at the site can be confirmed with both hydraulic fracturing and overcoring methods.

Boreholes for stress measurements is recommended to be located in all rock units, within which a reliable prediction is desired (number of boreholes ≥ 3), and at several levels (≥ 3) from 200 to 700 m depth. At each measurement level a number of measurements (≥ 4) close to each other is recommended.

11 References

Andersson J, Christiansson C, Hudson J A, 2002. Site Investigation – Strategy for Development of a Rock Mechanics Site Descriptive Model. SKB TR-02-01, Svensk Kärnbränslehantering AB.

Amadei A, Stephansson O, 1997. Rock stress and its measurement, Chapman and Hall, London, ISBN 0412447002.

Ask M S V, 1996. *In situ* Stress from Borehole Breakouts in Denmark. Licentiate Thesis, Royal Institute of Technology, Stockholm, TRITA-AMI LIC 2012, ISBN 9171706682.

Bjarnason B, Klasson H, Leijon B, Strindell L, Öhman T, 1989. Rock stress measurements in boreholes KAS02, KAS03 and KAS05 on Äspö. SKB PR 25-89-17, Svensk Kärnbränslehantering AB.

Bungum H, Alsaker A, Kvamme L B, Hansen R A, 1991. Seismicity and seismotectonics of Norway and nearby continental shelf areas. Journal of Geophysical Research, 96, 2249–2265.

Chandler N, Martin D, 1994. The influence of near surface faults on in situ stresses in the Canadian Shield. Nelson and Laubach (eds.). In Proc. 1st North American Rock Mechanics Symposium, Austin, pp 369–376. A A Balkema, Rotterdam, ISBN 9054103808.

Cosgrove J W, 1976. The formation of crenulation cleavage. Journal of the Geological Society London, 132, 155–178.

Cosgrove J W, 1997. Fluid induced fractures in sediments and rocks and the use of desiccation fractures as mechanical analogues. Journal of the Geological Society of China, 40, No. 1, 243–260.

Cheung L S, Haimson B C, 1989. Laboratory study of hydraulic fracturing pressure data- how valid is their conventional interpretation? Int J Rock Mech Min Sci and Geomech Abstr, 26, 595–604.

Donell L H, 1941. Stress Concentrations Due to Elliptical Discontinuities in Plates Under Edge Forces. In: Von Karman Anniversary Volume: Contributions to Applied Mechanics and Related Subjects. Pasadena:California Institute of Technology, pp. 293–309.

Engelder T, Geiser W, 1980. On the use of regional joint sets as trajectories of palaeostress fields during the development of the Appalachian Plateau, New York. Journal of Geophysical research, 85, 6319-41.

Erlstrom M, Thomas S A, Deeks, N, Sivhed U, 1997. Structure and tectonic evolution of the Tornquist Zone and adjacent sedimentary basins in Scania and the southern Baltic Sea area. Tectonophysics, 271, 191–215.

Gorbatschev R, Bogdanova S, 1993. Frontiers in the Baltic Shield. Precambrian Research, 64, 3–21.

Gou F, Morgenstern N R, Scott J D, 1993. Interpretation of hydraulic fracturing breakdown pressure. Int J Rock Mech Min Sci and Geomech Abstr, 30, 617–26.

Gregersen S, 1992. Crustal Stress Regime in Fennoscandia from Focal Mechanisms. Journal of Geophysical Research, 97, No. B8, 11, 821–827.

Gregersen S, Korhonen H, Husebye E S,1991. Fennoscandian dynamics: Present-day earthquake activity. Tectonophysics, 189, 333–344.

Grunthal G, Stromeyer D, 1992. The Recent Crustal Stress Field in Central Europe: Trajectories and Finite Element Modeling. Journal of Geophysical Research, 97, No. B8, 11, 805–820.

Gustafson G, Stanfors R, Wikberg P, 1989. Swedish Hard Rock Laboratory. Evaluation of 1988 year pre-investigation and description of the target area, the island of Äspö. SKB TR-89-16, Svensk Kärnbränslehantering AB.

Gölke M, Coblentz D,1996. Origins of the European regional stress field. Tectonophysics, 266, 11–24.

Hakala M, 2000. Interpretation of the Hästholmen in situ state of stress based on core damage observations. Posiva Oy, Helsinki, Finland, Report 2000-01.

Hakami E, Olofsson S-O, 2000. Thermo-mechanical effects from a KBS-3 type repository – Performance of pillars between repository tunnels. SKB TR-00-05, Svensk Kärnbränslehantering AB.

Hakami E, Olofsson S-O, 2002. Numerical modelling of fracture displacement due to thermal load from a KBS-3 repository. SKB TR-02-08, Svensk Kärnbränslehantering AB.

Itasca, 1998. User's Manual, 3DEC – Three-dimensional Distinct element code. Itasca Consultant Group Inc., Minneapolis, Minnesota.

te Kamp L, Konietzky H, Blüming P, 1999. Three-dimensional modeling of the planned Wellenberg repository site in Switzerland. In: Numerical Models in Geomechanics – NUMOG VII, Balkema, Rotterdam, 1999, 385–390.

Klasson H, Persson M, Ljunggren C, 2001. Overcoring Rock Stress Measurements at the Äspö HRL – Prototype Repository: Borehole KA3579G (Revised data) and K-tunnel: Borehole KK0045G01. SKB Report IPR-02-03, Svensk Kärnbränslehantering AB.

Konietzky H, Blüming P, Rummel F, 1995. In situ stress field in the Wellenberg area. NAGRA Bulletin 26, 38–47.

Lee M Y, Haimson B C, 1989. Statistical evaluation of hydraulic fracturing stress measurement parameters. Int J Rock Mech Min Sci and Geomech Abstr, 26, 447–456.

Martin C D, Christiansson R, 1991. Overcoring in highly stressed granite; comparison between the USBM and CSIR devices. Rock Mech. Rock Eng., 24, 207-35.

Martin C D, Christiansson R, Söderhäll J, 2001. Rock stability considerations for siting and constructing a KBS-3 repository. Based on experiences from Äspö HRL, AECL's URL, tunnelling and mining. SKB TR-01-38, Svensk Kärnbränslehantering AB.

Minster J B, Jordon T H, 1978. Present Day Plate Motions. Journal of Geophysical research. 83, 5331–354.

Morita N, Fuh G-F, Black A D, 1996. Borehole breakdown pressure with drilling fluids – II. Semi-analytical solution to predict borehole breakdown pressure. Int J Rock Mech Min Sci and Geomech Abstr, 33, 53–69.

Munier R, 1995. Studies of geological structures at Äspö – Comprehensive summary of results. SKB PR 25-95-21, Svensk Kärnbränslehantering AB.

Müller B, Zoback M L, Fuchs K, Mastin L, Gregersen S, Pavoni N, Stephansson O, Ljunggren C, 1992. Regional Patterns of Tectonic Stress in Europe. Journal of Geophysical Research, 97, No. B8, 11, 783–803.

Müller B, Reinecker J, Heidbach O, Fuchs K, 2000. The 2000 release of the World Stress Map (available online at www.world-stress-map.org).

Nisca D H, 1987. Aeromagnetic interpretation. SKB PR 25-87-23, Svensk Kärnbränsle-hantering AB.

Pollard D D, Segal P, 1987. Theoretical displacements and stresses near fractures in rock: with applications to faults, joints, veins dikes, and solution surfaces. In: Fracture Mechanics of Rock, Academic Press, London, pp. 277–349.

Price N J, 1966. Fault and joint development in brittle and semi-brittle rocks. Pergamon Press, 176 p.

Price N J, 1974. The development of stress systems and fracture patterns in undeformed sediments. In Advances in rock mechanics. Proc. of the 3rd. Int. Conf. Soc. Rock Mech., Denver, Colorado, 1A, 487 p.

Price N J, Cosgrove J W, 1990. Analysis of Geological structures. Cambridge University Press, pp. 502.

Ratigan J L, 1992. The use of fracture reopening pressure in hydraulic fracturing stress measurements. Rock Mech Rock Engng, 25, 225-36.

Rhén I, Gustafson G, Stanfors R, Wikberg P, 1997. ÄSPÖ HRL – Geoscientific evaluation 1997/5 – Models based on site characterization 1986–1995. SKB TR-97-06, Svensk Kärnbränslehantering AB.

Roberts D G, Thompson M, Mitchener B, Hossak J, Carmichael S, Bjornseth H-M, 1999. Palaeozoic to Tertiary rift and basin dynamics: mid-Norway to the Bay of Biscay – a new context for hydrocarbon prospectivity in the deep water frontier. In: Fleet, A. J. and Boldy, S. A. R. (eds) Petroleum Geology of Northwest Europe: Proceedings of the 5th Conference, 7-40. Geological Society of London.

Rosengren L, Stephansson O, 1990. Distinct element modelling of the rock mass response to glaciation at Finnsjön, Central Sweden. SKB TR-90-40, Svensk Kärnbränslehantering AB.

Rutqvist J, Tsang C-F, Stephansson O, 2000. Uncertainty in the maximum principal stress estimated from hydraulic fracturing measurements due to the presence of the induced fracture. Int. J. of Rock Mech and Mining Sciences, 37, 107–120.

Röshoff K, Lanaro F, Jing L, 2002. Strategy for a Rock Mechanics Site Descriptive Model – Development and testing of the Empirical Approach. SKB R 02-01, Svensk Kärnbränslehantering AB.

Sehlstedt S, Stråhle A, 1991. Identification of water conductive oriented fractures in the boreholes KAS02 and KAS06. SKB HRL PR-25-91-11, Svensk Kärnbränsle-hantering AB.

Slunga R, Norrman P, Glans A-C, 1984. Baltic Shield seismicity, the result of a regional network. Geophysical Research Letters, 11, (12), 1247–1250.

SKB, 1999. Deep repository for spent nuclear fuel – SR97 – Post closure safety. SKB TR-99-06, Svensk Kärnbränslehantering AB.

SKB, 2001. Site Investigations. Investigation methods and general execution programme. SKB TR-01-29, Svensk Kärnbränslehantering AB.

Staub I, Fredriksson A, Outters N, 2002. Strategy for a Rock Mechanics Site Descriptive Model – Development and testing of the theoretical approach. SKB R 02-02, Svensk Kärnbränslehantering AB.

Stephansson O, Ljunggren C, Jing L, 1991. Stress measurements and tectonic implications for Fennoscandia. Tectonophysics, 189, 317–322.

Stille H, Olsson P, 1990. Evaluation of Rock Mechanics. SKB HRL PR-25-90-08, Svensk Kärnbränslehantering AB.

Talbot C, Riad L, 1988. Natural fractures in the Simpevarp area. SKB PR-25-87-03, Svensk Kärnbränslehantering AB.

Ulmishek G, 1991. "Geological Evolution and Petroleum Resources of the Baltic Basin". In: Interior Cratonic Basins, AAPG Memoir 51, 603–631.

van Balen R T, Heeremans M, 1998. Middle Proterozoic-early Palaeozoic evolution of central Baltoscandian intracratonic basins: evidence for asthenospheric diapirs. Tectonophysics 300, 131–142.

Whyatt J K, 2000. Influence of Geologic Structures on Stress Variation and the Potential for Rock Bursting in Mines with Particular Reference to the Lucky Friday Mine, Idaho. PhD Thesis, University of Minnesota.

Zoback M L, 1992. First- and Second-order Patterns of Stress in the Lithosphere: The World Stress Map Project. Journal of Geophysical Research, 97, No. B8, 11, 703–728.